# AN APPARATUS FOR TENSILE CHARACTERIZATION OF THERMOPLASTICS AT INTERMEDIATE STRAIN RATES

By

Syed Fahad Hassan

## A DISSERTATION

Submitted to
Michigan State University
in partial fulfillment of the requirements
for the degree of

Mechanical Engineering – Doctor of Philosophy

2023

#### **ABSTRACT**

Thermoplastic polymers have seen rapid increase in automotive applications. Advances in nanofillers technology has seen these polymers compete with thermosets with respect to mechanical properties, light-weighting, rapid manufacturing and high-volume processing. Unlike metals and thermosets, thermoplastics are relatively soft and their material response at intermediate strain rates (1 - 100s<sup>-1</sup>), commonly experienced in automotive crashes, is not well-documented. The tendency of thermoplastics to undergo large deformations before yield and failure, places a limitation on the type of apparatus which can be used to characterize their tensile response at these strain rates. This complex polymeric material behavior has led to an apparent lack of experimental techniques required to generate reliable tensile stress–strain data and a resulting absence of robust constitutive equations needed for development of 'digital twins'.

To address this challenge, a three-pronged approach was implemented. First, a novel, symmetric, double-acting drop weight impact apparatus that allows for pure-tensile testing at desired strain rates was designed and developed 'in-house' at the composite vehicle research center (CVRC). Equipped with an accurate data acquisition system, this fixture allows for application of equal displacement on both ends of the test sample, which results in efficient stress transfer throughout its gage length and a smoother transition to dynamic equilibrium. Two in-line load cells were used on both ends of the sample to record load data and ensure symmetric load application. Digital image correlation along with high-speed camera was used for obtaining strain information. The data acquisition system was automated with an optical trigger to ensure repeatability of response and facilitate data processing.

Second, the test fixture was validated with Aluminum 6061-T6 data reported in the literature corresponding to two unique strain rates. The experimentally validated fixture was then

used for the third part of the work that focused on intermediate strain rate characterization of five commonly used automotive thermoplastics. The thermoplastics were divided into three classes based on their stiffness and ductility. Further, the effect of nanoparticle inclusions on resulting tensile response of one select polymer (Acrylonitrile Butadiene Styrene - ABS) was investigated. Three nanoparticles, two graphene platelets and one carbon nanotube, were used at 1 wt. %. The baseline for the rate dependent response of all thermoplastics was established by initially testing them at different strain rates within the quasi-static regime. Next, all thermoplastics were tested at three strain rates corresponding to fixed drop heights of 10 in., 20 in. and 25 in.

Results show a homogenous strain field in the gage length of all samples tested, indicating a stable impact velocity and load-rising rate. Further, the load recorded on both load cells was similar indicating symmetric loading. Importantly, little to no ringing was observed in the output load response eliminating the need for further signal processing.

In general, results indicate that with increasing strain rates, the tensile strengths increased whereas the failure strains (ductility) reduced. The material specific variations in strength and ductility for each polymer were different due to differences in microstructure and morphology. For example, at a strain rate of  $27s^{-1}$ , the tensile strengths of ABS increased by 84 % while failure strains reduced by 48 %, compared to its quasi-static response. ABS nanocomposites exhibited improved strengths at higher strain rates relative to their quasi-static response. Nevertheless, it was lower than the pristine ABS response at similar strain-rate levels. This can be attributed to the improper dispersion of the nanoparticles as they were incorporated by mechanical mixing, and no chemical compatibilization with host polymer was performed. Overall, the results showed that the new apparatus is reliable and repeatable for characterizing the tensile response of thermoplastic polymers at intermediate strain rates.

Copyright by SYED FAHAD HASSAN 2023

## "Standing on the Shoulders of Giants"

This metaphor has always inspired me, but today, as I am putting the finishing touches on my doctoral dissertation, I am truly understanding the meaning of it.

I am understanding that whatever I am and whatever I have become is the culmination of decades of hard work, perseverance and sacrifice which my parents undertook; it is the result of the countless sleepless nights and tiresome days which they endured, and the product of their patience, understanding and fortitude. Nothing I do or say would ever be enough to thank them. And yet, there is one more person who has been the boon of my existence and success for the last eight years, and the reason that I am on the cusp of completing my doctoral studies.

My wife.

The one person without whom I would never have been able to accomplish this. She has been my companion and my rock through the most difficult phases of my life. She is the one who kept me going when the times got tough. To her, I want say that I know what you have sacrificed for me. I know that you gave up your comfort, your lifestyle and most importantly your career, just to make sure that I can focus on my work. Nothing I do, will ever be enough to repay your kindness, understanding and love.

I also want to dedicate my work to my lovely sons, Mohammad and Ebrahim. My dear sons, you might not understand right now, but just know that your dad drew strength from your smiling faces and unconditional love when he was at his lowest. You both are, and always will be, the light in my life. I couldn't have done this without you.

I also want to thank Dr. Gary Cloud, my friends and colleagues, Dr. Suhail Hyder, soon to be Dr. Sarat Kundhurti, Dr. Erik Stitt, Dr. Rajendra Prasad, Dr. Oleksii Karpenko, Dr Evan Patton and Ciaron Hamilton. With your support, this whole journey would not have been possible.

Last but not the least, I want to thank my advisor Dr Mahmood Haq. Sir, I don't have enough words to thank you for all what you have done for me. Thank you for believing in me when even I was unsure; for trusting me, for your technical guidance, and most importantly for always treating me with respect and dignity.

## TABLE OF CONTENTS

CHAPTER 1 - INTRODUCTION	1
REFERENCES	16
CHAPTER 2 - LITERATURE REVIEW	21
REFERENCES	31
CHAPTER 3 - QUASI-STATIC STRAIN RATE TESTING OF THERMOPLASTIC	
POLYMERS	37
REFERENCES	64
CHAPTER 4 - DESIGN AND VERIFICATION OF THE TEST FIXTURE	68
REFERENCES	
CHAPTER 5 - INTERMEDIATE STRAIN RATE CHARACTERIZATION OF	
THERMOPLASTICS	98
REFERENCES	

#### **CHAPTER 1 - INTRODUCTION**

Dynamic loading scenarios like crash events, foreign body impacts, blasts, forming operations and natural calamities such as earthquakes, tsunamis and wind gusts etc. present a very common yet less understood phenomena in many real-life structural applications. Under these loads, materials tend to deviate from their quasi-static behavior which results in a change in material properties and modes of failure. Accurately capturing this change of material behavior is mandatory in analyzing the strength and reliability of structures and components.

At slow loading rates, the time required for the stress-wave to travel back and forth through the specimen under test is small relative to the loading time. The system therefore is in a state of quasi-static equilibrium. Under a dynamic load, the system no longer remains in this equilibrium and the inertial forces become significant. Depending upon the material, type of loading (tensile, compressive or shear), existing environmental temperature and pressure, and the applied strain rate, the nature of material deformation and failure processes can be affected under such loads as shown in Figure 1.1. A representative diagram explaining the effect of quasi-static and dynamic loading in a tensile dog-bone sample has been shown in Figure 1.1(a). For illustration purposes, the gage length of the sample has been divided into sections containing bands of molecules. When the quasi-static load is applied, the rate of change of applied force is negligible and static equilibrium can be assumed. This results in nearly identical stresses in all the sections and the distance between the bands remains same. However, when dynamic load is applied, the disturbance will force the molecular bands to stretch in the center of the gage length and then propagate outwards towards the edges, thus continually changing the distance between each other. This means that at each time interval during the dynamic loading event, the strains at one particular cross-section in the gage length will change. This time dependent deformation of

the gage length from its original shape is called the strain rate.

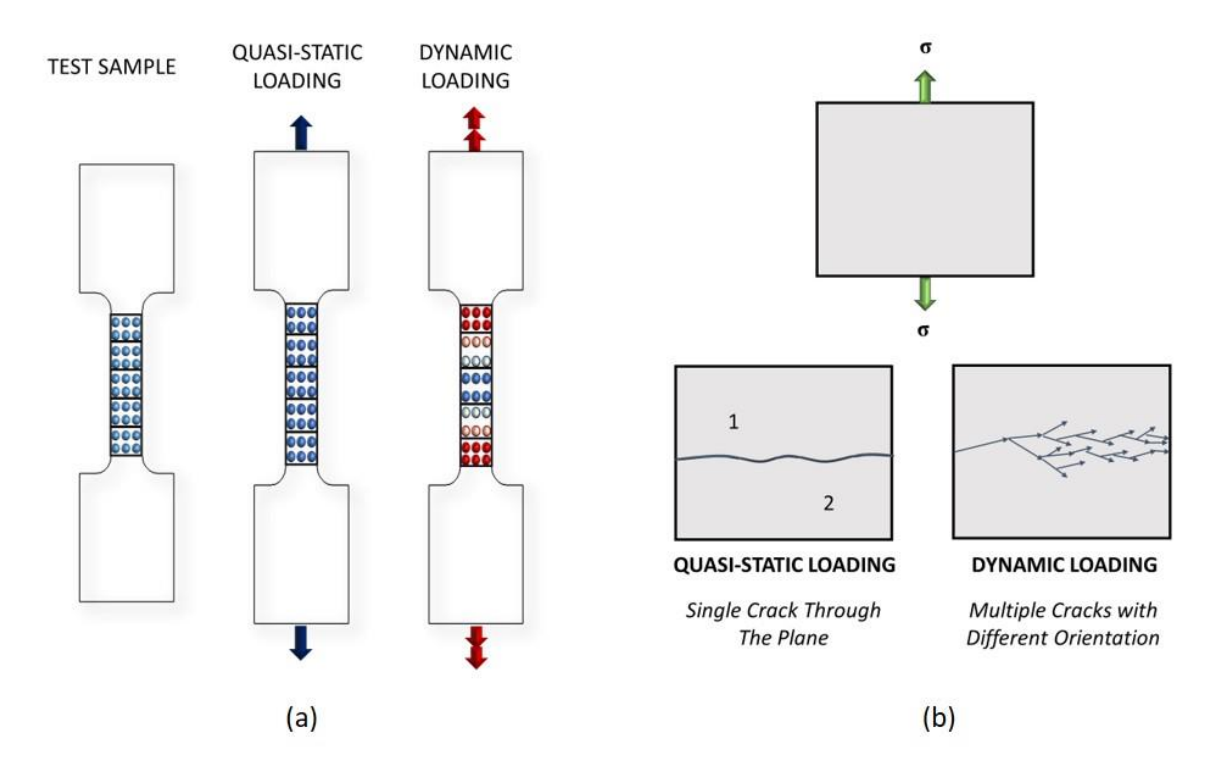


Figure 1.1: Quasi-Static vs Dynamic (a) Deformation (b) Failure. Adapted from [1]

At high strain rates, the failure mechanisms are also significantly different as compared to quasi-static loading [1]. As shown in Figure 1.1(b), a quasi-static load loading will generally result in a uniform crack propagation through the plane and divides the material into two parts. In dynamic loading however, the initial crack bifurcates and then branches out, propagating into multiple cracks at different orientations. Subsequently, this bifurcation leads to fragmentation of the material. It is important to note, that the bifurcation phenomena and the ensuing crack propagation only occurs at some critical velocity, which depends on the toughness of the material. Before that threshold, depending upon its microstructure and type of load applied, the material undergoes a series of deformations and extreme stress localizations due to the formation of crazes (more common in tensile loading) or shear bands (compressive loading) [2-4]. The formation of crazes and shear bands, and in effect the change in molecular structure and

mechanical properties of the material, are dependent on temperature and the rate of loading.

Characterizing the strain response of polymers at various rates is essential in understanding the deformation flow and failure strength. Deformation response in any material ultimately boils down to the microstructure of the material and the rate of imposed deformation. For example, there is a distinct difference between the deformation response of metals and polymers at any given loading rate. A typical stress-strain response of an amorphous polymer (containing randomly oriented molecular chains) and metal in uniaxial compression at quasi-static regime has been shown in Figure 1.2.

Unlike metals, the initial elastic behavior in the stress-strain curve of polymers is non-linear due to rate-dependent viscoelastic/plastic responses. Also, even though the yield stress of polymers is generally lower than the metals, they can withstand significantly higher strains before failure. Due to their viscoelastic nature, polymers are much more susceptible to strain rate loading than metals. As can be seen in Figure 1.3 below, a tangible variation in the stress strain response can be seen even at quasi-static regime. The same however is not generally observed in metals [5, 6].

Polymers generally exhibit time dependent mechanical behavior, which changes from rubbery to ductile to brittle. These transformations can occur over a range of strain rates and temperatures and are unique in every polymer, depending on the underlying microstructure. Figure 1.3 shows the stress-strain response of a commonly studied polymer.

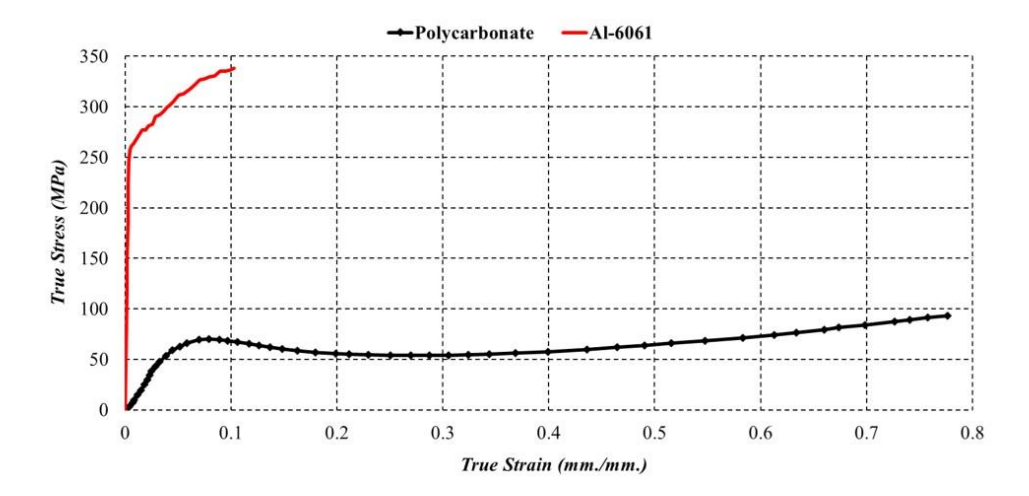


Figure 1.2: Comparison of Stress-Strain Response between Polymers (Polycarbonate[7]) and Metals (Aluminum 6061[8]) Subjected to Quasi-Static Loading

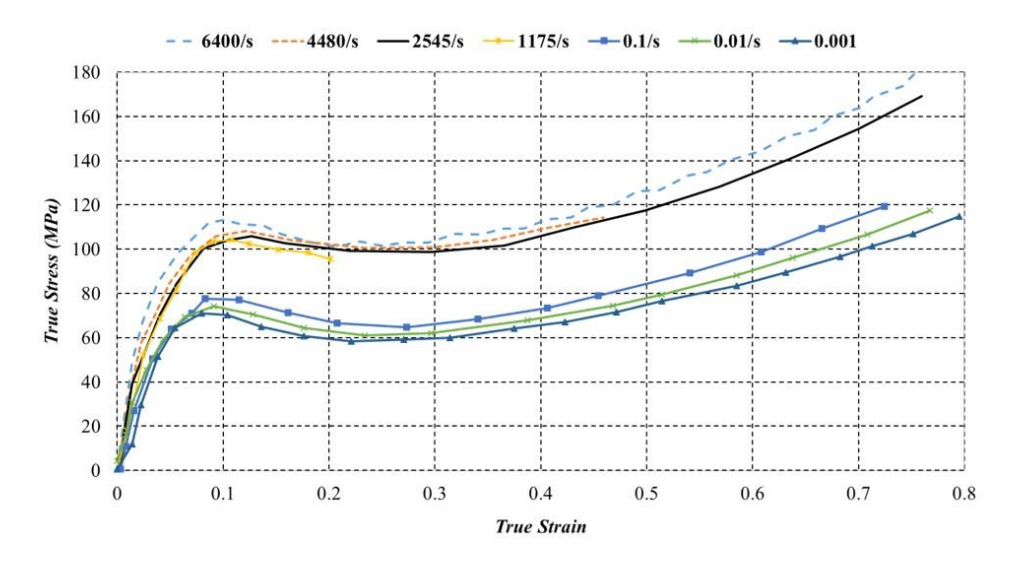


Figure 1.3: Stress – Strain Response of Polycarbonate (PC) at Various Strain Rates [9]

It can be clearly seen that the mechanical response of polycarbonate is sensitive to the loading rate. Almost a 100 % increase in the yield strength was recorded between the lowest and highest strain rate response, while the strain to failure decreased as compared to the quasi-static curve (the % reduction varies with the applied strain rate). A change in temperature can also affect the mechanical behavior of polymers [10]. Interestingly, this temperature dependence is strongly interlinked with the rate of loading [11, 12] and must be taken into consideration for

simulating the material response. Some studies have also highlighted the influence of hydrostatic confining pressure on the dynamic response of polymers [13, 14]. The yield strength, deformation flow, and failure stress of a polymer may vary with the hydrostatic pressure which translates into a different material response during tension and compression [10].

Polymers have unique internal morphology. Figure 1.4 illustrates a multi-scale schematic representation of these two types of polymers with essentially different microstructures.

Amorphous polymers consist of randomly oriented molecular chains which are physically entangled to each other and interact through the weak Van Der Waal forces. Semi-crystalline polymers are classified as such because they consist of both amorphous and crystalline phases.

Unlike amorphous polymers, where the mechanical response was only dependent on movement of randomly oriented chains, the elasto/visco-plastic behavior of semi-crystalline thermoplastic is dictated by the extent of crystallinity (typically 20 to 80 % by volume), lamellar thickness, crystallization procedures, and molecular arrangement etc. [15]. The microstructure of a semi-crystalline thermoplastic is composed of lamellar crystallites morphologically constrained by an assembly of randomly oriented amorphous macromolecules or molecular chains [16]. Lamella comprises of folded chains which have the ability to leave and re-enter the crystalline phase.

These chains get entangled with the chains present in the amorphous phase and form very strong covalent tie bonds along the interface [15].

The interaction between the amorphous and crystalline constituents is critical in determining the overall mechanical response of a semi-crystalline thermoplastic subjected to a deformation. Given that each polymer has a different percentage of crystallinity, initial crystallographic texture and molecular orientation, the evolution of stress-strain response when a load is imposed would be different. Typically, this response was considered to be dictated by the

evolution of the crystallographic structure during plastic straining up to large strains, however elastic response of each phase and the interplay between the elastic and visco-plastic behavior is also critical [17].

Due to their unique morphology, the intrinsic structural response of amorphous and semicrystalline polymers to mechanical loading is markedly different. Before investigating the dynamic loading responses of these polymers, it is therefore essential to develop a sound understanding of the various stages of deformation that occur within once a load is applied. Table 1.1 details the stress-strain response of amorphous and semi-crystalline polymers undergoing large plastic deformation. It is pertinent to mention that the description presented is valid only within the quasi-static regime. Beyond that, instabilities like necking and formation of micro-voids may appear in plastic regime causing accelerated failure.

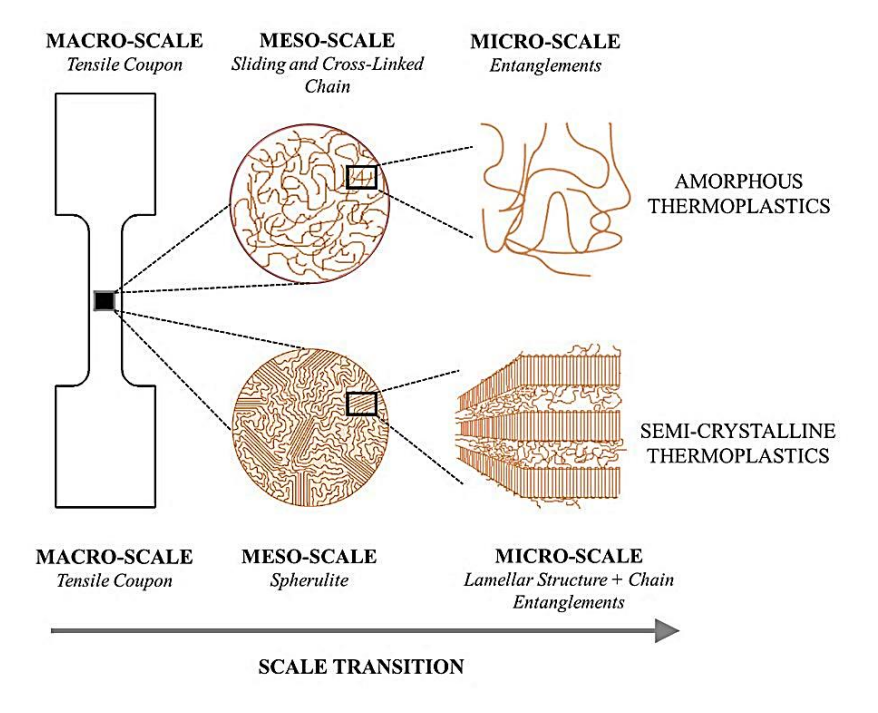


Figure 1.4: A Multi-Scale Structural Representation of Amorphous and Crystalline Thermoplastic Polymers. Adapted from [18, 19] (Spherulite is a stack of multiple lamellae more common in melt crystallized polymers)

Unlike amorphous polymers in which the deformation mechanisms are generally well understood [10, 20, 21], there is no unified theory presenting a clear and consistent description of large strain deformation mechanisms occurring inside semi crystalline polymers [15]. Over the years, a number of models, for instance.[16, 22-31] etc., have been formulated to explain this response. Based on the above-mentioned deformation models, a generic baseline description of the deformation flow inside semi-crystalline plastics has been established in Table 1.1, with the ultimate aim of creating a better understanding of dynamic loading effects in these polymers

Table 1.1: Deformation mechanisms in amorphous and semi-crystalline polymers

	Amorphous Polymers	Semi-Crystalline Polymers
	The chain segments get stretched	The polymers chains in the amorphous
	and tend to partially rotate and/or	phase start to uncoil and stretch. These
	slide with respect to each other.	chains exhibit the rubber-like
	With the advancing strain, local	properties similar to their response in
	clusters of chain segments start	amorphous polymers, but their
	overcoming the intermolecular	extensibility is limited by the length of
Viscoelastic	forces (Vander Wall) and move to	chain segments joining the nodes
Response	new positions. These localized	(short tie molecules which link the
	effects are random and result in	amorphous and crystalline phases). As
	non-linearity of the response. As	the strain increases, the chains reorient
	the stretching and reorientation of	along the line of load and the stress
	the molecular segments occurs,	increases.
	stress tends to increase.	

Table 1.1 (cont'd)

	Once enough accumulation of these	As the strain increases, the compliant
	localized effects has taken place,	chains are constrained by the crystal
	the polymer starts to yield. After	lamellae. Crystallographic defects,
	this point, there is a significant load	primarily slip, originate at this point
Yielding	drop and the thermoplastic starts to	and are accompanied by interlaminar
	deform.	shear of the amorphous phase. Once
		enough dislocations have moved out
		of the crystal core and into the
		interface, the thermoplastic yields.
	After the material yields, the	This phenomenon is generally not
	material flows without any	observed in semi-crystalline polymers.
	additional increase in stress. The	Instead a reduction of slope is
	intermolecular barriers which	observed. The tie molecules stretch
	prevent the chain segment rotation	resulting in an increase in localized
Strain	and/or sliding disappear under	stress. Due to this, slip dislocations
Softening	plastic strain thus making their	continue to move which results in the
	movement easier. Therefore, upon	cooperative bending or kinking of the
	further loading, there is a decrease	crystal lamellae and might even result
	in stress and material exhibits	in localized fragmentation of the
	structural changes.	lamellae. This leads to a reduction in
		deformation resistance and the slope.

Table 1.1 (cont'd)

As the load increases, the molecular At this stage, the molecular chains are chains align themselves in the fully stretched, which lead to further direction of the load, which makes slip instability and fragmentation of it difficult for the polymer to crystal lamellae into small blocks. As undergo further plastic the strain increases, become Strain deformation. Thus, the stress progressively oriented in the direction Hardening of maximum extension. The stress required is increased resulting in strain hardening and the material therefore continues to increase and becomes brittle. results in strain hardening. The molecular chains eventually assume a fibrillar shape before partial destruction.

The effect of microstructure on the deformation flow in amorphous and semi-crystalline polymers can also be observed through the schematic in Figure 1.5. It can be observed that the molecular chains in semi-crystalline structures assume a fibrillar shape before failing. The design architecture of semi-crystalline polymers ensures that they have more strength as compared to amorphous plastics [32].

Another important parameter which can affect the polymer properties are the processing conditions. Polymers can be subjected to very large plastic deformations during processing which can have a significant effect on the macromolecular orientation, crystallographic texture and direction and subsequently on the overall end-use mechanical properties. For example, for a

same polymeric material, a dog-bone tensile sample cut from a sheet produced through traditional cell cast method would have different properties from a sample cut from a sheet produced through the extrusion process. The latter sample would definitely exhibit chain orientation and better properties in the direction of extrusion.

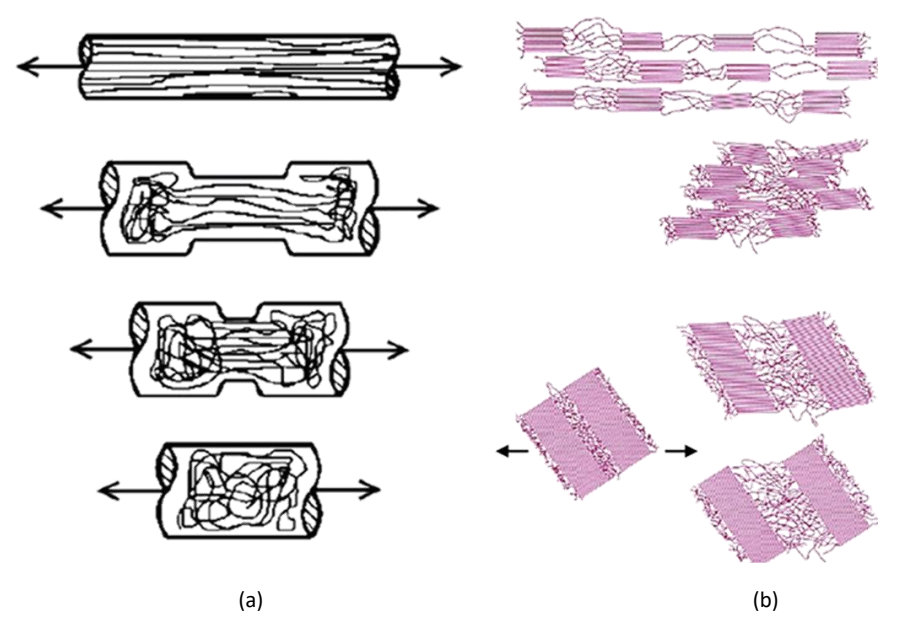


Figure 1.5: Tensile deformation flow in (a) Amorphous (b) semi-crystalline Polymers. Adapted from [32, 33]

It is pertinent to mention that the description presented in Table 1.1 is valid only within the quasi-static regime. Beyond that, instabilities like necking and formation of micro-voids may appear in plastic regime causing accelerated failure. Investigation into the post quasi-static behavior of select automotive plastics forms the basis of this dissertation.

#### 1.1 Background and Motivation

Advanced plastics and polymer composites are integral to automotive design. These plastics offer an unparalleled combination of properties that are essential to meet the ever evolving consumer expectations from safety and performance to efficiency and aesthetics [34]. Traditionally, thermosets, due to their lower viscosity, higher heat and chemical resistance and

greater overall strength and stiffness have been the preferred polymers/polymer composites for automotive applications [35]. However, with the recent advancements in molding technologies [36-38], their potential for medium to large scale production and adaptability to rapid manufacturing, high performance thermoplastics have gained traction in a range of structural applications from transportation and mass transit to aerospace and defense production [39]. While thermosets do not possess the ability to be recycled due to the cross-linking of polymer chains during the curing process, thermoplastics can be recycled repeatedly through application of heat. This cyclic reheating and reversibility of thermoplastics opens up the potential for increasing the service life of products through innovative healing/processing techniques [40-42]. Furthermore, with the advancement in filler technologies and permutations, attractive mechanical properties like improved specific stiffness and strength, better impact/damage tolerance and energy absorption, corrosion resistance and most importantly flexibility of design have resulted in an exponential rise in the use of thermoplastics/composites [39, 43] and an increased focus on their load dependent properties in different scenarios [7, 10, 43-61].

Filler materials are used in polymers to attain mechanical/electrical/ chemical properties greatly superior to that of the base resin. Most commercially available polymer materials are incorporated with a combination of different fillers to modify their strength, permanence, working properties, or other qualities, or to lower costs [62]. These fillers can vary from reinforcing fibers to conductive particulate fillers to coupling agents, flame retardants, and plasticizers etc. With increasing use of thermoplastic polymeric materials and their composites in automotive and various other transportation industries, effect of these fillers on the mechanical properties of these resins has become a subject of particular interest.

While most original equipment manufacturers (OEMs) supply quasi-static mechanical

properties of neat and reinforced thermoplastics, which suffice for static loading conditions, understanding the rate dependent response of these materials still remains a big question mark. Scenarios like crash events, foreign body impacts, blasts, forming operations etc. present a very common yet less understood phenomena.

#### 1.2 Problem Statement

The effect of dynamic loading on the tensile mechanical properties of neat and reinforced thermoplastic composites consisting of fibers, fabric or mats made of fiber has been the subject of a number of studies [43, 49, 52, 63-65]. However, due to their complex dynamic response at intermediate strain rates, the testing protocol are non-standardized. This has led to an apparent lack of reliable experimental data critical for predictive modelling of their response in a range of structural and non-structural applications. Hence, this work aims at developing an apparatus of high-strain tensile testing, its validation and then its use in predicting the behavior of thermoplastics.

#### 1.3 Methodology

To address this challenge, a four (04) step approach was adopted. In the first step, experimental characterization of the tensile properties of 'select' thermoplastics was carried out at four different strain rates within the quasi-static regime. This was done to assess the variation in material properties as a function of strain rate sensitivity. The selection of thermoplastics was done such that it was generic enough to include most common structural automotive thermoplastics yet specific enough to create 'performance-bounds' of resulting mechanical properties. The performance bounds for thermoplastics were created such that one (01) thermoplastic (Polyamide (6/6)) was selected in the "high-stiffness / low ductility" regime and one (02) thermoplastic (High density polyethylene (HDPE) and Polypropylene (PP)) were selected in the "low stiffness/ high

ductility regime. Lastly, two (02) thermoplastics (Acrylonitrile Butadiene Styrene (ABS) and Polycarbonate (PC)) that are in the intermediate stiffness/ductility were selected.

In the second step, a 'select' thermoplastic - ABS - was used to investigate the effect of carbon-based nanoparticles on the rate dependent mechanical response within the quasi-static loading limits. The choice of the carbon-based nanoparticles was based on the difference in their morphology while the thermoplastic selection was based on the experimental results derived from the first step.

As a third step, an open loop symmetric double acting drop weight tensile test fixture was conceptualized, designed and fabricated to carry out reliable and repeatable testing of soft thermoplastic polymers within the intermediate strain rate regime 1 - 100 s<sup>-1</sup> [66]. To validate the fixture design and operation, the intermediate strain rate response of a commonly used aluminum alloy 6061-T6 was compared against established experimental data available in literature [67]. After verification of the designed test fixture, mechanical characterization of the intermediate strain response of five selected thermoplastics was carried out at three different drop heights. Finally, as the last step, neat and particle reinforced configurations of ABS were tested at three (03) different intermediate strain rates and the quantitative changes in material response were measured and compared on the basis of the nanoparticle morphology.

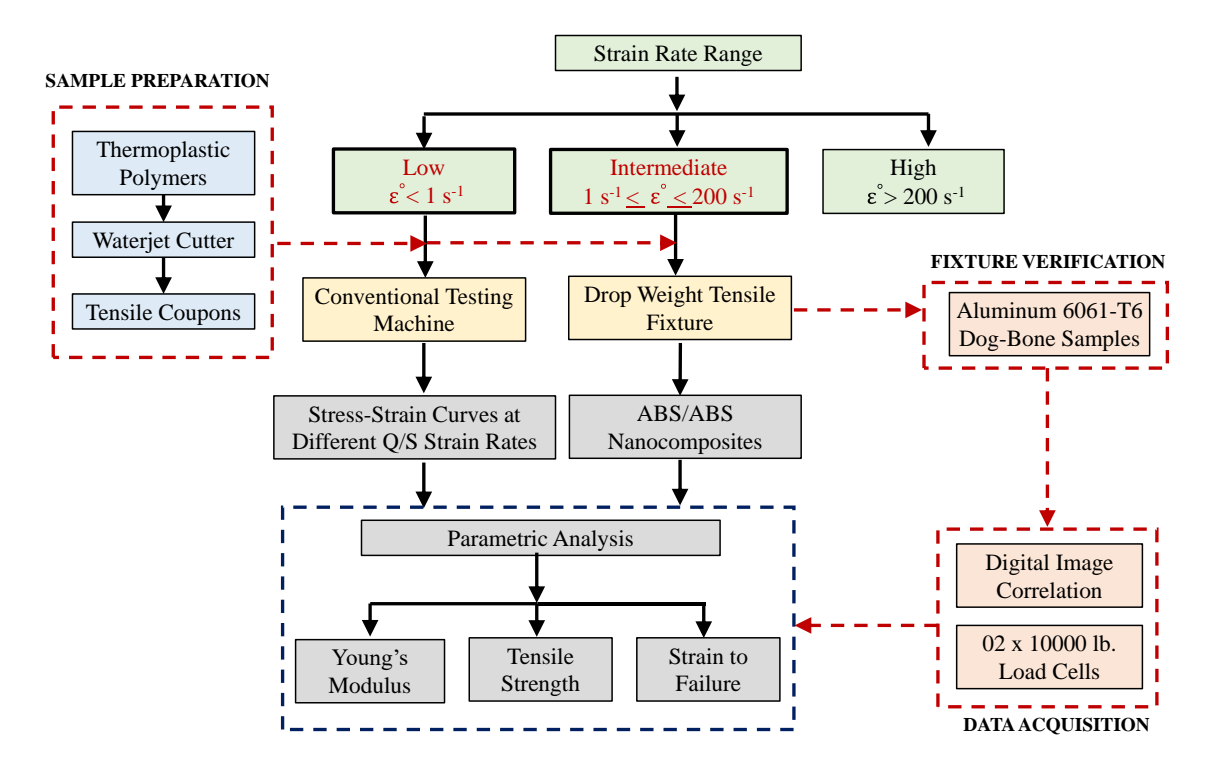


Figure 1.6: Research Methodology

## 1.4 Organization of Thesis

This aim of this dissertation is to understand the mechanics of neat and nanoparticle reinforced thermoplastics under tensile loading at intermediate strain rates. The dissertation is organized into five chapters. The first chapter introduces the work with a brief background, description of objectives and the method adopted to achieve the research goals. Chapter 2 focusses on the available literature on the tensile intermediate strain rate testing of neat and particle reinforced nanocomposites. It also provides an overview on the operational principles of already in-use test fixtures and critical parameters for designing a fixture to test thermoplastic samples at intermediate strain rates.

In Chapter 3, an investigation into the effect of strain rate variation within the quasi-static testing range is carried out on five commonly used automotive thermoplastics.

Testing protocols defined in ASTM standard D638-14 were followed to test the samples at four

(04) different strain rates from  $0.01 - 0.44 \, s^{-1}$ . This is followed by quasi-static material characterization of a select thermoplastic in neat and reinforced configurations at three different quasi-static strain rates. Three carbon-based nanoparticles were used to reinforce the select base thermoplastic. The sample dimension and shape were altered in the second characterization to conform to the sample geometry used in intermediate strain rate characterization.

In Chapter 4, the design concept of the newly designed symmetric double acting tensile testing fixture was introduced and a detailed investigation into its operational reliability and repeatability was carried out. The output response of the test fixture was verified against established literature using Aluminum 6061-T6 samples at two different strain rates within the intermediate strain rate regime.

In Chapter 5, investigation into the dynamic behavior of five selected thermoplastics was carried out by testing at three different drop heights using the newly designed/experimentally validated test fixtures. These drop heights were selected to introduce intermediate strain rates in the test samples. This was followed by intermediate strain rate characterization of selected neat and particle reinforced thermoplastics. This was done to study the effect of nanoparticle morphology on the dynamic material response of thermoplastics.

#### REFERENCES

- [1] T.Z. Blazynski, Materials at high strain rates, Springer Science & Business Media, 1987.
- [2] A.G. Odeshi, S. Al-ameeri, M.N. Bassim, Effect of high strain rate on plastic deformation of a low alloy steel subjected to ballistic impact, Journal of Materials Processing Technology, 162-163 (2005) 385-391.
- [3] J. Rösler, H. Harders, M. Bäker, Mechanical behaviour of engineering materials: metals, ceramics, polymers, and composites, Springer Science & Business Media, 2007.
- [4] K. Friedrich, Crazes and shear bands in semi-crystalline thermoplastics, in: Crazing in polymers, Springer, 1983, pp. 225-274.
- [5] H. Huh, J.H. Lim, S.H. Park, High speed tensile test of steel sheets for the stress-strain curve at the intermediate strain rate, International Journal of Automotive Technology, 10 (2009) 195-204.
- [6] X. Chen, Y. Peng, S. Peng, S. Yao, C. Chen, P. Xu, Flow and fracture behavior of aluminum alloy 6082-T6 at different tensile strain rates and triaxialities, PLOS ONE, 12 (2017) e0181983.
- [7] A.D. Mulliken, Low to high strain rate deformation of amorphous polymers: experiments and modeling, in, Massachusetts Institute of Technology, 2004.
- [8] Z. Hu, K. Lynne, F. Delfanian, Characterization of materials' elasticity and yield strength through micro-/nano-indentation testing with a cylindrical flat-tip indenter, Journal of Materials Research, 30 (2015) 578-591.
- [9] M. Kendall, C. Siviour, Experimentally simulating high-rate behaviour: rate and temperature effects in polycarbonate and PMMA, Philosophical Transactions of the Royal Society A: Mathematical, Physical and Engineering Sciences, 372 (2014) 20130202.
- [10] A.D. Mulliken, M.C. Boyce, Mechanics of the rate-dependent elastic–plastic deformation of glassy polymers from low to high strain rates, International Journal of Solids and Structures, 43 (2006) 1331-1356.
- [11] E.M. Arruda, M.C. Boyce, R. Jayachandran, Effects of strain rate, temperature and thermomechanical coupling on the finite strain deformation of glassy polymers, Mechanics of Materials, 19 (1995) 193-212.
- [12] M. Boyce, E. Arruda, An experimental and analytical investigation of the large strain compressive and tensile response of glassy polymers, Polymer Engineering & Science, 30 (1990) 1288-1298.
- [13] J. Sauer, Deformation, yield and fracture of polymers at high pressure, Polymer Engineering & Science, 17 (1977) 150-164.

- [14] K. Pae, S. Bhateja, The effects of hydrostatic pressure on the mechanical behavior of polymers, Journal of Macromolecular Science—Reviews in Macromolecular Chemistry, 13 (1975) 1-75.
- [15] Z. Bartczak, Deformation of semicrystalline polymers—the contribution of crystalline and amorphous phases, Polimery, 62 (2017).
- [16] C. G'sell, A. Dahoun, Evolution of microstructure in semi-crystalline polymers under large plastic deformation, Materials Science and Engineering: A, 175 (1994) 183-199.
- [17] J.v. Van Dommelen, D. Parks, M. Boyce, W. Brekelmans, F. Baaijens, Micromechanical modeling of the elasto-viscoplastic behavior of semi-crystalline polymers, Journal of the Mechanics and Physics of Solids, 51 (2003) 519-541.
- [18] P. Technology, Injection Molding: Melting Amorphous vs. Semi-Crystalline Plastics, in, 2018.
- [19] W.D. Callister, Materials science and engineering an introduction, John Wiley, 2007.
- [20] L. Anand, N.M. Ames, V. Srivastava, S.A. Chester, A thermo-mechanically coupled theory for large deformations of amorphous polymers. Part I: Formulation, International Journal of Plasticity, 25 (2009) 1474-1494.
- [21] V. Srivastava, S.A. Chester, N.M. Ames, L. Anand, A thermo-mechanically-coupled large-deformation theory for amorphous polymers in a temperature range which spans their glass transition, International Journal of Plasticity, 26 (2010) 1138-1182.
- [22] R.J. Young, A dislocation model for yield in polyethylene, The Philosophical Magazine: A Journal of Theoretical Experimental and Applied Physics, 30 (1974) 85-94.
- [23] A. Peterlin, Molecular model of drawing polyethylene and polypropylene, Journal of Materials Science, 6 (1971) 490-508.
- [24] C. G'Sell, S. Boni, S. Shrivastava, Application of the plane simple shear test for determination of the plastic behaviour of solid polymers at large strains, Journal of Materials Science, 18 (1983) 903-918.
- [25] C. G'Sell, J.J. Jonas, Determination of the plastic behaviour of solid polymers at constant true strain rate, Journal of Materials Science, 14 (1979) 583-591.
- [26] C. G'Sell, N.A. Aly-Helal, J.J. Jonas, Effect of stress triaxiality on neck propagation during the tensile stretching of solid polymers, Journal of Materials Science, 18 (1983) 1731-1742.
- [27] Z. Bartczak, A.S. Argon, R.E. Cohen, Deformation Mechanisms and Plastic Resistance in Single-Crystal-Textured High-Density Polyethylene, Macromolecules, 25 (1992) 5036-5053.

- [28] Z. Bartczak, R.E. Cohen, A.S. Argon, Evolution of the crystalline texture of high-density polyethylene during uniaxial compression, Macromolecules, 25 (1992) 4692-4704.
- [29] A. Galeski, Z. Bartczak, A.S. Argon, R.E. Cohen, Morphological alterations during texture-producing plastic plane strain compression of high-density polyethylene, Macromolecules, 25 (1992) 5705-5718.
- [30] L. Lin, A.S. Argon, Deformation Resistance in Oriented Nylon 6, Macromolecules, 25 (1992) 4011-4024.
- [31] R. Séguéla, Dislocation approach to the plastic deformation of semicrystalline polymers: Kinetic aspects for polyethylene and polypropylene\*, Journal of Polymer Science Part B: Polymer Physics, 40 (2002) 593-601.
- [32] D.R. Jones, M.F. Ashby, Engineering materials 2: an introduction to microstructures and processing, Butterworth-Heinemann, 2012.
- [33] I.R. Harrison, Polymer materials science, Jerold M. Schultz, Prentice-Hall, Englewood Cliffs, N.J., 1974, 524 pp, Journal of Polymer Science: Polymer Letters Edition, 12 (1974) 603-604.
- [34] A.C. Council, Automotive Plastics, in, 2010-2020.
- [35] P. Mallick, Thermoset—matrix composites for lightweight automotive structures, in: Materials, Design and Manufacturing for Lightweight Vehicles, Elsevier, 2010, pp. 208-231.
- [36] M. Tufail, Processing investigation and optimization for hybrid thermoplastic composites, Journal of University of Science and Technology Beijing, Mineral, Metallurgy, Material, 14 (2007) 185-189.
- [37] M. Schade, O. Diestel, K.M. Cherif Ch, W. Hufenbach, J. Franeck, Development and technological realization of complex shaped textilereinforced thermoplastic composites, in: Proceedings of composites in automotive and aerospace (5th international congress on composites), Munich, 2009, pp. 14-15.
- [38] W. Hufenbach, F. Adam, J. Beyer, M. Zichner, M. Krahl, S. Lin, U. Hanke, Development of an adapted process technology for complex thermoplastic lightweight structures based on hybrid yarns, in: Proceedings of ICCM-17 conference. Edinburgh, 2009, pp. 27-31.
- [39] U. Vaidya, K. Chawla, Processing of fibre reinforced thermoplastic composites, International Materials Reviews, 53 (2008) 185-218.
- [40] P. Zhang, G. Li, Advances in healing-on-demand polymers and polymer composites, Progress in Polymer Science, 57 (2016) 32-63.
- [41] S.H. Vattathurvalappil, Experimental and Numerical Characterization of Bonded Joints Using Reversible Adhesives, in, Michigan State University, Ann Arbor, 2020, pp. 191.

- [42] S.H. Vattathurvalappil, S.F. Hassan, M. Haq, Healing potential of reversible adhesives in bonded joints, Composites Part B: Engineering, 200 (2020) 108360.
- [43] K.A. Brown, R. Brooks, N.A. Warrior, The static and high strain rate behaviour of a commingled E-glass/polypropylene woven fabric composite, Composites Science and Technology, 70 (2010) 272-283.
- [44] M. Schoßig, C. Bierögel, W. Grellmann, T. Mecklenburg, Mechanical behavior of glassfiber reinforced thermoplastic materials under high strain rates, Polymer Testing, 27 (2008) 893-900.
- [45] B.L. Peterson, R.N. Pangborn, C.G. Pantano, Static and high strain rate response of a glass fiber reinforced thermoplastic, Journal of composite materials, 25 (1991) 887-906.
- [46] Y. Wang, E.M. Arruda, Constitutive modeling of a thermoplastic olefin over a broad range of strain rates, (2006).
- [47] A.D. Mulliken, Mechanics of amorphous polymers and polymer nanocomposites during high rate deformation, in, Massachusetts Institute of Technology, 2006.
- [48] D.A. Şerban, G. Weber, L. Marşavina, V.V. Silberschmidt, W. Hufenbach, Tensile properties of semi-crystalline thermoplastic polymers: Effects of temperature and strain rates, Polymer Testing, 32 (2013) 413-425.
- [49] K.A. Brown, R. Brooks, N.A. Warrior, Characterizing the strain rate sensitivity of the tensile mechanical properties of a thermoplastic composite, Jom, 61 (2009) 43.
- [50] C.A. Weeks, C.T. Sun, Modeling non-linear rate-dependent behavior in fiber-reinforced composites, Composites Science and Technology, 58 (1998) 603-611.
- [51] J. Fitoussi, M. Bocquet, F. Meraghni, Effect of the matrix behavior on the damage of ethylene–propylene glass fiber reinforced composite subjected to high strain rate tension, Composites Part B: Engineering, 45 (2013) 1181-1191.
- [52] W. Hufenbach, A. Hornig, B. Zhou, A. Langkamp, M. Gude, Determination of strain rate dependent through-thickness tensile properties of textile reinforced thermoplastic composites using L-shaped beam specimens, Composites science and technology, 71 (2011) 1110-1116.
- [53] K.A. Brown, Finite element modelling of the static and dynamic impact behaviour of thermoplastic composite sandwich structures, in, University of Nottingham, 2007.
- [54] S. Bartus, U. Vaidya, Performance of long fiber reinforced thermoplastics subjected to transverse intermediate velocity blunt object impact, Composite structures, 67 (2005) 263-277.
- [55] K. Yoon, C. Sun, Characterization of elastic-viscoplastic properties of an AS4/PEEK thermoplastic composite, Journal of Composite Materials, 25 (1991) 1277-1296.

- [56] R. Recht, Catastrophic thermoplastic shear, (1964).
- [57] S. Kolling, A. Haufe, A constitutive model for thermoplastic materials subjected to high strain rates, in: PAMM: Proceedings in Applied Mathematics and Mechanics, Wiley Online Library, 2005, pp. 303-304.
- [58] C. Cady, W. Blumenthal, G. Gray III, D. Idar, Determining the constitutive response of polymeric materials as a function of temperature and strain rate, in: Journal de Physique IV (Proceedings), EDP sciences, 2003, pp. 27-32.
- [59] C.L. Clark, D.J. Locke, High strain rate testing of engineering thermoplastics for head impact applications, in, SAE Technical Paper, 1996.
- [60] Y. Li, Z. Lin, A. Jiang, G. Chen, Experimental study of glass-fiber mat thermoplastic material impact properties and lightweight automobile body analysis, Materials & design, 25 (2004) 579-585.
- [61] N.S.J. Al-Maliky, Strain rate behaviour of thermoplastic polymers, in, Loughborough University, 1997.
- [62] A.S.f.T. Materials, ASTM D-883-99, Terminology Relating to Plastics, in, ASTM Standards Philadelphia, 1999.
- [63] F. Coussa, J. Renard, S. Joannes, J.C. Teissedre, R. Bompoint, N. Feld, A consistent experimental protocol for the strain rate characterization of thermoplastic fabrics, Strain, 53 (2017) e12220.
- [64] J. Lienhard, F. Huberth, Strain rate dependent thermo-mechanical aspects of glass fiber reinforced thermoplastic based on experimental data, International Journal of Impact Engineering, 131 (2019) 57-65.
- [65] S. Duan, F. Mo, X. Yang, Y. Tao, D. Wu, Y. Peng, Experimental and numerical investigations of strain rate effects on mechanical properties of LGFRP composite, Composites Part B: Engineering, 88 (2016) 101-107.
- [66] X. Xiao, Dynamic tensile testing of plastic materials, Polymer Testing, 27 (2008) 164-178.
- [67] D. Zhu, B. Mobasher, S.D. Rajan, P. Peralta, Characterization of dynamic tensile testing using aluminum alloy 6061-T6 at intermediate strain rates, Journal of Engineering Mechanics, 137 (2011) 669-679.

#### **CHAPTER 2 - LITERATURE REVIEW**

## 2.1 Intermediate Tensile Strain Rate Testing - Neat Thermoplastics

Extensive experimental data characterizing the compressive stress—strain response over a range of strain rates for a broad range of polymers is available in literature. Review references [1-4] provide elaborate details on compressive of polymers. The literature however predominantly focusses on loading on thermosets. Further, the focus of most research in this domain has been on compressive loading of polymer. In-line tensile testing is a relatively less explored subject, especially in thermoplastics.

The interest in dynamic tensile response of thermoplastics materials dates back to Bauwens et al. [5, 6] who studied the effect of temperature on the yield stress of polycarbonate (PC) and polyvinyl chloride (PVC). There have been numerous studies which actually focus on the effect of strain rate on mechanical properties of thermoplastics, both amorphous [7-14] and semi-crystalline [15-18], however most of the experimental data is limited to low and high strain rate testing. Investigations into the intermediate strain rate behavior of thermoplastics poses a significant challenge since experimental evaluation within this range is influenced by complex dynamic phenomena like system ringing, inertia, specimen size load rising time and wave propagation, etc. Optimizing these parameters is essential to ensure dynamic equilibrium along the gage length of the sample. Details of these parameters are provided in section 2.4.

Only a select number of studies are available on tensile strain rate testing on neat thermoplastic samples between the ranges of 1-200 s<sup>-1</sup>. Serban et al [19] studied the strain rate sensitivity of PA-12 based semi-crystalline thermoplastic material in the interval from 2.8 s<sup>-1</sup> to 9.4 s<sup>-1</sup> using high speed servo hydraulic machine. The authors reported an increase in tensile modulus and strength with the increase in strain rate. They however did not test the materials at

higher strain rates within the intermediate strain rate regime. Foster et al. [7] studied the rate dependent tensile response of Polycarbonate (PC) and Poly-methyl methacrylate (PMMA) from low  $(0.001~\text{s}^{-1})$  to high strain rates  $(1600~\text{s}^{-1})$ . A servo hydraulic fixture was used to study the intermediate strain rate effect with the help of Digital Imaging Correlation (DIC) at 500fps. For both the thermoplastics, the authors found an increase in tensile modulus from low to intermediate strain rates ( $\sim 100~\text{s}^{-1}$ ), with an eventual increase at higher rates of loading. The study focused on a wider range of strain rates, but only a single test point was selected in the intermediate range.

El-Quobaa et al. [12] investigated the tensile mechanical behavior of Polyether ether ketone (PEEK) at room temperature over a large range of strain rates (from 0.001 - 1000 s<sup>-1</sup>). The authors used a tensile crossbow system for intermediate and high strain rates. Only one strain rate (151 s<sup>-1</sup>) was reported in this work. The tensile yield stress of PEEK was observed to be highly sensitive to strain rate and increased with the increase in loading rate. Zrida et al. [18] studied the mechanical behavior of copolymer polypropylene at various strain rates ranging from 0.8 to 200 s<sup>-1</sup> using a servo hydraulic machine. The study showed an increase in Young's modulus with the increase in strain rate. A microscopic analysis of the fractured surfaces showed an increase in surface roughness at higher strain rates.

#### 2.2 Intermediate Strain Rate Testing - Particle Reinforced Thermoplastics

Nanoparticles have widely gained acceptance as possible reinforcing structures because of their low cost and ease of incorporation [20]. Particulate reinforcements/fillers can provide increase in specific stiffness, specific strength and toughness in polymeric matrices, albeit to a lesser extent as compared to fiber reinforced composites [21]. Detailed investigations into the effect of various particulate reinforcements, like carbon nanotubes, graphene, nanoclay, talc,

halloysite, etc. on the mechanical properties of thermoplastics can be found in literature [22-30]. An overview of the enhancement in mechanical properties of a few representative thermoplastic resins by the addition of various nanoparticles has been given in Table 2.1.

Table 2.1: Improvement in mechanical properties of a few representative thermoplastics with the addition of nanoparticles. Adapted from [27]

Thermoplastic	Nanoparticle Reinforcement	Neat Resin Strength (MPa)	Neat Resin Modulus (GPa)	Nanoparticle Composite Strength (MPa)	Nanoparticle Composite Modulus (GPa)
Polyether Imide (PEI)	CNT (1.2 Vol %)	79	2.6	126	4.7
Polyether Ether  Ketone  (PEEK)	Hydroxyapatite (7.8 wt. %)	88-90	2.0-2.2	85-90	3.3-3.4
Polypropylene (PP)	Graphene (10 Vol %)	36-42	1.1-1.3	50-52	3.1-3.4
Nylon (PA)	Nylon-6 Clay (4.6 wt. %)	69	1.1	107	2.1
Polycarbonate (PC)	Multilayered Graphene/PC Films (0.08 Vol %)	120	2	160	2.7

Table 2.1 (cont'd)

77-86	3.6-4.0
77 00	3.0 1.0
7	<i>1</i> 7-86

The effects of nano-reinforcement on the mechanical response of the host resin subjected to different strain rates is not a widely researched topic. Only a few experimental studies have focused on the strain rate sensitivity of particle reinforced thermoplastics at different speeds, albeit within the quasi-static regime [31-39]. The research gap becomes more noticeable at intermediate and high strain rate loading. Delhaye et al. [40] carried out an experimental investigation into the mechanical behavior of a rubber-modified polypropylene copolymer under different stress states and strain rates, in compression, tension, and shear. A direct impact Hopkinson bar was used at the intermediate strain rate level (100 s<sup>-1</sup>) to measure the stress-strain response. It was found that the rate sensitivity seems to be slightly more pronounced in shear than in tension and compression modes. The tensile results showed an increase in stress with the increase in strain rate, but a quicker yielding and smaller strain to failure. The study does not provide a comparative analysis of PP, with and without rubber particle reinforcement. Also, data was only presented for a single point in the intermediate strain rate range.

The lack of experimental data for nanoparticle reinforced thermoplastics in the intermediate and high strain rate ranges mandates the need for extensive testing to better understand the mechanical behavior of such composites under dynamic loading conditions. As mentioned before, while high strain rate testing can be performed in standardized experimental

fixtures, there is no universally accepted fixture for testing neat and reinforced thermoplastics (polymers in the intermediate strain rate range). In the next section, a brief overview of the experimental fixtures used for polymer characterization over a range of strain rates is provided, with a narrowed focus on the set-ups used in literature for tensile testing in the intermediate strain rate regime.

#### 2.3 Experimental Techniques for Tensile Strain Rate Testing in Polymers

A wide variety of experimental techniques are used to capture polymer/polymer composite behavior at high- strain rate loadings. Many of these techniques have especially been modified for polymer characterization. These special modifications are required to accommodate the slower elastic wave speed experienced in plastics, as compared to metals [41]. An overview of these techniques has been given in Table 2.2.

The most widely used apparatus in this regard is the Split Hopkinson Pressure Bar (SHPB) [42-44]. It is a reliable and widely used strain rate testing technique, however it can only be employed to generate data in the higher strain rate range. As mentioned before, a large number of real-life applications including crash and impact scenarios in cars (0.01 to  $500 \, \text{s}^{-1}$ [41]) and aircrafts ( $10^{-2}$  to  $10^{2} \, \text{s}^{-1}$ [45]) occur at a lower range of strain rates. These strain rates are also typical in a number of forming operations like extrusion [ $10^{-1}$  to  $100 \, \text{s}^{-1}$ ], forming [1 to  $100 \, \text{s}^{-1}$ ], and rolling [1 to  $10^{3} \, \text{s}^{-1}$ ] etc.[46, 47].

Characterizing the material response of polymers in this range is therefore critical in prediction of failure strength and post-impact behavior. However, investigative experimental techniques required to generate tensile stress—strain data at intermediate strain rates are not well established [41]. Traditionally, high rate servo hydraulic machines have been used to gather reliable data for intermediate rates of strain. References [19, 48-51] are some of the studies in

which these servo machines have been used to gather tensile stress-strain data in polymers and their composites. However, servo hydraulic machines are expensive and not easily accessible. Furthermore, the ringing issues in servo hydraulic machines are also well documented [41, 52, 53]. These factors have over time necessitated the design and development of alternative fixtures. In the last few decades, a number of researchers have introduced fixtures such as fly wheel systems [54, 55], cam plastometer [56], expanding ring [57], wedge bar [58] and a very long Hopkinson bar [59] for testing of polymers in intermediate strain rate range. However due to their ease of implementation and lack of complexity, tensile tests using drop weight systems have gained the most traction recently.

A select number of studies have conceptualized the principle of converting the compressive impact energy of the impactor into tensile loading on a test specimen [60-64]. The strain rate can be controlled by controlling the impacting force on the top plate of the movable frame. The current work will focus on the drop weight concept in designing the fixture such that the sample is in pure tension. The details of the design work and final fixture would be provided in the next chapter.

### 2.4 Factors Affecting Dynamic Response of Polymers at Intermediate Strain Rates

#### 2.4.1 Ringing

Ringing is a very important issue in tensile testing machines used for measurement of rate dependent material response. This phenomenon occurs when the natural oscillations of the test fixture coincides with the frequency of the load measuring device and/or the testing fixture. This results in high amplitude stress waves in the output and a significantly distorted data. Numerous studies have detailed damping measures including the use of double coated vinyl foam tapes [50] to placing rubber plates between the impacting metallic surfaces [61].

Table 2.2: Experimental Techniques for Testing Polymers at Different Strain Rates

STRAIN RATE RANGE	CATEGORY	TESTING DEVICES
10 <sup>-8</sup> to 10 <sup>-4</sup>	Creep and Stress	Creep Testers
(Inertia Negligible)	Relaxation	Conventional Cross Head Load Frame
10 <sup>-4</sup> to 10 <sup>-1</sup>		Hydraulic Machine
(Inertia Negligible)	Quasi-Static	Servo Hydraulic System
		Screw Driven Testing Machine
10° to 10²	Intermediate	High Rate Servo Hydraulic System
(Inertia Important)	Strain Rate	Drop Weight Test
10 <sup>2</sup> to 10 <sup>4</sup>	High Strain Rate	Split Hopkinson Pressure Bar
(Inertia Important)		Expanding Ring
10 <sup>4</sup> to 10 <sup>8</sup>	Shock/Impact	Taylor Impact
(Inertia Important)		Plate Impact
		Air gun Apparatus

## 2.4.2 Inertia

Inertia of the test fixture is another critical phenomenon that can affect the validity of the measured output. At quasi-static loading, since the load is applied very slowly, the acceleration of the system and sample can be assumed as negligible. Therefore, the equilibrium equation shown as Equation 1 below becomes purely a function of the system stiffness (k) and displacement vector (x). At dynamic strain rates though, rapid acceleration is experienced and the inertia of the system becomes important. The system equilibrium therefore also becomes a function of velocity and acceleration;

$$F = kx + c\dot{x} + m\ddot{x}$$
 Equation 2.1

Where  $\dot{x}$  and  $\ddot{x}$  are the velocity and acceleration vectors, c is the damping coefficient and m is the mass of the system.

For rate dependent materials, k is always a function of loading rate and depending upon the material its effect can be large even within the quasi-static range. During dynamic event, the material experiences deformation and its properties change due to a combination of strain rate and inertia. As both effects are superimposed, distinguishing between them can be very challenging from an experimental design point of view. Therefore, for any fixture design, it is critical to either overcome/minimize the effects of inertia or apply an inertia correction to the resulting stress-strain curves.

## 2.4.3 Specimen Dimensions and Stress Wave Propagation

Selection of the right specimen type is critical for tensile strain rate testing at intermediate strain rates. For plastics in general, tensile dog-bone samples are used to ensure that the deformation is constrained to the narrower gage section and fracture does not initiate at the ends. Further, to successfully obtain the elongation data, a sample with extended grip section is required. In any tensile dog-bone test sample, wave propagation takes place along the length of the sample. The wave speed (C) is a function of the Young's Modulus (E) and density  $(\rho)$  of the test material as indicated by Equation 2 below;

$$C = \sqrt{\frac{E}{\rho}}$$
 Equation 2.2

The generated wave is reflected and transmitted at any point of impedance change along its line of travel. These points may include the transition from gage length to the grip area in a

sample, sample to grips and grip to load cell etc. [50]. The varying impedance at each of these transition points results in stress waves of varying amplitude in the specimen. These stress wave negate the condition of equilibrium and homogenous stress/strain distribution in the gage length. To avoid these localized variations in quasi-static testing, a larger gage length should be ensured. However, the same does not apply to dynamic loading.

For intermediate and high-strain experiments, quasi-homogenous stress and strain state can be safely assumed if the number of waves (n) travelling through sample are high – at least 10 reflected elastic waves [65]. This condition is very difficult to ensure in softer materials like thermoplastic and elastomers. A quantitative measure of  $n \ge 3$ , based on Split Hopkinson Pressure Bar testing has been shown to provide reasonable results for plastics [41, 42]. Depending on the material and damping conditions, even lower values of 'n' are difficult to achieve.

## 2.4.4 Load Rising Time

Another critical factor for achieving dynamic equilibrium is the load rising time(T), also described as stable impact duration. It is the time in which a certain number of stress waves can make a roundtrip inside the sample and is dependent on the length of the sample (L), the elastic stress wave-speed (C) and the number of stress wave round-trips (n), see Equation 3 below;

$$T = \frac{2L}{c} \cdot n$$
 Equation 2.3

Ideally the load rising time should be large enough to allow the reflected waves to makes multiple roundtrips and load up the sample. Fixture design plays an important part in optimizing the system slack. A quick load time would result in a lower value of n and unusable data. On the other hand, slower load actuations may result in the generation of undesired strain rates.

#### 2.4.5 Load Measurement

Load measurement also affects the accuracy of the measured output. In this regard, straingage type load cells and piezoelectric load washers are the two most common choices [66]. The most important parameter during the selection of a load cell is its frequency response, which should be fast enough to capture high strain rates [41, 67]. It is also pertinent to mention that the frequency response of the associated amplifiers and data acquisition system should also be compatible.

## 2.4.6 Strain Measurement

Strain measurement is generally performed by tracking the fiducial markers along the gage length of the samples using digital image correlation (DIC) technique. For the loading rates experienced within the intermediate range, a 3D visualization of the test specimen using two or more cameras is recommended [61, 66].

#### REFERENCES

- [1] S. Walley, J. Field, Strain rate sensitivity of polymers in compression from low to high rates, DYMAT j, 1 (1994) 211-227.
- [2] R.L. Sierakowski, Strain Rate Effects in Composites, Applied Mechanics Reviews, 50 (1997) 741-761.
- [3] S. Barre, T. Chotard, M. Benzeggagh, Comparative study of strain rate effects on mechanical properties of glass fibre-reinforced thermoset matrix composite, Composites Part A: Applied Science and Manufacturing, 27 (1996) 1169-1181.
- [4] A.M.S. Hamouda, M.S.J. Hashmi, Testing of composite materials at high rates of strain: advances and challenges, Journal of Materials Processing Technology, 77 (1998) 327-336.
- [5] C. Bauwens-Crowet, J.C. Bauwens, G. Homès, The temperature dependence of yield of polycarbonate in uniaxial compression and tensile tests, Journal of Materials Science, 7 (1972) 176-183.
- [6] J.C. Bauwens, C. Bauwens-Crowet, G. Homes, Tensile yield-stress behavior of poly (vinyl chloride) and polycarbonate in the glass transition region, Journal of Polymer Science Part A-2: Polymer Physics, 7 (1969) 1745-1754.
- [7] M. Foster, B. Love, R. Kaste, P. Moy, The Rate Dependent Tensile Response of Polycarbonate and Poly-methylmethacrylate, Journal of Dynamic Behavior of Materials, 1 (2015) 162-175.
- [8] S. Sarva, A.D. Mulliken, M.C. Boyce, Mechanics of Taylor impact testing of polycarbonate, International Journal of Solids and Structures, 44 (2007) 2381-2400.
- [9] S. Fu, Y. Wang, Y. Wang, Tension testing of polycarbonate at high strain rates, Polymer Testing, 28 (2009) 724-729.
- [10] S. Sarva, M. Boyce, Mechanics of polycarbonate during high-rate tension, Journal of Mechanics of Materials and Structures, 2 (2007) 1853-1880.
- [11] S. Tzibula, Z. Lovinger, D. Rittel, Dynamic tension of ductile polymers: Experimentation and modelling, Mechanics of Materials, 123 (2018) 30-42.
- [12] Z. El-Qoubaa, R. Othman, Tensile Behavior of Polyetheretherketone over a Wide Range of Strain Rates, International Journal of Polymer Science, 2015 (2015) 275937.
- [13] N.K. Naik, Y. Perla, Mechanical behaviour of acrylic under high strain rate tensile loading, Polymer Testing, 27 (2008) 504-512.

- [14] Z.N. Yin, T.J. Wang, Deformation response and constitutive modeling of PC, ABS and PC/ABS alloys under impact tensile loading, Materials Science and Engineering: A, 527 (2010) 1461-1468.
- [15] E. Brown, N., P. Rae, J., G. Gray, T., The influence of temperature and strain rate on the tensile and compressive constitutive response of four fluoropolymers, J. Phys. IV France, 134 (2006) 935-940.
- [16] E.N. Brown, P.J. Rae, E.B. Orler, The influence of temperature and strain rate on the constitutive and damage responses of polychlorotrifluoroethylene (PCTFE, Kel-F 81), Polymer, 47 (2006) 7506-7518.
- [17] B. Jiang, L. Cao, F. Zhu, Dynamic tensile behavior of polypropylene with temperature effect, Composites Part B: Engineering, 152 (2018) 300-304.
- [18] M. Zrida, H. Laurent, V. Grolleau, G. Rio, M. Khlif, D. Guines, N. Masmoudi, C. Bradai, High-speed tensile tests on a polypropylene material, Polymer Testing, 29 (2010) 685-692.
- [19] D.A. Şerban, G. Weber, L. Marşavina, V.V. Silberschmidt, W. Hufenbach, Tensile properties of semi-crystalline thermoplastic polymers: Effects of temperature and strain rates, Polymer Testing, 32 (2013) 413-425.
- [20] C.C. Ibeh, Thermoplastic materials: properties, manufacturing methods, and applications, CRC Press, 2011.
- [21] M.C. Tanzi, S. Farè, G. Candiani, Chapter 1 Organization, Structure, and Properties of Materials, in: M.C. Tanzi, S. Farè, G. Candiani (Eds.) Foundations of Biomaterials Engineering, Academic Press, 2019, pp. 3-103.
- [22] J. Jancar, A. Dianselmo, A. Dibenedetto, The yield strength of particulate reinforced thermoplastic composites, Polymer Engineering & Science, 32 (1992) 1394-1399.
- [23] L. Nicolais, L. Nicodemo, The effect of particles shape on tensile properties of glassy thermoplastic composites, International Journal of Polymeric Materials, 3 (1974) 229-243.
- [24] C.L. Wu, M.Q. Zhang, M.Z. Rong, K. Friedrich, Tensile performance improvement of low nanoparticles filled-polypropylene composites, Composites Science and Technology, 62 (2002) 1327-1340.
- [25] Y. Zhou, V. Rangari, H. Mahfuz, S. Jeelani, P. Mallick, Experimental study on thermal and mechanical behavior of polypropylene, talc/polypropylene and polypropylene/clay nanocomposites, Materials Science and Engineering: A, 402 (2005) 109-117.
- [26] J. Johnsen, F. Grytten, O.S. Hopperstad, A.H. Clausen, Influence of strain rate and temperature on the mechanical behaviour of rubber-modified polypropylene and cross-linked polyethylene, Mechanics of Materials, 114 (2017) 40-56.

- [27] A.K. Naskar, J.K. Keum, R.G. Boeman, Polymer matrix nanocomposites for automotive structural components, Nature nanotechnology, 11 (2016) 1026-1030.
- [28] J.-X. Li, J. Wu, C.-M. Chan, Thermoplastic nanocomposites, Polymer, 41 (2000) 6935-6937.
- [29] S. Sathyanarayana, C. Hübner, Thermoplastic Nanocomposites with Carbon Nanotubes, in: J. Njuguna (Ed.) Structural Nanocomposites: Perspectives for Future Applications, Springer Berlin Heidelberg, Berlin, Heidelberg, 2013, pp. 19-60.
- [30] K. Majdzadeh-Ardakani, A.H. Navarchian, F. Sadeghi, Optimization of mechanical properties of thermoplastic starch/clay nanocomposites, Carbohydrate Polymers, 79 (2010) 547-554.
- [31] B. Soltannia, I. Haji Gholami, S. Masajedian, P. Mertiny, D. Sameoto, F. Taheri, Parametric Study of Strain Rate Effects on Nanoparticle-Reinforced Polymer Composites, Journal of Nanomaterials, 2016 (2016) 9841972.
- [32] S. Absar, R. Tandon, H. Choi, Study about the Effect of Addition of Carbon Nanofibers on the Strain-Rate Sensitivity of Thermoplastic Polymer Matrix Nanocomposites Manufactured by Ultrasonic Processing, Procedia Manufacturing, 48 (2020) 400-406.
- [33] S.M. Zebarjad, S.A. Sajjadi, On the strain rate sensitivity of HDPE/CaCO3 nanocomposites, Materials Science and Engineering: A, 475 (2008) 365-367.
- [34] S. Mojtaba Zebarjad, S. Golmakaniyoon, Influence of strain rate on the toughening effect of CaCO3 in polypropylene/CaCO3 composites, Journal of Vinyl and Additive Technology, 19 (2013) 271-275.
- [35] I. Ali, R. Elleithy, Toughness of HDPE/CaCO3 microcomposites prepared from masterbatch by melt blend method, Journal of Applied Polymer Science, 122 (2011) 3303-3315.
- [36] J. Ingram, Y. Zhou, S. Jeelani, T. Lacy, M.F. Horstemeyer, Effect of strain rate on tensile behavior of polypropylene and carbon nanofiber filled polypropylene, Materials Science and Engineering: A, 489 (2008) 99-106.
- [37] S.P. Bao, S.C. Tjong, Mechanical behaviors of polypropylene/carbon nanotube nanocomposites: The effects of loading rate and temperature, Materials Science and Engineering: A, 485 (2008) 508-516.
- [38] Y. Zhou, P.K. Mallick, Effects of temperature and strain rate on the tensile behavior of unfilled and talc-filled polypropylene. Part I: Experiments, Polymer Engineering & Science, 42 (2002) 2449-2460.

- [39] A. Zhang, G. Zhao, J. Gao, Y. Guan, Effect of Acrylonitrile-Butadiene-Styrene High-Rubber Powder and Strain Rate on the Morphology and Mechanical Properties of Acrylonitrile-Butadiene-Styrene/Poly (Methyl Methacrylate) Blends, Polymer-Plastics Technology and Engineering, 49 (2010) 296-304.
- [40] V. Delhaye, A.H. Clausen, F. Moussy, R. Othman, O.S. Hopperstad, Influence of stress state and strain rate on the behaviour of a rubber-particle reinforced polypropylene, International Journal of Impact Engineering, 38 (2011) 208-218.
- [41] X. Xiao, Dynamic tensile testing of plastic materials, Polymer Testing, 27 (2008) 164-178.
- [42] T. George, G. Gray, Classic split-Hopkinson pressure bar testing, ASM Handbook, 8 (2000) 1027-1068.
- [43] U. Lindholm, Some experiments with the split hopkinson pressure bar\*, Journal of the Mechanics and Physics of Solids, 12 (1964) 317-335.
- [44] W. Chen, F. Lu, M. Cheng, Tension and compression tests of two polymers under quasi-static and dynamic loading, Polymer testing, 21 (2002) 113-121.
- [45] N.R.S. Toso, Contribution to the modelling and simulation of aircraft structures impacting on water, (2009).
- [46] S.P.F.C. Jaspers, J.H. Dautzenberg, Material behaviour in metal cutting: strains, strain rates and temperatures in chip formation, Journal of Materials Processing Technology, 121 (2002) 123-135.
- [47] W. Liu, Identification of strainrate dependent hardening sensitivity of metallic sheets under in-plane biaxial loading, in, Rennes, INSA, 2015.
- [48] P. Bastias, S. Kulkarni, K.-Y. Kim, J. Gargas, Noncontacting strain measurements during tensile tests, Experimental mechanics, 36 (1996) 78-83.
- [49] D. Zhu, S.D. Rajan, B. Mobasher, A. Peled, M. Mignolet, Modal Analysis of a Servo-Hydraulic High Speed Machine and its Application to Dynamic Tensile Testing at an Intermediate Strain Rate, Experimental Mechanics, 51 (2011) 1347-1363.
- [50] S.I. Hill, P. Sjöblom, Practical considerations in determining high strain rate material properties, in, SAE Technical Paper, 1998.
- [51] J. Fitoussi, F. Meraghni, Z. Jendli, G. Hug, D. Baptiste, Experimental methodology for high strain-rates tensile behaviour analysis of polymer matrix composites, Composites Science and Technology, 65 (2005) 2174-2188.
- [52] P. Béguelin, M. Barbezat, H. Kausch, Mechanical characterization of polymers and composites with a servohydraulic high-speed tensile tester, Journal de Physique III, 1 (1991) 1867-1880.

- [53] R. Othman, P. Guégan, G. Challita, F. Pasco, D. LeBreton, A modified servo-hydraulic machine for testing at intermediate strain rates, International Journal of Impact Engineering, 36 (2009) 460-467.
- [54] P. Viot, Polymer foams to optimize passive safety structures in helmets, International Journal of Crashworthiness, 12 (2007) 299-310.
- [55] R. Bouix, P. Viot, J.-L. Lataillade, Polypropylene foam behaviour under dynamic loadings: Strain rate, density and microstructure effects, International Journal of Impact Engineering, 36 (2009) 329-342.
- [56] F. Scarpa, L. Ciffo, J. Yates, Dynamic properties of high structural integrity auxetic open cell foam, Smart Materials and Structures, 13 (2003) 49.
- [57] N. Al-Maliky, D. Parry, A freely expanding ring technique for measuring the tensile properties of polymers, Measurement Science and Technology, 7 (1996) 746.
- [58] T. Cloete, S. Oxtoby, A new technique for compression tests at intermediate strain rates: Prototype results, in: Dymat 2009: 9th International Conference on the Mechanical and Physical Behaviour of Materials under Dynamic Loading, 2009, pp. 249-255.
- [59] B. Song, C. Syn, C. Grupido, W. Chen, W.-Y. Lu, A long split Hopkinson pressure bar (LSHPB) for intermediate-rate characterization of soft materials, Experimental mechanics, 48 (2008) 809.
- [60] R. Fernie, N. Warrior, Impact test rigs for high strain rate tensile and compressive testing of composite materials, Strain, 38 (2002) 69-73.
- [61] N. Perogamvros, T. Mitropoulos, G. Lampeas, Drop tower adaptation for medium strain rate tensile testing, Experimental Mechanics, 56 (2016) 419-436.
- [62] N. Perogamvros, G. Lampeas, Experimental investigation of composite lockbolt fastened joints under in-plane low velocity impact, Composites Part A: Applied Science and Manufacturing, 90 (2016) 510-521.
- [63] S. Gurusideswar, R. Velmurugan, N. Gupta, Study of rate dependent behavior of glass/epoxy composites with nanofillers using non-contact strain measurement, International Journal of Impact Engineering, 110 (2017) 324-337.
- [64] S. Gurusideswar, N. Srinivasan, R. Velmurugan, N. Gupta, Tensile response of epoxy and glass/epoxy composites at low and medium strain rate regimes, Procedia engineering, 173 (2017) 686-693.
- [65] J. Achenbach, On harmonic guided waves in elastic cylinders, in: Wave propagation in elastic solids. Applied mathematics and mechanics, North-Holland Publishing Company Amsterdam, 1973, pp. 202-258.

- [66] C.M. Roland, J.N. Twigg, Y. Vu, P.H. Mott, High strain rate mechanical behavior of polyurea, Polymer, 48 (2007) 574-578.
- [67] W.W. Chen, Experimental Methods for Characterizing Dynamic Response of Soft Materials, Journal of Dynamic Behavior of Materials, 2 (2016) 2-14.

# CHAPTER 3 - QUASI-STATIC STRAIN RATE TESTING OF THERMOPLASTIC POLYMERS

## 3.1 Choice of Thermoplastics

Polymers, especially thermoplastics, are extremely strain rate sensitive [1-3]. However, their initial elastic response, the transitioning of this elastic response to viscoplastic behavior with the increasing strain, and the subsequent variation in the maximum stress experienced at different strain rates is dependent upon the inherent morphology (amorphous, semi-crystalline) and the interplay between them [4]. For structural polymer applications in automotive industry, the interest in thermoplastics and their composites has been comparatively lower due to their relatively inferior strength characteristics compared to thermosets [5]. However due to modern advances in molding techniques, accurate residual stress estimations during processing [6] and adaptability to rapid manufacturing, thermoplastics are finding increased utilization in a range of mechanical and structural applications which were typically associated with either metals/alloys or thermosets and their composites [7-9].

Strain rate sensitive response of thermoplastics is essential in developing any type of numerical model. Considering the wide range of structural automotive thermoplastic configurations available in the market, detailed characterization of strain rate response for each of these materials is not feasible. To address this issue, an attempt was made to investigate the strain rate sensitivity of six most commonly used thermoplastics in the automotive sector. The initial aim, was to carry out dynamic tensile characterization of 'select' thermoplastics within the quasi-static regime. The selection of thermoplastics was made such that it was generic enough to include most common structural thermoplastics yet specific enough to create 'performance-bounds' of resulting mechanical properties. These performance bounds were created such that

two <sup>1</sup>(02) thermoplastics were selected in the "high-stiffness / low ductility" regime and two (02) thermoplastics were selected in the "low stiffness/ high ductility regime. Lastly, two (02) thermoplastics in the intermediate stiffness/ductility were selected. The objective was to understand the varying phenomena in each class of thermoplastics as it corresponds to increasing strain rates.

The concept of selecting thermoplastics based on stiffness-ductility 'performance bounds' is shown in Figure 3.1. This was ensured by keeping factors like manufacturing, processing, external conditions, etc., as uniform as possible. The intrinsic morphology (amorphous/semi-crystalline) of the thermoplastic was intentionally kept inconsistent across the three ranges, since the inspiration of material selection was their usage in the automotive industry, and their suitability for various structural, semi-structural and non-structural parts.

Generally, it is difficult to compare a wide range/class of thermoplastics purely in terms of their tensile mechanical properties as there are large variations due to their intrinsic chemical formulations, crystallinity, processing parameters, etc., Nevertheless, since the literature on intermediate strain rate behavior of thermoplastics is limited, one of the objectives of this work is to create a benchmark/starting point for industry / researchers alike in this area.

<sup>&</sup>lt;sup>1</sup> Only one thermoplastic was tested in this range.

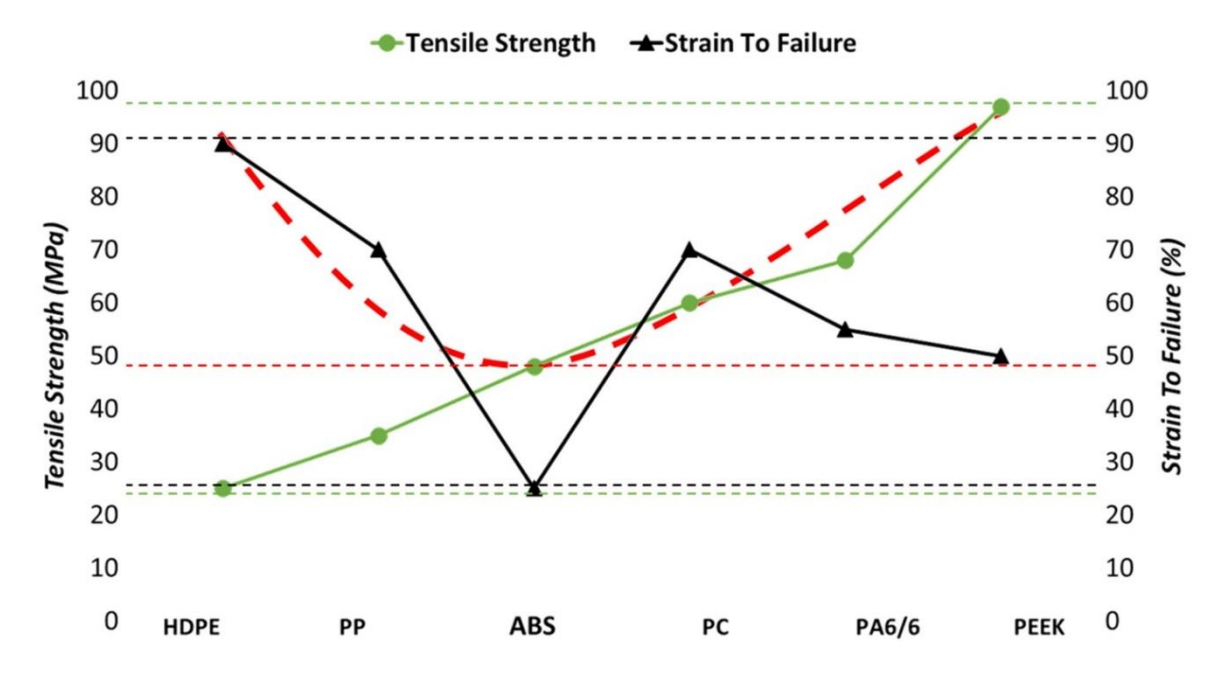


Figure 3.1: Thermoplastic polymers classification on the basis of strength and failure strain. The red dotted line shows the U-Shape characterizing the generic variation of tensile behavior in the selected polymers [10-16]

It is important to note that this initial classification of materials into groups was done based on the generalized quasi-static data available in literature. The actual response of the thermoplastics selected in this study can differ due to a range of reasons, including manufacturing technique, molding/ cutting process etc. Table 3.1 detailing the selected thermoplastics and their applications is given below. The material properties cited in the table are referenced from well-established literature (see Table 3.1) and only represent the quasi-static behavior of these materials. While Polyether Ether Ketone testing was initially planned for this work, it was not tested due to lack of availability of the material within the duration of this work.

# 3.2 Quasi-static Tensile Testing

Quasi-static tensile tests on the five thermoplastic polymers (HDPE, PP, ABS, PC and PA6/6) were conducted in a 100 kN MTS Insight screw driven testing machine at cross-head speeds of 5 mm/min, 50 mm/min, 100 mm/min and 200 mm/min, which correspond to nominal

strain rates of ~ 0.01 s<sup>-1</sup>, 0.1s<sup>-1</sup>, 0.22 s<sup>-1</sup> and 0.44 s<sup>-1</sup>. The nominal strain rates were calculated by dividing the speed with the gage length of the samples. Tensile strength and strain to failure were determined for the samples as per ASTM D638-14. All test specimens conformed to the Type V sample dimensions and were cut from sheet material using water jet cutting. Before testing, all the samples were conditioned in a vacuum oven for 48 hrs. at a temperature of 60°C to remove any residual moisture.

Table 3.1: Thermoplastic Categorization for Low and Intermediate Strain Rate Testing

Range	Polymer	Туре	Tensile Modulus (GPa)	Tensile Strength (MPa)	Failure Strain (%)	Automotive Applications
	High Density Polyethylene (HDPE) [13, 17]	Semi- Crystalline	1	20-30	80-100	Fuel Tank, Water Bottle, Inner Fenders, Fuel Filter Housing
Low	Polypropylene (PP) [10, 17]	Semi- Crystalline	1.2-1.9	30-40	60-80	Battery Case, Cooling fan blades, Heating Ducts, Instruments Panel, Bumper Beam, Interior Console, Splash Shield

Table 3.1 (cont'd)

						Bumpers,
Medium	Acrylonitrile	Amorphous	2.0 -2.2	40-55	15-30	Dashboards, Wheel
	Butadiene					Covers, Radiator
	Styrene (ABS)					Grills, Mirror
	[14, 17]					Housing, Interior
						Consoles
	Polycarbonate	Amorphous	2.6	60	50-110	Head Lamp Lens,
	(PC) [12, 17]					Instrument Panel,
						Bumpers
		Semi- Crystalline	2.8-3.5	60-75	55-70	Engine Covers,
	D-1111					Intake Manifold,
High	Polyamide 6/6					Cooling Fan Blades,
	(PA6/6) [16,					Gears, Bushes, Cams,
	17]					Bearings, Weather
						Proof Coatings
	Polyether	Amorphous	4	97	40-50	Bearings, Pistons,
	Ether Ketone					Pumps, Cable
	(PEEK) [11, 17]					Insulation, Gears

# 3.2.1 High Density Polyethylene (HDPE)

Figure 3.2 shows the stress-strain response of high-density polyethylene (HDPE), a semi-crystalline thermoplastic, in the low stiffness/strength category. For all the crosshead

speeds, the stress-strain response is approximately linear elastic up to the maximum point of ~10MPa. Following that, the strain rate starts dictating the tensile strength and strain-to-failure. As the testing speed increases, an increase in maximum stress and decrease in strain to failure was observed.

# 3.2.2 Polypropylene (PP)

The quasi-static strain rate response of Polypropylene (PP) is shown in Figure 3.3. The initial linear elastic response in this case extends approximately up to 18 MPa. An average reduction of 45 % in the strain-to-failure was observed at the highest cross-head speed corresponding to a strain rate 0.44s<sup>-1</sup>.

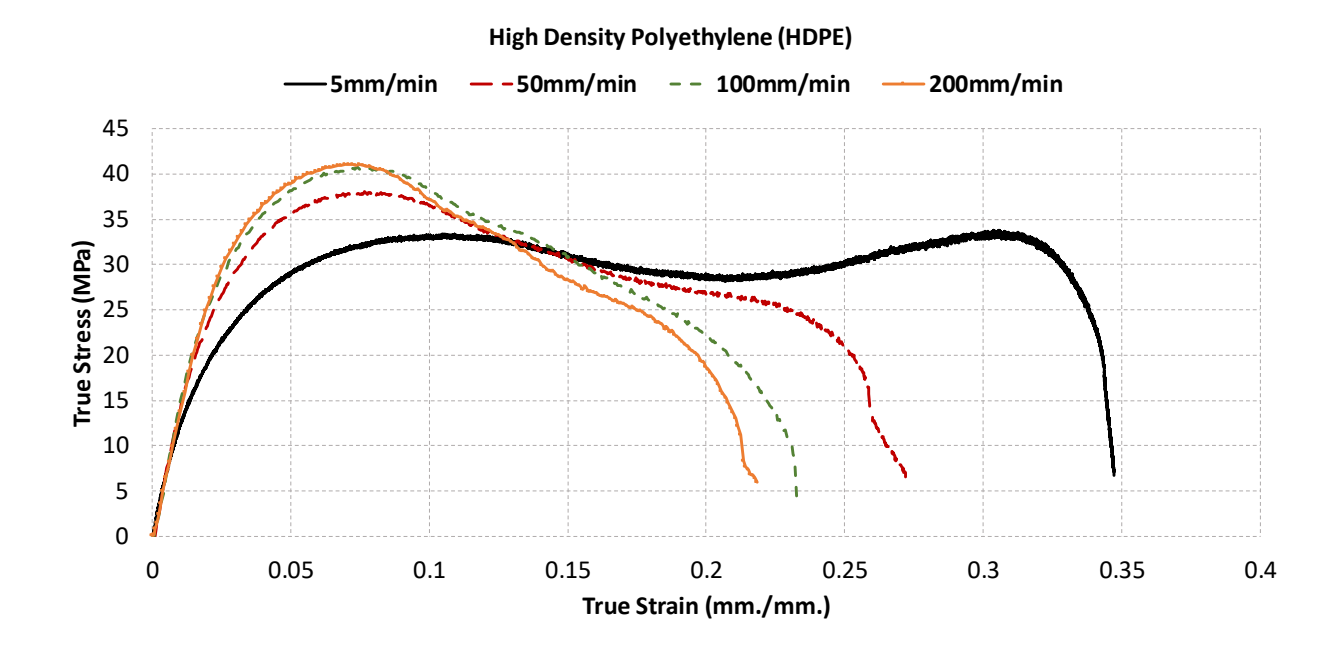


Figure 3.2: Representative True stress strain curves for HDPE at different cross-head speed

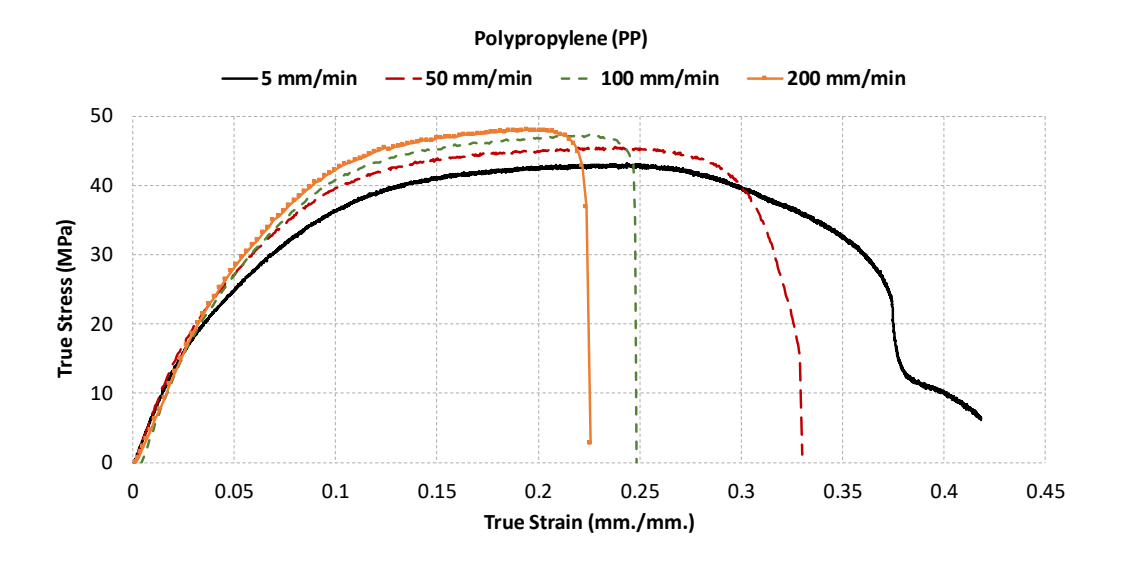


Figure 3.3: Representative True stress strain curves for PP at different cross-head speeds

# 3.2.3 Acrylonitrile Butadiene Styrene (ABS)

There was a distinct increase in the tensile strength and reduction in failure strain as the strain rates increased from 0.01 - 0.44 s<sup>-1</sup> as shown in Figure 3.4. It is pertinent to mention that ABS was selected in the medium strength – medium ductility group. Although the polymer exhibited good strength at higher rates, the percentage elongation was the lowest in comparison to all the other tested polymers.

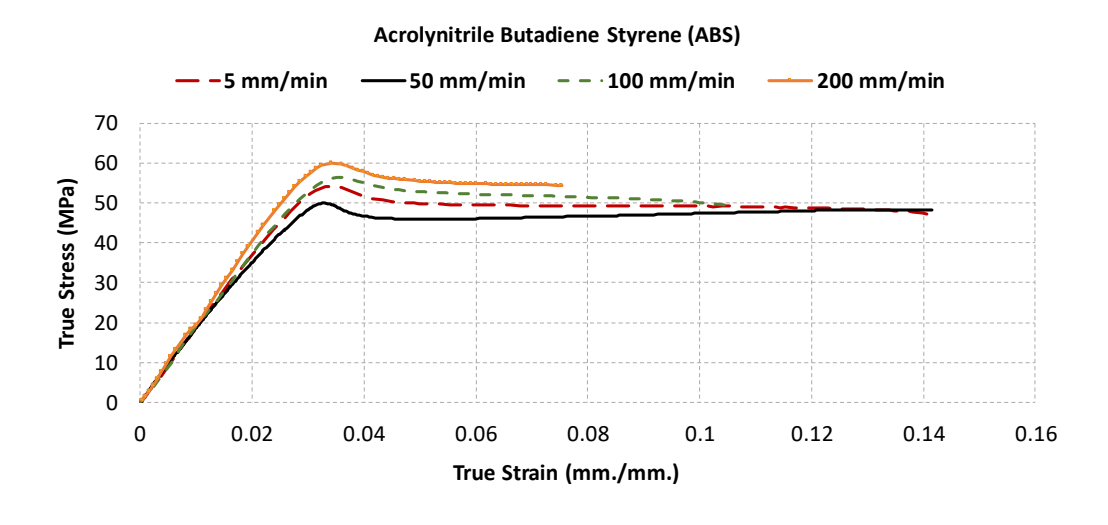


Figure 3.4: Representative True stress strain curves for ABS at different cross-head speeds

# 3.2.4 Polycarbonate (PC)

The strain rate dependent deformation behavior of Polycarbonate (PC), is shown in Figure 3.5. The polymers showed distinctly lesser ductility than HDPE and PP, however the average percentage elongation was ~ 10 % greater than that of ABS. As compared to the range defined in Table 1, the percentage failure strain was significantly lower in the tested samples.

# 3.2.5 Polyamide 6/6 (PA6/6)

Figure 3.6 shows the stress-strain response for Polyamide 6/6 (PA6/6) at different speeds. This thermoplastic polymer has the highest ductility compared to other variants of PA6 which makes it ideal for automotive applications. The stress-strain behavior shows an increasing modulus and strength and decreasing strain with increasing strain rate. An average increment of ~10 % in tensile strength was observed at a strain rate of 0.44s<sup>-1</sup> when compared with the quasi-static value obtained at 0.01s<sup>-1</sup>. Despite being in high strength – low ductility classification, PA (6/6) showed better elongation properties when compared to ABS and PC.

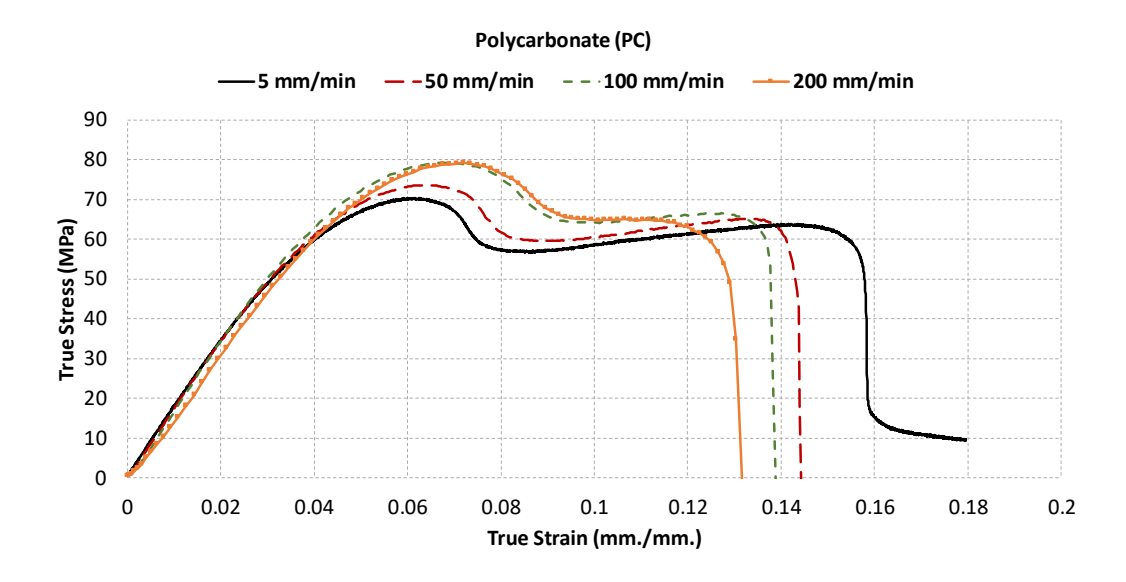


Figure 3.5: Representative True stress strain curves for PC at different cross-head speeds

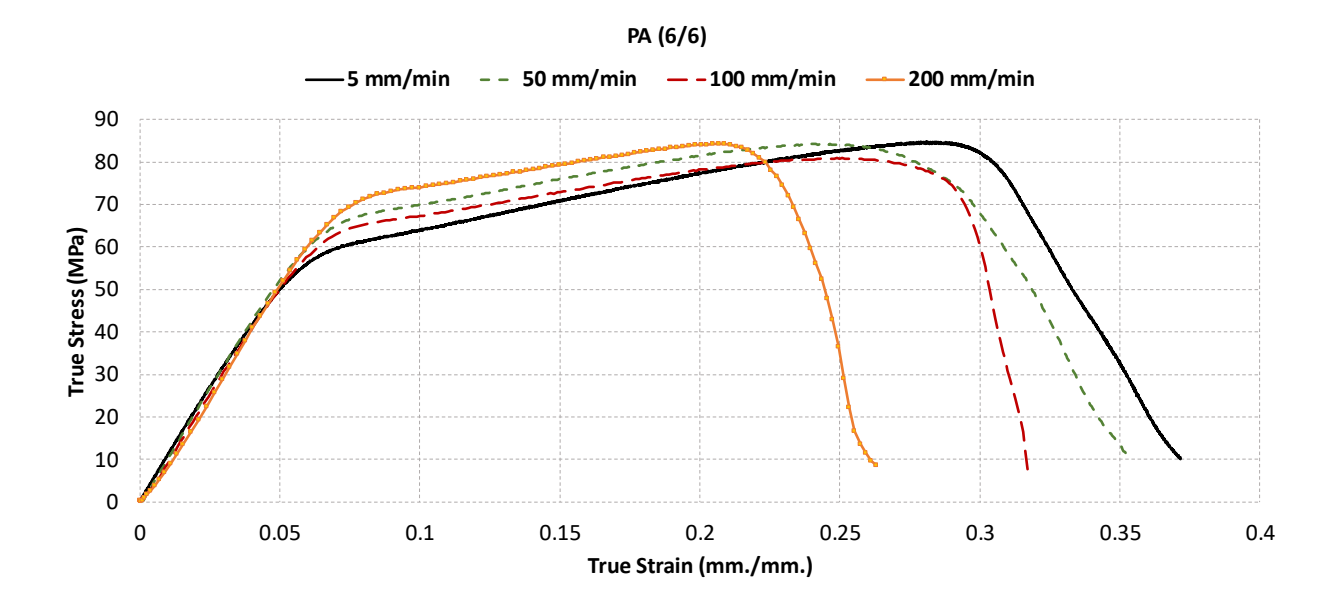


Figure 3.6: Representative True stress strain curves for PA (6/6) at different cross-head speeds

# 3.3 Material Characterization

The variation of the tensile strength versus the log of crosshead speeds is shown in Figure 3.7. As expected the tensile strength of all the tested polymers increased with the increasing cross head speeds. This behavior can be attributed to the strain hardening experienced by the polymers at higher test speeds. The dynamics of the change in molecular mobility due to strain hardening however differ in each polymer due to their unique microstructures. This is reflected by the different percentage increase in strengths for different polymers. For example, the average increase in tensile strength from the lowest to the highest strain rate is approximately 16.5 % in HDPE as compared to just 7.2 % in PA (6/6). The strain-to-failure of selected thermoplastics shows decreasing trend with the increase in strain rate as shown in Figure 3.8. At higher rates of loading, polymers generally display brittle behavior which leads to reduction in elongation to failure, however many other factors including morphology and processing conditions can also have a significant effect on the average percentage of elongation.

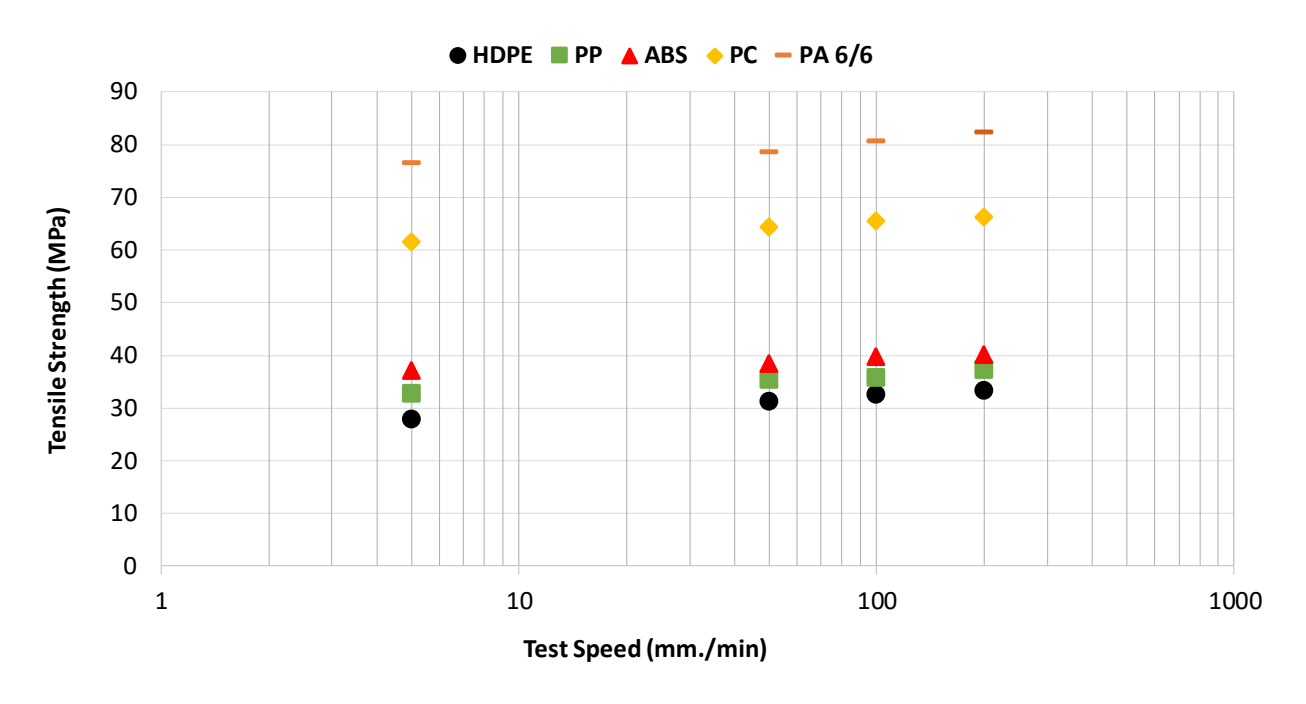


Figure 3.7: Variation of tensile strength for selected thermoplastics with log of crosshead speeds

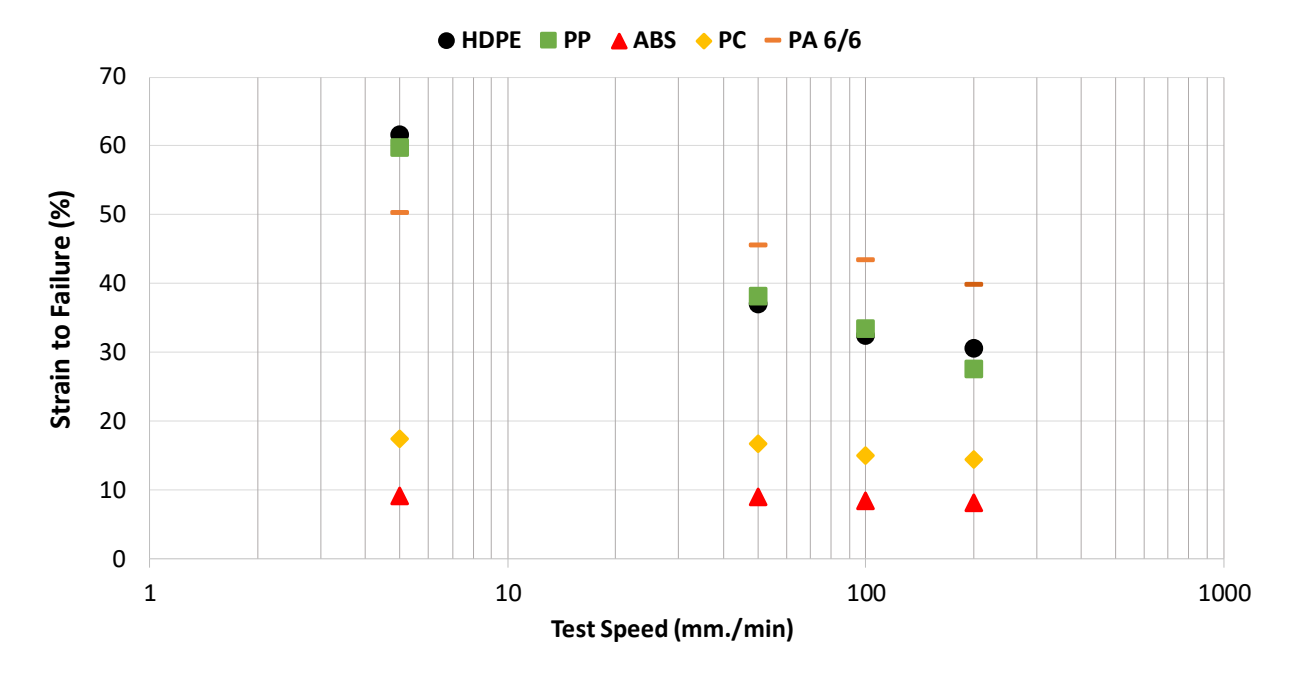


Figure 3.8: Variation in strain-to-failure for selected thermoplastics with log of crosshead speeds

From the experimental observations above, it can be clearly deduced that at higher rates of loading, thermoplastic polymers generally become brittle which leads to an increase in tensile strength and reduction in the failure strain.

# 3.4 Quasi-Static Strain Rate Testing of Nano-particle Reinforced ABS

After a detailed investigation into the effect of increasing quasi-static strain rates on the tensile mechanical response of different polymers, tests were carried out to study the effect of nanoparticle incorporation on the strain rate sensitivity of thermoplastics. In this regard, ABS was chosen due to its superior mechanical properties in impact related scenarios, adaptability to additive manufacturing and ease of processability [18].

ABS is one of the most commonly used thermoplastics in automotive industry [17]. However, despite its excellent impact resistance and energy absorption, the current applicability of ABS in advanced structural applications is restricted by its relatively lower strength and stiffness as compared to semi-crystalline thermoplastics and thermosets [19]. To overcome that challenge, incorporation of particulate reinforcements to enhance the thermal, mechanical, electrical and chemical performance of ABS is a common technique [20-23]. The presence of fillers with different morphologies and their interaction with the matrix also dictates the strain rate behavior and presents an interesting avenue of research. Integration of nanoparticles or fillers into the thermoplastic polymer can be used to tailor the properties and impart multifunctionality to the resulting material. To this end, filler particles with higher specific surface areas allow for a large matrix-particle interface, thereby ensuring a stronger interaction [24] and better enhancement of resulting properties.

Due to the nature of its applications, detailed analysis of the plastic deformation behavior of ABS and its composites at different rates of loading is extremely critical from an engineering

design point of view. Despite that, there are only a limited number of studies which have investigated the effects of strain rates on the mechanical properties of neat ABS, and ABS reinforced by particulate fillers.

One of the earliest investigation into the tensile quasi-static behavior of ABS was performed by Truss et al. [25]. The main aim of this work was to assess the effects of temperature and strain rate on the tensile deformation characteristic of several grades of ABS, differentiated on the basis of rubber content and molecular weight, and to assess the applicability of Eyring rate equation to model the yield stress variation. Strain rates tests were conducted within a range of 10<sup>-4</sup> to 10<sup>-1</sup> s<sup>-1</sup>. Dundar et al. [26] carried out tensile tests at various strain rates ranging from 0.0001 – 0.2 s<sup>-1</sup> on ABS material and observed an increase in tensile stress and strain to failure. In another related work [27], the authors carried out quasi-static testing on ABS in tension, compression and shear and observed an increase in tensile modulus and strength with the increase in deformation rate. They also found that ABS is more strain-sensitive in compression as compared to tension. Lee et al. [28] also observed an increase in tensile strength and modulus with increasing strain rates of ABS samples, however observed that the strain rate dependency of ABS was more pronounced at high strain rates (>10<sup>-3</sup> s<sup>-1</sup>) and in compression.

ABS has become an important cog of the rapidly developing additive manufacturing sector. Gordelier et al. [18] has recently reviewed a number of studies in which ABS has been used as the base material to refine the 3D printing technology and improve the mechanical properties of the printed test materials. Fused Deposition Modelling (FDM) is one of the most common 3D printing techniques and experimental tensile testing of such coupons at different rates has also been the focus of some recent research. Rodriguez [29] carried out an experimental study into the mechanical behavior of fused deposition (FD) ABS, by comparing it with ABS

nano-filaments at different quasi-static strain rates. The tensile tests indicated a generic increase of tensile strength with the increasing strain rate for both type of ABS samples, although the FFD ABS was lower in strength and modulus. Vairis et al. [30] studied the tensile strain rate response of ABS fabricated through FDM at three different test speeds and observed an increase in tensile strength and modulus at higher speeds. Quasi-static tensile response of ABS was also investigated by Owolabi et al. [31], as part of a study to characterize the strain rate sensitivity of the polymer. The authors conducted tensile tests on 3D printed ABS coupons and observed a direct relation between displacement rate and tensile strength. They however did not observe any variation in the tensile modulus. Chevrychinka et al. [32] also studied the mechanical response of 3D printed ABS samples in quasi-static and dynamic regimes and described the rate dependence of ABS strength in terms of incubation time criterion.

The current experimental work is part of a wider investigation into the effect of nanoparticles on the strain rate sensitivity of thermoplastics, at different testing regimes, ranging from quasi-static to high strain rates. For this study, quasi-static strain rate characteristics of neat ABS tensile coupons would be investigated as a baseline at different speeds, followed by tensile testing of similarly shaped ABS samples, reinforced with three different carbon-based nanoparticles (nanofillers). This research is focused on analyzing the effect of different particle reinforcements on the tensile dynamic response of the matrix, including its tensile strength and displacement to failure.

#### 3.5 Experimental Details

#### 3.5.1 Materials & Manufacturing

The polymer was processed using a DSM 15cc mini-extruder. Prior to the extrusion process, the ABS adhesive pellets were oven dried for three (03) hours at 80 °C to remove any

absorbed moisture. In each batch, 10 grams of ABS or ABS/nanoparticle mixture was fed into the DSM extruder barrel, maintained at a temperature of 240 °C (processing temperature of ABS). The ABS/ABS mixture was mixed for three (03) minutes with the help of two (02) contrarotating screws at 100 RPM. The molten polymer was transferred from the barrel into a transfer cylinder (piston) maintained at 240 °C. Using a pneumatic pressure of 100 psi, the polymer was transferred from the piston cylinder into ASTM closed tensile molds to manufacture tensile dogbone samples having consistent dimensions as shown in Figure 3.9 below. The tensile molds are maintained at a constant temperature of 80 °C, which allows the adhesive to cool down and assume the mold shape.

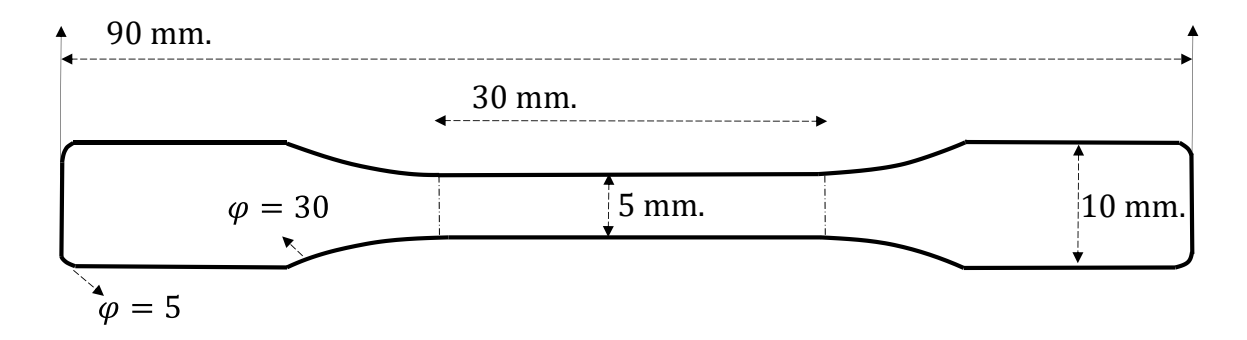


Figure 3.9: Dimensions of the tensile dog-bone sample, thickness 1.5 mm.

## 3.5.2 Nanoparticles – Selection and Particle Concentration

Carbon based nanoparticles, MWCNT's and two different grades of Graphene, have been used in the work. Graphene/CNT's and their derivatives are widely used in polymer composites owing to their inherently outstanding mechanical properties and low density at the nano-scale [33-36]. Most importantly, these nanoparticles have excellent geometric characteristics providing greater potential of high surface interaction with polymers, which is essential for fabrication of high strength polymer composites [37].

Two different grades of Graphene M-5 and C-750, along with a highly dispersible nanotube structure was used in this study. Both grades of Graphene were acquired from XG Sciences [38] whereas the carbon nanotubes were acquired from Cabot [39]. These CNT's had an average surface area of 200 m²/g and a purity of ~ 97 % as compared to 90-93 % carbon percentage in typical nanotubes. Having a surface area of 200 m²/g, these CNT's display better mechanical properties due to lesser entanglement of nanotubes and higher crosslinking between tubes [38]. Graphene nanoparticles, M-5 and C-750, had similar thicknesses, however M-5 with an average diameter of 5μm and surface area of 150 m²/g, is larger as compared to C-750 which has a diameter of 2μm and a surface area of 750 m²/g [39]. All nano-particels were used 'as-is' and were not surface treated or chemically functionalized. The scanning electron microscopy (SEM) images of these nanoparticles are shown in Figure 3.10.

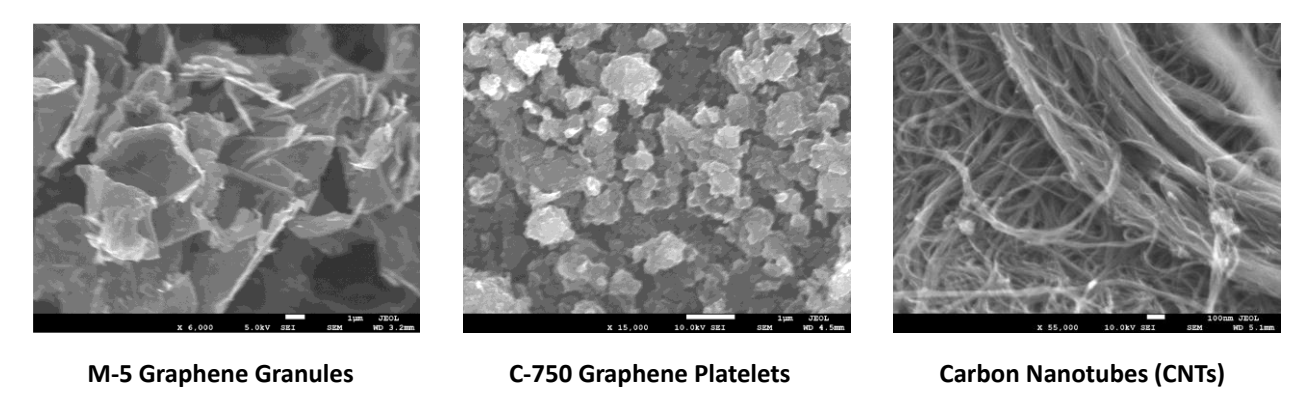


Figure 3.10: SEM micrographs of M-5, C-750 and CNT nanoparticles

Optimization of the filler content is also critical in dictating the mechanical response of a polymer composite. Small concentrations do not provide the required strength or stiffness enhancements, whereas a larger concentration can result in agglomeration of particles which lead to discontinuities, voids and stress concentrations. In this work, the authors have used 1 wt. % nanoparticle concentration in ABS for both graphene grades and the CNT's. This concentration

was selected on the basis of previous research [40] which showed that the mechanical properties of the nanocomposites can be easily processed and characterized at these concentrations. Further, deterioration of mechanical properties can occur when the filler concentration of carbon-based nanoparticles is increased beyond 1wt. %.

# 3.5.3 Mechanical Testing

The tensile tests were carried out using an electromechanical Universal Testing Systems (UTS) machine at three different speeds corresponding to strain rates of 0.001, 0.01 and 0.1 s<sup>-1</sup>. Care was taken to ensure that the tensile coupons experienced uniform strain rates during the deformation process. By recording the applied load (load cell) and resulting displacements (laser extensometer), the corresponding engineering quasi-static stress-strain relationships were established. True stress-strain relations were obtained using the following equations;

$$\varepsilon_T = ln(1 + \varepsilon_E)$$
 Equation 4

$$\sigma_T = \sigma_E (1 + \varepsilon_E)$$
 Equation 5

where  $\epsilon$  and  $\sigma$  represent strain and stress respectively. Subscript 'T' represents true strain/stress while subscript 'E' was used for engineering strains/stress. Before testing, all the samples were conditioned in a vacuum oven for 48 hrs. at a temperature of 60°C to ensure complete moisture removal. The true stress-strain curves were post-processed to obtain the elastic tensile modulus, tensile strength and strain to failure. All the samples were tested at a uniform room temperature of 23 °C.

#### 3.5.4 Scanning Electron Microscopy

Scanning Electron Microscopy (SEM) of tensile coupon cross-sections was carried out to visualize the dispersion of different nanoparticles inside the polymer matrix. As shown in Figure 3.10, the graphene nanoparticles are randomly distributed along the surface of the cross-section,

however the CNT's can be seen protruding from the surface. In this study, chemical functionalization of nanoparticles was not carried out i.e., the particles were mechanically dispersed in the ABS matrix. One of the reason for this approach is that the low concentration of nanoparticles significantly reduces the chances of agglomeration [40].

#### 3.6 Results and Discussions

Tensile coupons made from ABS and its nanocomposites were tested at three different decades of strain rates within the quasi-static range to ensure a thorough examination of the variations observed in the mechanical properties. To ensure uniformity of results, five samples were tested for every material configuration and testing speed. Thus, a total of 60 tensile coupons were tested. It is important to re-iterate that non-functionalized ('as-received') nanoparticles were used in this work.

The deformation behavior of amorphous thermoplastics like ABS has been well documented [41, 42]. When a load is applied, polymer chain segments get stretched and tend to partially rotate and/or slide with respect to each other. With the advancing strain, local clusters of chain segments start overcoming the intermolecular forces and move to new positions. As the stretching and reorientation of the molecular segments occurs, stress tends to increase. Once enough accumulation of these localized effects has taken place, the polymer starts to yield. After this point, there is a significant load drop and the thermoplastic starts to deform without any additional increase in stress. The intermolecular barriers which prevent the chain segment rotation and/or sliding disappear under plastic strain thus making their movement easier. Therefore, upon further loading, there is a decrease in stress and material exhibits structural changes. As the load increases, the molecular chains align themselves in the direction of the load, which makes it difficult for the polymer to undergo further plastic deformation. Thus, the stress

required is increased resulting in strain hardening and the material becomes brittle.

An increase in strain rate, will make the molecular chains stiffer and restrict the initial molecular mobility, which leads to yielding. Thus, the tensile strength of the polymer tends to increase and a reduction in displacement/strain to failure is observed. This time-dependent shift in the mechanical behavior of neat ABS, which changes from rubbery to ductile to brittle over a range of strain rates has been shown in Figure 3.11.

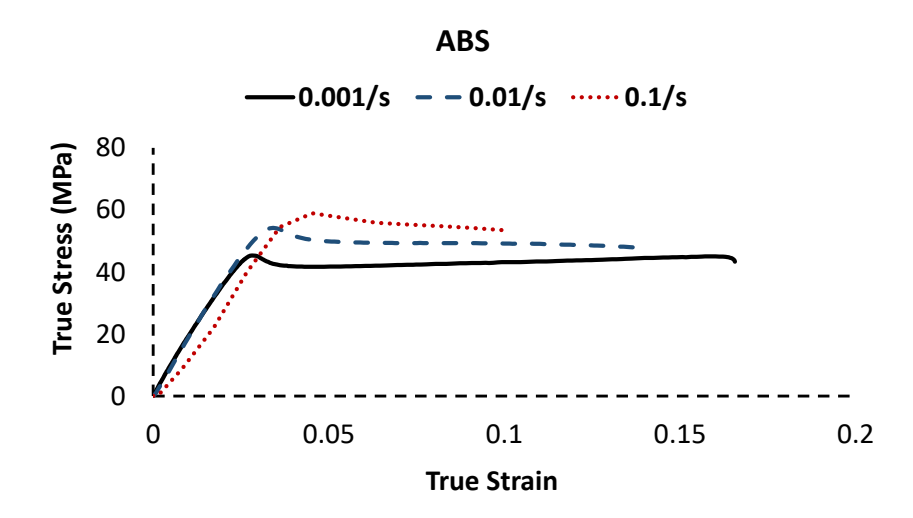


Figure 3.11: Representative curves of neat ABS at three different strain rates

As expected, a distinct increase in the yield strength and tensile strength was observed with the increasing rate of loading as shown in Figure 3.12. However, the strain to failure decreased at higher strain rates. It is also clear form Figure 3.11 that the stress-strain curve at 0.1s<sup>-1</sup> has a relatively shallower and explicitly non-linear slope. This results in a reduction of modulus.

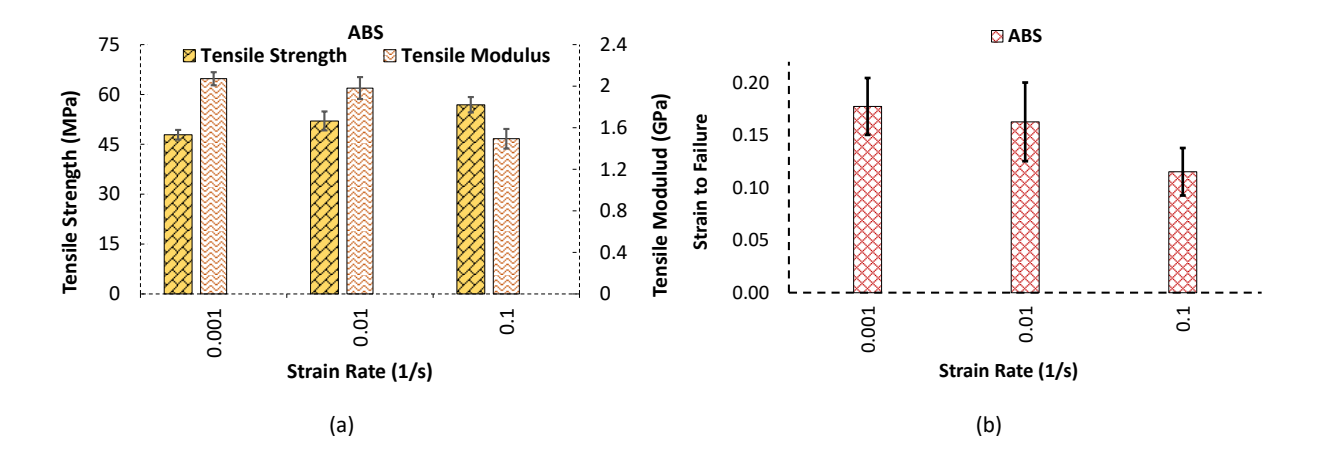


Figure 3.12: (a) Tensile Strength and Modulus of neat ABS at different strain rates (b) Strain to Failure values of neat ABS at different strain rates

The values indicated for the tensile strength, modulus and strain to failure in Figures 3.12 (a) and (b) are an average of all test results along with the standard deviation error.

The representative curves of ABS nanocomposites are shown in Figure 3.13. It is evident that the addition of nanoparticles does not alter the basic amorphous thermoplastic behavior under different rates of loading i.e., there is an increase in tensile strength and decrease in failure strain with increasing strain rate. However, depending upon the rate of loading and morphology of the particle used to reinforce the ABS plastic, the variation in the mechanical response can be controlled. A detailed account on how the three nanoparticles used in this study influence the tensile strength, strain to failure and tensile modulus at different strain rates is provided in the next sections.

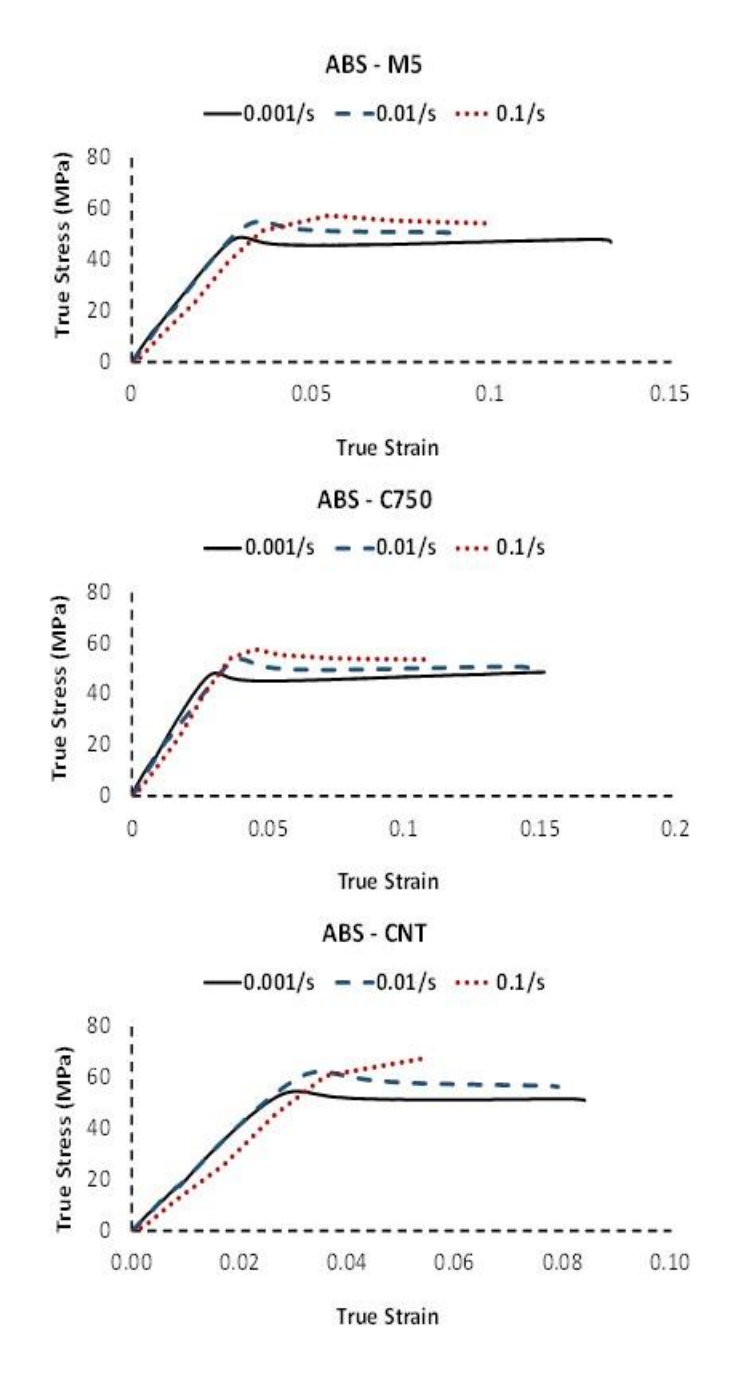


Figure 3.13: Representative curves for ABS nanocomposites

# 3.6.1 Effect of Strain Rate

# 3.6.1.1 Tensile Strength

The graphical comparison of tensile strengths for neat ABS and its nanocomposites is shown in Figure 3.14. There is a distinct increase in tensile strength as the strain rates are

increased from 0.001 to 0.1s<sup>-1</sup>. The average percentage increase for each test material across the two decades of strain rates are shown in Table 3.2.

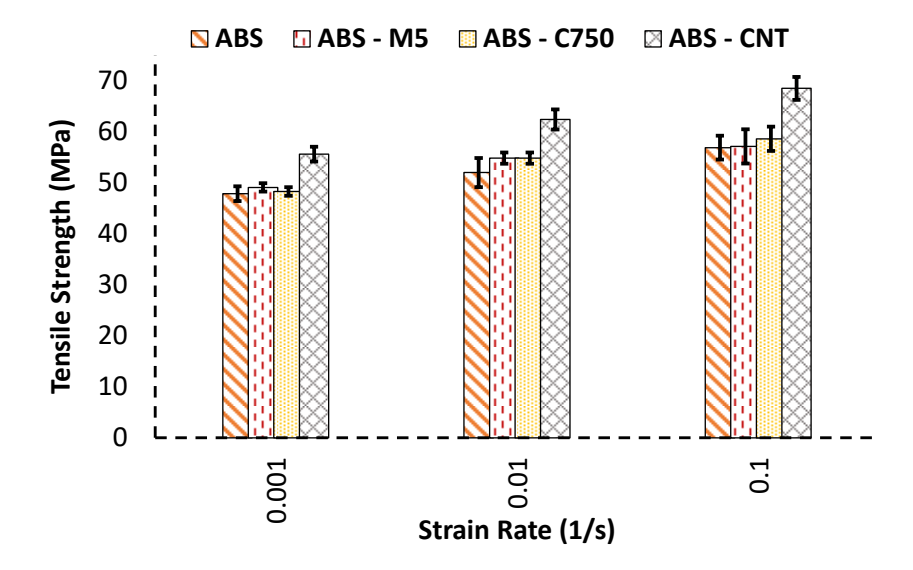


Figure 3.14: Comparison of tensile strength of ABS and ABS nanocomposites at different strain rates

Table 3.2: Average percentage increase in Tensile Strength of ABS/ABS nanocomposites at varying incremental strain rates

	Average Percentage Increases in Tensile Strength						
Material	0.001-0.01s <sup>-1</sup>	0.01-0.1 s <sup>-1</sup>	0.001-0.1 s <sup>-1</sup>				
Neat ABS	7.98	8.57	15.87				
ABS - M5	10.49	4	14.08				
ABS - C750	11.91	6.44	17.58				
ABS - CNT	10.93	8.9	18.86				

The comparison in the table below shows the effect of strain rate on the tensile strength of individual test materials. An inter-material comparison highlighting the effect of nanoparticle morphology would be carried out in section 3.6.2. The highest increase of ~19 % in tensile strength as the strain rates were increased was observed in ABS-CNT nanocomposites, which was only marginally higher than neat ABS and other graphene nanocomposites.

#### 3.6.1.2 Strain to Failure

The strain to failure in the tensile coupons of ABS and its nanocomposites decreased significantly with the increase in strain rate as shown in Figure 3.15. This can be attributed to the increase in strain hardening experienced by the polymer when subjected to higher rates of loading. The addition of nanoparticles to neat ABS further decreases the failure strain, however the individual effect of different nanoparticles is unique and will be discussed later in section 3.6.2. Overall the largest decrease in strain to failure was observed in the ABS-M5 nanocomposites which showed an average decrease of ~50 % in strain to failure across the two decades of strain rate. This average was around 30 % in neat ABS and other nanocomposites.

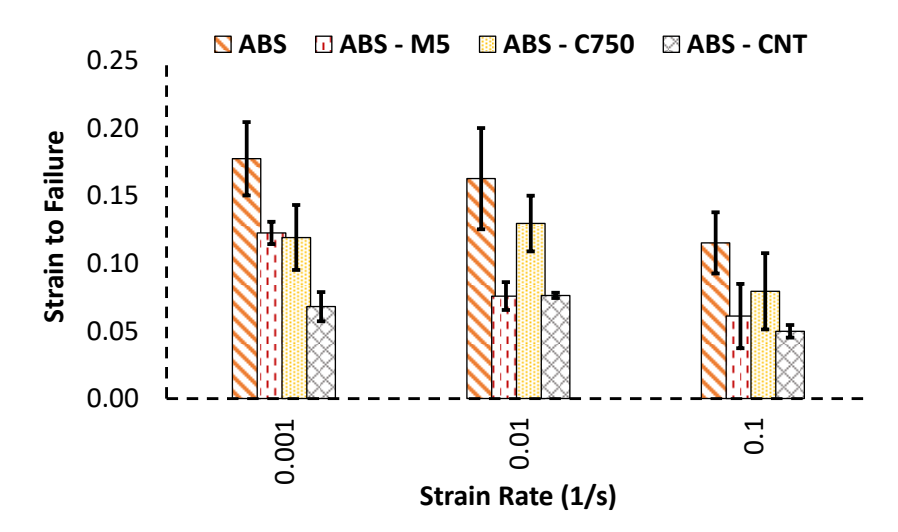


Figure 3.15: Comparison of strain to failure of ABS and ABS nanocomposites at different strain rates

# 3.6.2 Effect of Morphology

The addition of nanoparticles in ABS matrix results in a distinct increase in the tensile strength of polymer as shown in Figure 3.14. Out of the three nanoparticle reinforced ABS samples, the ABS/CNT's showed the highest increase in tensile strength. This behavior can be attributed to their large aspect ratios. The importance of the aspect ratio has been described by

micromechanical models such as Halpin Tsai model [43], Mori-Tanaka model [44] and Shear Lag model [45], which illustrate that higher aspect ratio facilitates better load transfer between the matrix and the particles. When a tensile load is applied on a polymer dog-bone sample, the load is transferred from matrix to the particles through shear stresses generated at the interface, and normal stresses at the particle extremities. Hence, if the particle of higher aspect ratio is used, the interfacial length and the subsequent load bearing capacity of the polymer would also increase. Among the two graphene nanoparticles, M-5 has a larger nanoplatelet size and therefore a higher aspect ratio. At a testing speed of 5mm/min (equivalent to a strain rate of 0.001s<sup>-1</sup>), there is an average increase of ~ 2.5 % in the strength of ABS-M5 nanocomposite relative to a nearly ~1 % increase in the strength of ABS-C750. These average percentage increases in strengths are statistically insignificant and can be considered to be similar to pristine ABS. Nevertheless, at higher rates of loading however, this pattern breaks and the strengths become higher than that of the control/quasi-static strengths.

The significance of the effect of aspect ratio of nanoparticles can be clearly emphasized by analyzing the average percentage increase in tensile strength of ABS-CNT nanocomposites. The rod-shaped CNT's have the highest aspect ratio among the three nanoparticles used in this work, therefore their test coupons show the highest strength at all rates of loading as shown in Figure 3.16. Compared to neat ABS, an average percentage increase of ~ 14, 17 and 19 % was observed in the tensile stiffness values of ABS-CNT nanocomposites at the three strain rates i.e. 0.001, 0.01 and 0.1 s<sup>-1</sup> respectively.

It is important to note that although the effect of particle aspect ratio is significant, it is not the only determining factor in improving the mechanical properties of a nanocomposite.

There are a host of other factors, including the filler strength, specific surface area and chemical

functionalization to enhance bond between particles and the host polymer. A higher filler strength would increase the composite strength, however a strong adhesion between the matrix and the nanoparticle is crucial to achieve it. In case of a weak interfacial adhesion, the load transfer between the particle and the matrix would be insufficient to enhance the particle strength, leading to interfacial debonding. Ultimately, this phenomenon can lead to large stress concentrations, a reduced tensile strength and failure strains.

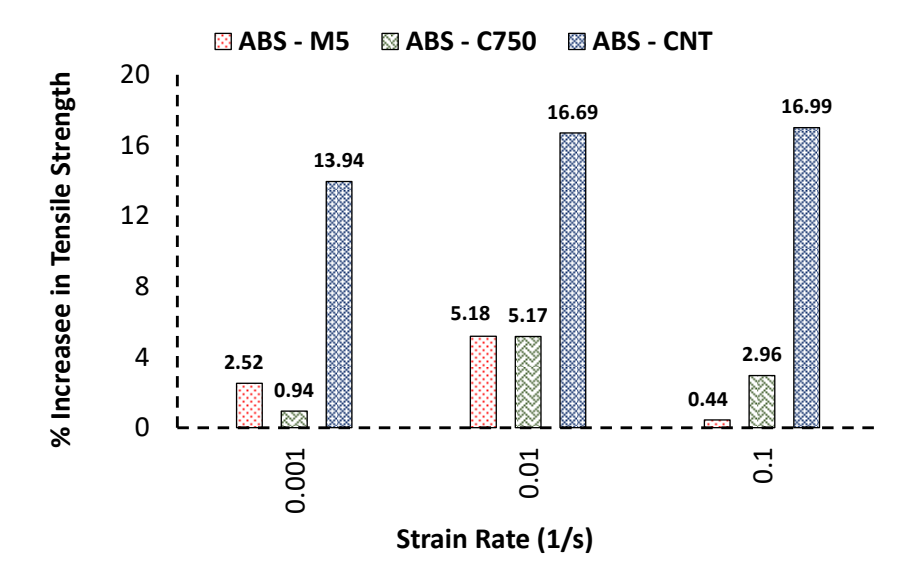


Figure 3.16: Percentage increase in tensile strength of ABS Nanocomposites as compared to neat samples

The adhesion of nanoparticles to matrix can be enhanced by functionalization and incorporation off oxygen functional groups to the surface of the particles. For example, the Graphene C-750 nanoparticles have naturally more oxygen functional groups attached to its surface as compared to M-5 [46]. This leads to a comparatively better interfacial adhesion with the host ABS, as can be seen by the significant increase in strain to failure values of its nanocomposite in Figure 3.15.

The reduction in the strain to failure of the three tested ABS nanocomposites is shown in

Figure 3.17. In all three cases, the overall strain to failure is lesser than what was observed in neat ABS. However, the ABS-C750 nanocomposite shows the lowest reduction in strain to failure. At a loading rate of 0.01s<sup>-1</sup>, the average failure strain of ABS-C-750 nanocomposite sample was only 20 % less relative to neat ABS, however at the same testing speed, there is ~ 53 % reduction in both ABS-M5 and ABS-CNT nanocomposites. Similarly, at 0.1s<sup>-1</sup>, the value of strain to failure in ABS-C750 is approximately 23% and 37 % lower than ABS-M5 and ABS-CNT respectively.

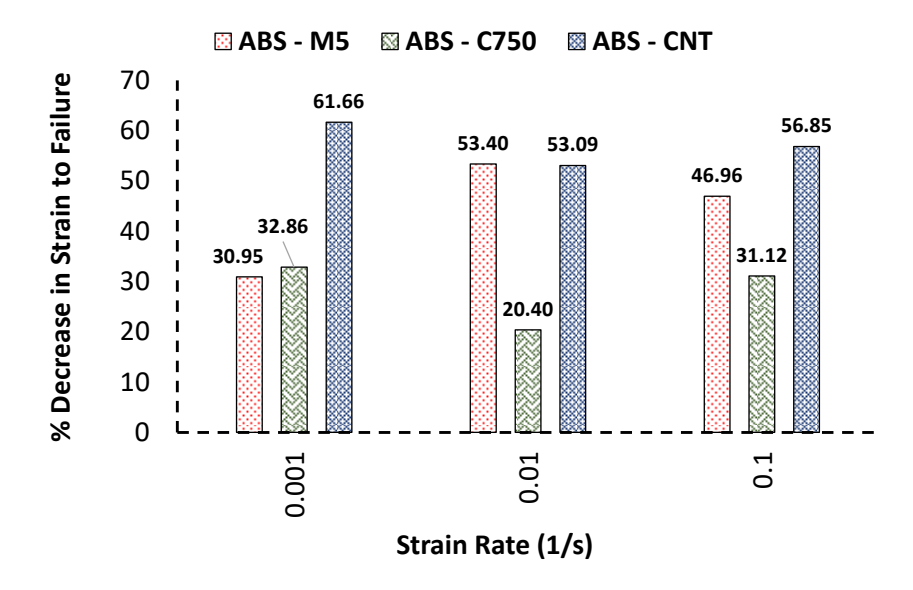


Figure 3.17: %age decrease in strain to failure of ABS Nanocomposites as compared to neat samples

The large specific surface area of C-750 nanoplatelets might also help in explaining this behavior. In general, a large specific surface area is expected to positively affect the mechanical properties of the corresponding nanocomposite, because it increases the bonding/contact area with the host matrix [40]. The C-750 nanoplatelets have by far the highest specific area – C-750  $(750 \text{ m}^2/\text{g}) > \text{CNT} (200 \text{ m}^2/\text{g}) > \text{M-5} (150 \text{ m}^2/\text{g})$  – leading to improved toughness characteristics.

Particle dispersion can also have a significant effect on the strength of the composite. In

any polymer nanocomposite, if the larger dimension of the nanoparticle is aligned in-line with the load direction, there will be a significant improvement in the loading transfer capability from the matrix to the nanoparticle, leading to better strength. In this study however, treatment of nanoparticles to ensure a homogeneous, well-dispersed mixture was not carried out. A major reason for this approach was the low concentration of nanoparticles (1wt. %) which significantly reduces the chances of agglomeration[40]. The loss of stiffness was therefore assumed to be negligible at quasi-static strain rates. Further, unlike typical CNT's which tend to bundle up, the CNTs used in this work consist of a forest of cross-linked branched nanotubes which disperse more easily. Therefore, although no prior treatment was carried out before mixing, enough proportion of nanotubes stay still in-line with the load to significantly increase the stiffness of the ABS-CNT nanocomposite as seen in Figure 3.18 below.

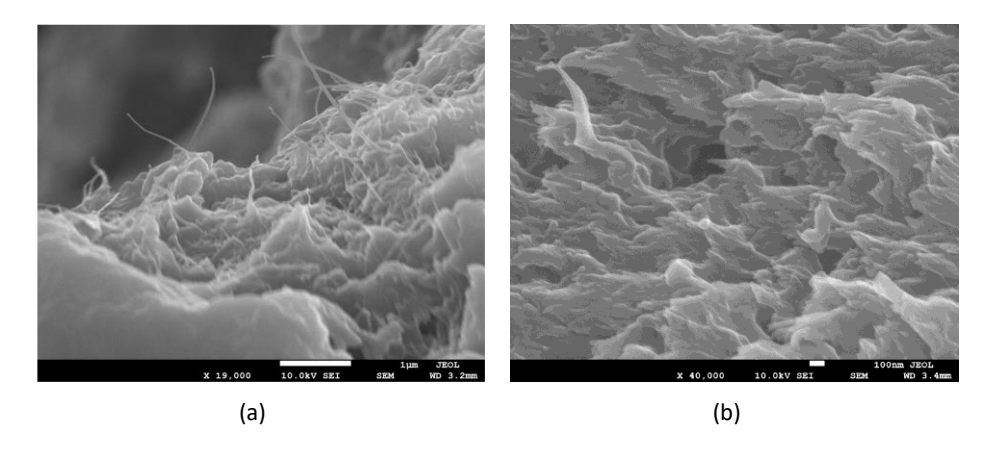


Figure 3.18: SEM images of cross-sectional cut-outs showing fracture surfaces of (a) CNT and (b) C750 nanocomposite tensile coupons

The cutouts shown above also signify the effect of the three-dimensional morphology of the CNTs. In Figure 3.18, cross-sectional cut-outs of ABS-CNT and ABS-C750 tensile coupons were analyzed in a scanning electron microscope (SEM). From Figure 3.18 (a), it was observed that the carbon nanotubes are projecting out of the cross-sectional cutout, whereas in Figure 3.18

(b) which represents ABS-C750 nanocomposites, the surface is relatively plain. These images indicate clearly that the rod-shaped carbon nanotubes basically act like very small load-aligned fibers in the matrix media and therefore lead to an increase in ductility (strain to failure).

#### 3.7 Conclusions

In this chapter, a research goal was formulated to understand the quasi-static response of different classes of thermoplastic polymers ranging from low stiffness - highly ductile plastics to stronger – less/moderate ductile materials. Further, the effect of nanoparticles on the strain rate properties of one select polymer – ABS – by incorporating three different carbon-based nanoparticles. As expected, the tested thermoplastic polymers showed strain rate sensitivity even at quasi-static strain rates. The extent of strain rate sensitivity was unique in each polymer, and as such a correlation in material behavior based on the stiffness-ductility groups could not be established. From the experimental observations it was concluded that at higher rates of loading, thermoplastic polymers become brittle leading to an increase in tensile strength but reduction in the failure strain. The incorporation of 1 wt. % unfunctionalized carbon-based nanoparticles in the ABS matrix led to an increase in its strength, with the highest increases (~17 %) observed in the ABS-CNT nanocomposite. At quasi-static rates of loading, both aspect ratio and surface area were found to be significant in terms of resulting tensile properties. Future work should focus on chemical functionalization of the nanoparticles to fully exploit the benefits offered by these materials. The results presented here create the control/baseline data for the 'as-received' materials and any further improvements will only attract the use of these materials for a wide range of applications.

#### REFERENCES

- [1] D. Goble and E. Wolff, "Strain-rate sensitivity index of thermoplastics," Journal of materials science, vol. 28, pp. 5986-5994, 1993.
- [2] A. Dasari and R. Misra, "On the strain rate sensitivity of high density polyethylene and polypropylenes," Materials Science and Engineering: A, vol. 358, pp. 356-371, 2003.
- [3] S. Walley and J. Field, "Strain rate sensitivity of polymers in compression from low to high rates," DYMAT j, vol. 1, pp. 211-227, 1994.
- [4] J. v. Van Dommelen, D. Parks, M. Boyce, W. Brekelmans, and F. Baaijens, "Micromechanical modeling of the elasto-viscoplastic behavior of semi-crystalline polymers," Journal of the Mechanics and Physics of Solids, vol. 51, pp. 519-541, 2003.
- [5] P. Mallick, "Thermoset—matrix composites for lightweight automotive structures," in Materials, Design and Manufacturing for Lightweight Vehicles, ed: Elsevier, 2010, pp. 208-231.
- [6] S. F. Hassan, S. Kundurthi, S. H. Vattathurvalappil, G. Cloud, and M. Haq, "A hybrid experimental and numerical technique for evaluating residual strains/stresses in bonded lap joints," Composites Part B: Engineering, vol. 225, p. 109216, 2021/11/15/2021.
- [7] J. Kerns, "Replacing metal with plastic," Machine design, vol. 88, pp. 34-42, 2016.
- [8] R. Stewart, "Thermoplastic composites—recyclable and fast to process," Reinforced Plastics, vol. 55, pp. 22-28, 2011.
- [9] R. E. Murray, R. Beach, D. Barnes, D. Snowberg, D. Berry, S. Rooney, et al., "Structural validation of a thermoplastic composite wind turbine blade with comparison to a thermoset composite blade," Renewable Energy, vol. 164, pp. 1100-1107, 2021.
- [10] MakeItFrom.com. (2009-2020). Unfilled PP Homopolymer. Available: https://www.makeitfrom.com/material-properties/Unfilled-PP-Homopolymer
- [11] MakeItFrom.com. (2009-2020). Unfilled PEEK. Available: https://www.makeitfrom.com/material-properties/Unfilled-PEEK
- [12] MakeItFrom.com. (2009-2020). Unfilled PC. Available: https://www.makeitfrom.com/material-properties/Unfilled-PC
- [13] MakeItFrom.com. (2009-2020). Unfilled HDPE. Available: https://www.makeitfrom.com/material-properties/Unfilled-HDPE
- [14] MakeItFrom.com. (2009-2020). Unfilled ABS. Available: https://www.makeitfrom.com/material-properties/Unfilled-ABS

- [15] R. Sreidel Jr and C. Makerov, "The tensile properties of some engineering materials at moderate rates of strain," Univ. of California, Livermore1960.
- [16] MakeItFrom.com. (2009-2020). Dry Unfilled PA 6/6. Available: https://www.makeitfrom.com/material-properties/Dry-Unfilled-PA-6-6
- [17] P. K. Mallick, "5 Thermoplastics and thermoplastic—matrix composites for lightweight automotive structures," in Materials, Design and Manufacturing for Lightweight Vehicles, P. K. Mallick, Ed., ed: Woodhead Publishing, 2010, pp. 174-207.
- [18] T. J. Gordelier, P. R. Thies, L. Turner, and L. Johanning, "Optimising the FDM additive manufacturing process to achieve maximum tensile strength: a state-of-the-art review," Rapid Prototyping Journal, 2019.
- [19] E. ToolBox. (2008). Polymers Physical Properties. Available: https://www.engineeringtoolbox.com/polymer-properties-d\_1222.html
- [20] FastRadius, "An overview of thermoplastic additives," 2021.
- [21] S. H. Vattathurvalappil, "Experimental and Numerical Characterization of Bonded Joints Using Reversible Adhesives," PhD, Civil and Environmental Engineering, Michigan State University, East Lansing, 2020.
- [22] S. H. Vattathurvalappil, S. F. Hassan, and M. Haq, "Healing potential of reversible adhesives in bonded joints," Composites Part B: Engineering, vol. 200, p. 108360, 2020.
- [23] S. H. Vattathurvalappil and M. Haq, "Thermomechanical characterization of Nano-Fe3O4 reinforced thermoplastic adhesives and single lap-joints," Composites Part B: Engineering, vol. 175, p. 107162, 2019.
- [24] S.-Y. Fu, X.-Q. Feng, B. Lauke, and Y.-W. Mai, "Effects of particle size, particle/matrix interface adhesion and particle loading on mechanical properties of particulate—polymer composites," Composites Part B: Engineering, vol. 39, pp. 933-961, 2008/09/01/2008.
- [25] R. Truss and G. Chadwick, "Tensile deformation behaviour of ABS polymers," Journal of Materials Science, vol. 11, pp. 111-117, 1976.
- [26] M. A. Dundar and G. S. Dhaliwal, "Investigation for impact behavior of acrylonitrile-butadiene-styrene amorphous thermoplastic," Polymer Testing, vol. 89, p. 106624, 2020.
- [27] M. A. Dundar, G. S. Dhaliwal, E. Ayorinde, and M. Al-Zubi, "Tensile, compression, and flexural characteristics of acrylonitrile—butadiene—styrene at low strain rates: Experimental and numerical investigation," Polymers and Polymer Composites, p. 0967391120916619, 2020.
- [28] W.-s. Lee and H.-L. Lin, "The Strain Rate Dependence of Deformation and Fracture Behaviour of Acrylonitrile-Butadiene-Styrene (Abs) Copolymer in Impact Test," in European Structural Integrity Society. vol. 32, ed: Elsevier, 2003, pp. 231-240.

- [29] J. F. Rodríguez, J. P. Thomas, and J. E. Renaud, "Mechanical behavior of acrylonitrile butadiene styrene (ABS) fused deposition materials. Experimental investigation," Rapid Prototyping Journal, 2001.
- [30] A. Vairis, M. Petousis, N. Vidakis, and K. Savvakis, "On the strain rate sensitivity of abs and abs plus fused deposition modeling parts," Journal of Materials Engineering and Performance, vol. 25, pp. 3558-3565, 2016.
- [31] G. Owolabi, A. Peterson, E. Habtour, J. Riddick, M. Coatney, A. Olasumboye, et al., "Dynamic response of acrylonitrile butadiene styrene under impact loading," International Journal of Mechanical and Materials Engineering, vol. 11, pp. 1-8, 2016.
- [32] A. Chevrychkina, A. Evstifeev, and G. Volkov, "Analysis of the Strength Characteristics of Acrylonitrile–Butadiene–Styrene Plastic under Dynamic Loading," Technical Physics, vol. 63, pp. 381-384, 2018.
- [33] Y. Wang, H. Mi, Q. Zheng, Z. Ma, and S. Gong, "Flexible infrared responsive multi-walled carbon nanotube/form-stable phase change material nanocomposites," ACS applied materials & interfaces, vol. 7, pp. 21602-21609, 2015.
- [34] X. Yu, W. Zhang, P. Zhang, and Z. Su, "Fabrication technologies and sensing applications of graphene-based composite films: advances and challenges," Biosensors and Bioelectronics, vol. 89, pp. 72-84, 2017.
- [35] R. K. Poduval, S. Noimark, R. J. Colchester, T. J. Macdonald, I. P. Parkin, A. E. Desjardins, et al., "Optical fiber ultrasound transmitter with electrospun carbon nanotube-polymer composite," Applied physics letters, vol. 110, p. 223701, 2017.
- [36] Z. Spitalsky, D. Tasis, K. Papagelis, and C. Galiotis, "Carbon nanotube–polymer composites: chemistry, processing, mechanical and electrical properties," Progress in polymer science, vol. 35, pp. 357-401, 2010.
- [37] H. Abbasi, M. Antunes, and J. I. Velasco, "Recent advances in carbon-based polymer nanocomposites for electromagnetic interference shielding," Progress in Materials Science, vol. 103, pp. 319-373, 2019.
- [38] Carbon Nanostructures | Cabot Corporation. Available: cabotcorp.com/solutions/product-plus/advanced-carbons/carbon-nanostructures
- [39] XG Sciences Our Proprietary xGnP Graphene Formulas. Available: xgsciences.com/graphene/
- [40] M. Oh, W. D. Kim, M. Zhang, T. Kim, D. Yoo, S. H. Kim, et al., "Mechanical behavior of ABS plastic-matrix nanocomposites with three different carbon-based nanofillers," Polymer Bulletin, vol. 78, pp. 3751-3762, 2021/07/01 2021.

- [41] A. D. Mulliken and M. C. Boyce, "Mechanics of the rate-dependent elastic—plastic deformation of glassy polymers from low to high strain rates," International Journal of Solids and Structures, vol. 43, pp. 1331-1356, 2006/03/01/2006.
- [42] D. Garcia-Gonzalez, A. Rusinek, A. Bendarma, R. Bernier, M. Klosak, and S. Bahi, "Material and structural behaviour of PMMA from low temperatures to over the glass transition: Quasi-static and dynamic loading," Polymer Testing, vol. 81, p. 106263, 2020/01/01/2020.
- [43] J. Halpin, "Stiffness and expansion estimates for oriented short fiber composites," Journal of composite materials, vol. 3, pp. 732-734, 1969.
- [44] T. Mori and K. Tanaka, "Average stress in matrix and average elastic energy of materials with misfitting inclusions," Acta metallurgica, vol. 21, pp. 571-574, 1973.
- [45] X.-L. Gao and K. Li, "A shear-lag model for carbon nanotube-reinforced polymer composites," International Journal of Solids and Structures, vol. 42, pp. 1649-1667, 2005.
- [46] F. Wang, L. T. Drzal, Y. Qin, and Z. Huang, "Mechanical properties and thermal conductivity of graphene nanoplatelet/epoxy composites," Journal of materials science, vol. 50, pp. 1082-1093, 2015.

#### CHAPTER 4 - DESIGN AND VERIFICATION OF THE TEST FIXTURE

Dynamic testing is essential for performance prediction and failure analysis of materials at both component and structural scales. It is an important material characterization tool and can help design engineers understand and predict the mechanical response of different materials at automotive crash speeds. The automotive industry uses a tremendous number of materials to build vehicles, including steel, aluminum, rubber, glass, plastics, etc., Depending upon their microstructure and morphology, these materials can exhibit unique responses at crash speeds which typically introduce strain rates ranging between 10° up to 10° s-1, commonly referred to as the intermediate strain rates [1].

To establish a precise correlation between the rate of loading (strain rate), microstructure of the test object, ambient temperature, pressure and a range of other factors [2-4] that can affect the overall material response at intermediate strain rates, a vast data of repeatable and reliable experimental results is required. To this end, experimental data for quasi-static rates of loading (<10<sup>1</sup>) and high strain rate loading (>10<sup>3</sup>) of metals, polymers and composites is readily available in literature [5-11]. However, strain rates ranging from 10<sup>0</sup> - 10<sup>2</sup> require challenging testing protocols [5, 12]. Testing at intermediate strain rates is affected by a number of factors like ringing, inertia, stress wave propagation, sample preload and stable load rising. A detailed explanation of these aforementioned factors was provided in Chapter 2. These factors severely affect the accuracy of response and render conventional high-speed testing setups like high rate servo-hydraulic machines and split Hopkinson bar unreliable. The issues become more pronounced in case of polymers, especially thermoplastics, which tend to experience large deformations before material failure leading to ineffective propagation of stress waves.

The unavailability of reliable experimental data in the intermediate strain rate testing range has also led to the lack of high-fidelity strain rate sensitive material model development for numerical analysis. This glaring information gap, despite the critical nature of in-use and potential applications, has eventually forced researchers to focus on the design and use of special instruments.

Specialized testing techniques used to test materials at intermediate strain rates basically fall under four categories, high rate servo hydraulic machines, modified high rate apparatus, drop weight towers and hybrid testing platforms. These test devices are classified on the basis of how load is applied to the test sample. In the section below, a brief overview of the various testing devices which have been used to bridge the data gap between low and high-speed strain rate testing are provided.

High rate servo hydraulic machines have developed the reputation of an industrial standard for intermediate strain rate testing of materials including polymers and composites. These machines employ the operational blueprint of conventional servo hydraulic machines, i.e. fixing the sample via an upper grip and introducing the dynamic load via the lower grip. A slack adapter module is incorporated at the lower grip to eliminate the inertia of the lower grip and the actuating system. The slack adapter mechanism allows the lower grip to get activated at the specified velocity, however the sudden engagement of the upper grip causes system oscillations which can lead to ringing and a distorted output from the load cell. These distortions can be eliminated using filtration techniques. However, in doing so, the signal accuracy is compromised. There are a number of studies which have employed high rate servo hydraulic machines to test metals and polymers [13-25].

The inherent drawbacks and the high costs associated with high rate servo hydraulic testing machines have necessitated the inception of innovative test apparatuses, depending on the type of material and the property to be determined. There are some studies which have used the classical drop tower concepts to test metals and composites at intermediate strain rates [24, 26-32]. These test apparatuses traditionally comprise two frames - a fixed frame connected to the upper grip and the load cell and a movable frame connected to the lower grip. Their working principle depends on the ability to transform the compression loading of a drop tower machine into tension loading on the specimen. A schematic of a typical drop tower apparatus is shown in Figure 4.1.

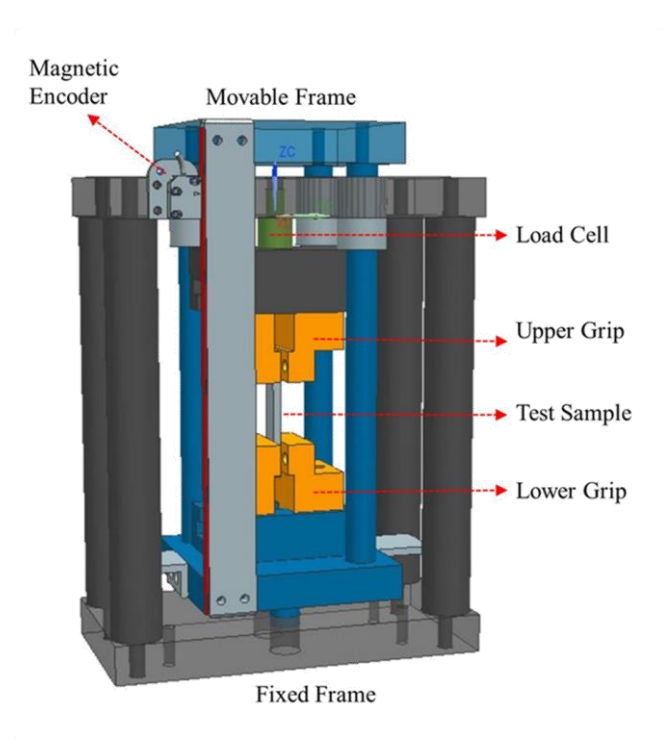


Figure 4.1: A typical schematic of a Drop Tower Apparatus

The force measurements are generally carried out using a strain gauge or piezoelectric load cell whereas the strain measurements can be performed either by using indirect methods like magnetic encoder and Linear Variable Differential Transformer (LVDT) or non-contact

techniques like Digital Image Correlation (DIC). Drop tower apparatuses also present some significant drawbacks which affect the data acquisition. These issues range from system/sample dimensions and alignment to more critical factors like system inertia, ringing, and stable impact duration and system symmetry.

Hybrid test apparatuses, combining either servo hydraulic concept with a split Hopkinson bar [33, 34], drop tower apparatuses with split Hopkinson bar [35], serpentine systems [36, 37] and specially instrumented servo-hydraulic load frames [38] have also been used to test specimens at intermediate strain rates with some success. Additionally some works have used the fly-wheel test apparatus to evaluate intermediate and high strain rate responses of different materials [39, 40].

There are a number of design drawbacks associated most in-use intermediate strain rate fixtures, which can compromise the reliability and repeatability of its output response. The most critical drawback is the lack of homogenous strain field along the sample gage length. In almost all text fixtures used for intermediate strain rate testing of materials, the sample is loaded from one end only. This necessitates the passage of enough stress waves through the gage length of the sample to ensure a quasi-homogenous strain field. High rate servo hydraulic machines and most test apparatuses use a slack adapter to ensure a stable impact duration, however there is no such mechanism in place in traditional drop tower machines. Ringing is also a very important issue and occurs when the natural oscillations of the test fixture coincide with the frequency of the load measuring device. This results in high amplitude stress waves in the output and a significantly distorted data. In high rate servo hydraulic machines, the issue of ringing becomes critical, especially at strain rates greater than 50 s<sup>-1</sup> [12].

Inertia of the test fixture is another critical phenomenon that can affect the validity of the measured output. Under dynamic load at constant temperature and pressure, the deformation flow of any test material is a function of both strain rates and inertia. If the inertia of the system is high, the output load response of the material would also reflect the superimposed effect of the inertia. To ensure that the inertial effects do not compromise the reliability of the output load signal, it is critical to either overcome/minimize the effects of inertia or have a provision to apply an inertia correction to the stress-strain curves. With regards to inertial correction, most in-use test fixtures require the sample to be installed for test calibrations and do not have the provision of testing the system response without the sample. It therefore becomes impossible to subtract the test system inertia from the output response. These fixtures generally use special instruments like slack adaptor to control the inertia of the lower grip and the actuator.

Another major drawback, especially associated with drop tower and other open loop intermediate strain rate test fixtures is the preload on the sample. The design blueprint of these apparatuses causes a preload on the test sample, equivalent to the weight of the movable carriage, the gripping assembly and the associated components. When testing softer metal alloys and plastics this can result in pre-deformation.

To address these challenges, an innovative drop weight apparatus with a unique testing blueprint for tensile testing in intermediate strain rates was conceptualized. The test fixture was developed in-house at the composite vehicle research lab (CVRC) at MSU. The working principle of this symmetric double acting drop weight test fixture was inspired from literature [41].

# 4.1 Fixture Design

The working principle of the designed fixture utilizes the compressive force of vertical impact and bifurcates it into two equal horizontal forces on both sides of the test sample. This was achieved by using a cable and pulley mechanism in conjunction with an innovative lightweight gripping system. The operational layout of the fixture and its main components are shown in Figure 4.2.



Figure 4.2: Basic layout of the newly developed symmetric double-acting tensile test fixture for intermediate strain rate testing

### **4.1.1** Hammer Mechanism

The hammer mechanism comprises of a stack carriage capable of moving freely on two sturdy vertical rods. Bush bearings were used on either ends of the carriage to ensure a uniform inline motion. These provisions add the flexibility of changing the impact force simply by changing the height of impact. The impact force can also be controlled by adding or removing specially designed weights to the stack carrier. The carriage can be moved and secured at any position along the vertical rods using an electric winch. As the system is operated, the stack carriage slides freely on the vertical rods, before striking the impact bar. The weight of the stack carriage (without any additional weight) was 58 lbs.

# 4.1.2 Impact Bar

Impact bar takes the impact of the hammer mechanism and transfers it to the test samples via the cable and pulley system. The entire surface of the stack carriage and the impact bar do not come into contact. The ends of the impact bar were protruded on both sides to absorb the impact of the carriage as it freely falls downward. The protruded ends of the impact bar were protected by polyethylene plugs and rubber dampers as shown in Figure 4.3. This was intentionally done to eliminate metal-to-metal contact, dampen the system and reduce vibration.

## 4.1.3 Electromagnets

The impact bar was suspended using two solenoid lift holding electromagnets having a rated voltage of 12V DC and a lifting capacity of 200kg / 2000N. The electromagnets were powered by two independent DC power supplies. Upon connection with the power source, these electromagnets become active and create a magnetic field. The shell of the electromagnet was made of pure iron to reduce magnetic remanence after power failure. The electromagnets were used for non-contact suspension of the 52 lbs. impact bar. The placement of these magnets is

critical to the overall operation of the test fixture. They were housed in specially designed fixtures that can slide up and down the side rails of the fixture as shown in Figure 4.4. The tension in the cables can be adjusted by sliding the electromagnetic housing vertically (up and down).



Figure 4.3: Impact bar architecture

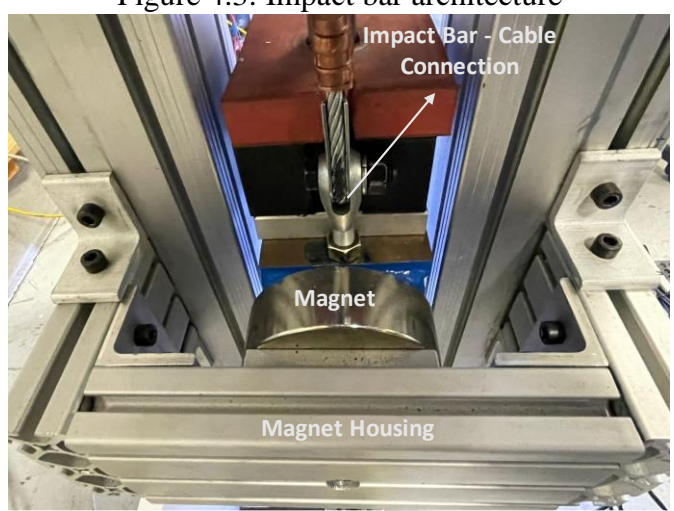


Figure 4.4: Electromagnet Housing

# 4.1.4 Optical Laser Triggered Data Acquisition System

The release mechanism of the impact bar was controlled by an optical laser as shown in Figure 4.3. As soon as the stack carriage passes the laser, the electromagnets are deactivated. The position of the laser pass requires careful and extensive calibration to ensure that the electromagnets deactivate at the exact same time a surface-to-surface contact initiates between the carriage and the impact bar. This allows for a seamless and resistance free vertical impact force to be imparted to the cable and pulley system.

The optical laser also acts as a trigger to activate the data acquisition system. The force data acquisition was carried out using two inline load cells placed directly behind the test sample grips. The placement of the load cells is critical to ensure that the exact load of the specimen is recorded on both sides and the output response is not affected by the reaction forces generated due to impact. The inline load cells are full-bridge strain gauge devices with a maximum capacity of 44 KN in tension/compression. The sensors were connected to analog amplifiers for in-line amplification with mV/V range output. The amplifiers had a maximum bandwidth of 25 kHz. A high rate analog-to-digital converter (ADC) was used to process the load signal, with the final output extracted by using a user-defined code in C-Sharp.

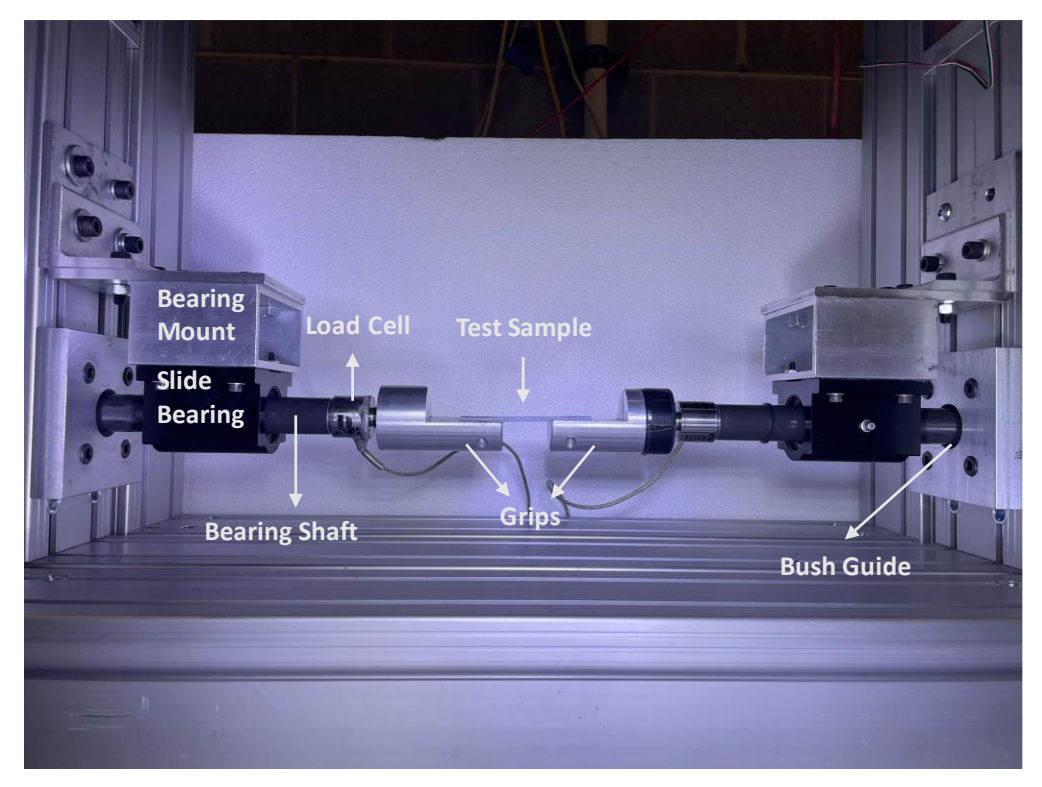
The displacement/strain measurements were carried out using a non-contact Digital Image Correlation (DIC) technique [42, 43]. To test the samples, a stochastic pattern was applied to the surface of the sample using an aerosol spray. A high-speed camera was used to track the motion of these speckled markers. Only a single camera was used to record the data in 2D, since the tests were purely tensile. The images were then processed using a special-use software to extract the full displacement and strain contours of the dog bone sample as it undergoes deformation at intermediate strain rates.

## 4.1.5 Cable and Pulley Assembly

The test fixture employed a system having a total of 04 pulleys and 02 stainless steel cable rope slings with crimpled and reinforced thimble eyes. A basic overview of the cable and pulley assembly was shown in Figure 4.2. The rope sling with a diameter of 0.25" was connected to the impactor bar at one end and the gripping assembly on the other. In between, it passed through two pulleys. The tightness of the cable was controlled via the motion of the electromagnetic housing. It is critical that the cables are carefully adjusted such that the tension in cables is just enough to keep them taut without exerting any significant preload on the sample. If there is a slack in the cable, the initial part of the exerted impact force would be wasted in tensioning the system. This would result in an unstable impact velocity and non-homogenous strain field in the gage length of the sample.

# 4.1.6 Gripping Assembly

It is important to note that the newly developed fixture can be tested with and without the sample, which allows for correction of inertial superimposition into the dynamic response of the sample. For the designed test fixture, the only inertia important to the output response of the load cells is that of the gripping assembly. To minimize that effect, the assembly was designed to be extremely lightweight. The gripping system for the test fixture comprised of six components as shown in Figure 4.5.



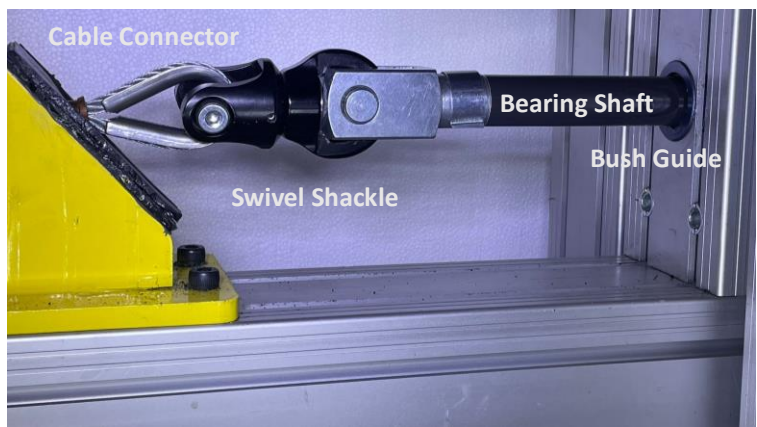


Figure 4.5: Gripping Assembly

# 4.1.7 Twist bearing

The cable passing through the pulleys connects to the gripping assembly via twist bearings. These bearings are basically high capacity swivel shackles with sealed ball bearings and high strength stainless axles. The shackles have a maximum load rating of 36 kN, and isolate the gripping mechanism from any twist induced due to the cable weave. This ensures that the

sample test conditions are purely tensile. Further, these shackles were made of high strength aluminum and were extremely light weight (0.3 lbs.) which is critical for minimizing the inertial effects.

# 4.1.8 Bearing shaft

The bearing shaft connects the swivel shackles to the slide bearing via a bearing bush block. These shafts were made of high strength aluminum alloy and have female threads on both sides. The shaft is hollow and has total weight of 0.54 lbs. The size of these shafts can be adjusted to accommodate test samples of different linear dimensions.

# 4.1.9 Bearing bush block

Two bearing bushes were installed in the main structure of the test fixture to ensure that the bearing shafts can pass through them without any friction and play. The bush block had an internal diameter of 25 mm. and an anodized aluminum housing. The sliding surface of the block was made of highly wear resistant and high-performance plastic. The block was flanged into the main structure of the test fixture.

#### 4.1.10 Slide bearings

After going through the bush block, the bearing shaft passes through a high speed mounted linear sleeve bearing. The slide bearings were installed to eliminate the possibility of bending leading to mode-I failure of the test sample due to a possible play at the interface of the bearing shaft and the bush block. Despite the tight tolerances, the shaft-bush interface rotation cannot be completely eliminated to ensure a frictionless sliding motion. The subsequent deflection was however arrested using high-speed sleeve bearings on both ends. The bearings used were self-aligning and capable of handling rapid acceleration and deceleration using a ceramic liner. The slide bearings are also sealed to ensure optimum lubrication and protection

from dirt contamination. The slide bearings were attached to the vertical rail of the fixture using a low carbon steel rectangular tube mount.

#### 4.1.11 Load cells

The strain gauge loads cells had male threads on both sides. The active end of the load cells was screwed directly into the high strength aluminum grips while the fixed end of the load cells was screwed into the bearing shaft. As mentioned before, the load cells were intentionally attached to the grips to ensure a load signal devoid of any noise. The lightweight load cells were  $\sim 0.5$  lbs. each.

## **4.1.12** Grips

The grips were made of high strength aluminum alloys and have a female thread at one end to connect with the load cell. A groove matching the test sample profile was machined into each grip to ensure that there is no sample slippage. After inserting the sample into the grips, a grip cover is screwed on top to ensure a tight fit. Once the grip covers are installed on both ends, only the gage length of the sample is visible to the high-speed camera. Further, the sample grips can be altered to accommodate samples with different shapes and configurations. The total weight of each grip is 0.79 lbs.

The eventual aim of this dissertation is to use the newly developed test fixture for testing automotive thermoplastics at intermediate strain rates. To reach that step however, a detailed investigation into the reliability of the newly designed test fixture was carried out. This was done by carrying out tensile testing on Aluminum 6061-T6 samples at intermediate strain rates. The resultant stress-strain curves compared with the data from established literature [14]. There are only limited number of studies which have detailed the intermediate strain rate response of Aluminum 6061-T6 samples [14, 17, 26, 35, 37]. This particular study was chosen for verification

purposes firstly because it uses a high rate servo hydraulic machine to test the samples which despite its drawbacks is still considered as an industrial standard. Secondly, the dimensions of the test samples used in the cited work closely resemble that of the aluminum and polymers samples tested in the current study. Thirdly, at least two iterations of stress-strain data below 50 s<sup>-1</sup> was available. High rate servo hydraulic machines do not require extensive filtration below this strain rate. Nevertheless, signal filtration was carried out using the spring mass model. Lastly, the stress-strain curves in the cited work were verified using the Johnson-Cook model.

## 4.2 Material and Specimen Geometry

The test material used in this study was Aluminum alloy 6061-T6. It is one of the most commonly used structural aluminum alloys and possesses an ideal combination of properties, especially weldability and corrosion resistance, making it ideal for a number of structural applications. These applications range from aerospace, road & water transportation to bridges and shipbuilding. As mentioned above, AA6061-T6 was specifically selected for this study due to the availability of its reliable dynamic tensile test data at intermediate strain rates [14]. The dimensions of the sample are shown in Figure 4.6.

An effort was made to keep the dog bone sample size and dimensions comparable to literature. Aluminum 6061-T6 sheets with a uniform thickness of 1.6 mm. were cut into dog bone sample using water jet cutting. The resulting samples had a uniform gage length of 30mm. which closely corresponds to the cited literature being used for verification.

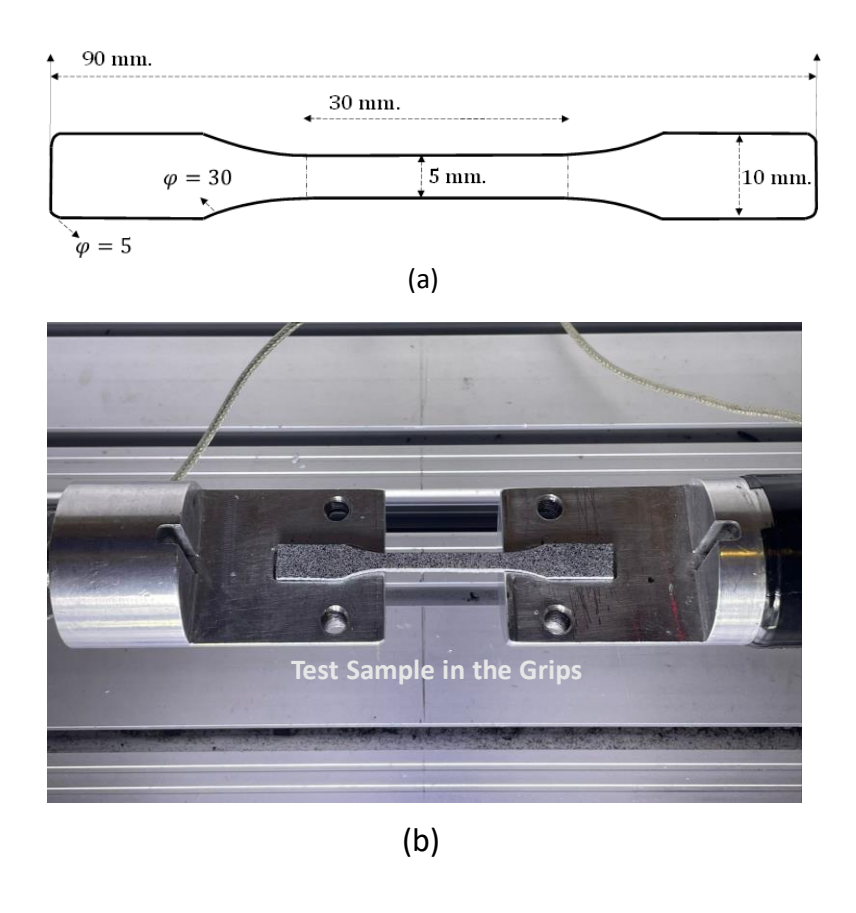


Figure 4.6: (a) Sample dimensions (b) Sample inserted inside the grip cavity

## **4.3** Verification of the Design Concept

The basic premise behind the design of this test fixture was that unlike traditional drop weight and high rate servo hydraulic devices, the test sample should be subjected to uniform load and displacements on both ends. This would facilitate the generation of simultaneous, uniform and stable intermediate impact speeds on both ends of the sample, leading to a homogeneous strain field in its gauge length. This design philosophy leads to a stable impact duration, causing the sample to load up quickly.

To achieve this, great care was taken to precisely machine different parts of the fixture, specifically ensuring that all the corresponding components of the gripping assembly and the cable assembly at both ends have same weights and dimensions. After the pre-test adjustments,

the test fixture was operated with and without samples and further calibrations were performed to ensure a synchronous and uniform response from both load cells. Figure 4.7 shows the comparison of load response of the test material (Aluminum 6061-T6) at two different strain rates, 36 s<sup>-1</sup> and 45s<sup>-1</sup>. The graph clearly shows that both the load cells generate a similar output response. This uniformity of response validates the symmetry and equal loading on both sides of the samples as observed during the entire duration of the impact event.

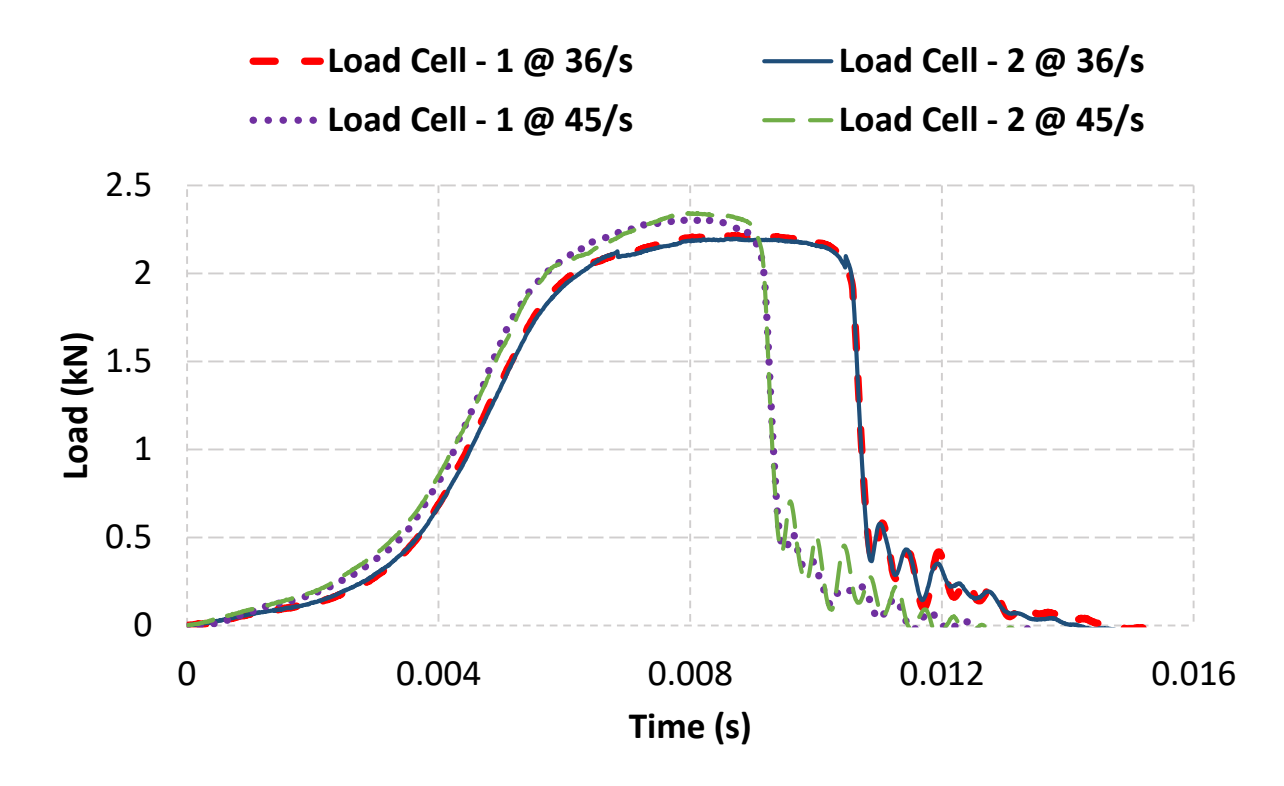


Figure 4.7: Comparison of load cell response at two different strain rates

These results indicate that the alternative loading method devised in this work is viable and can be successfully incorporated in the testing protocol to analyze the intermediate strain rate response of different materials.

Another important feature of the new test system is there is little to negligible ringing in the output response of the system. This was ensured by incorporating appropriate anti-vibration measures. Heavy duty vibration resistant self-locking sleeve anchor to fix the test fixture on the floor. The anchors were complemented by wedge locking washers, which utilize tension instead of friction in order to secure bolted joints exposed to severe vibration and dynamic loads. Further, the base of the fixture was padded by one-inch thick anti-vibration pads. As mentioned earlier in section 4.1.2 above, there is no metal to metal contact during the impact event which dampens the oscillation of the system. The use of a full Wheatstone bridge strain gauge ensures highest sensitivity, the fewest error components, and the highest output that reduces the effects of noise on the measurements. This ensures a smoother load response which did not require any data filtration. It is important to mention here that since large forces are involved in the test operation, the use of strain gauge load cells instead of piezoelectric load cells is totally pertinent. All these steps ensured that the system output had little to no ringing effects and filtration was not required. This is confirmed as shown in Figure 4.8. The original load response – the unfiltered load curve is smooth. A low pass filter was introduced to the output to observe if there was any potential improvement. However, as can be seen from the figure, the introduction of the low pass filter introduces an abnormal artifact to the load vs. time response.

# 4.4 Experimental Verification

The verification of the newly developed tensile test apparatus was carried out by characterizing Aluminum 6061-T6 test samples at strain rates similar to the cited literature [14]. Figure 4.9 (a) and (b) show a comparison of the stress strain curves at two different strain rates  $27s^{-1}$  and  $45s^{-1}$  respectively. It can be clearly seen, that there is excellent agreement between the literature-based and experimental results. Instead of displaying an average curve in the verification graphs, actual stress-strain curves obtained at these loading rates were compared

with the literature curve to highlight the repeatability of results. Three (03) experimental stress strain curves are shown both at  $27s^{-1}$  and  $45s^{-1}$ .

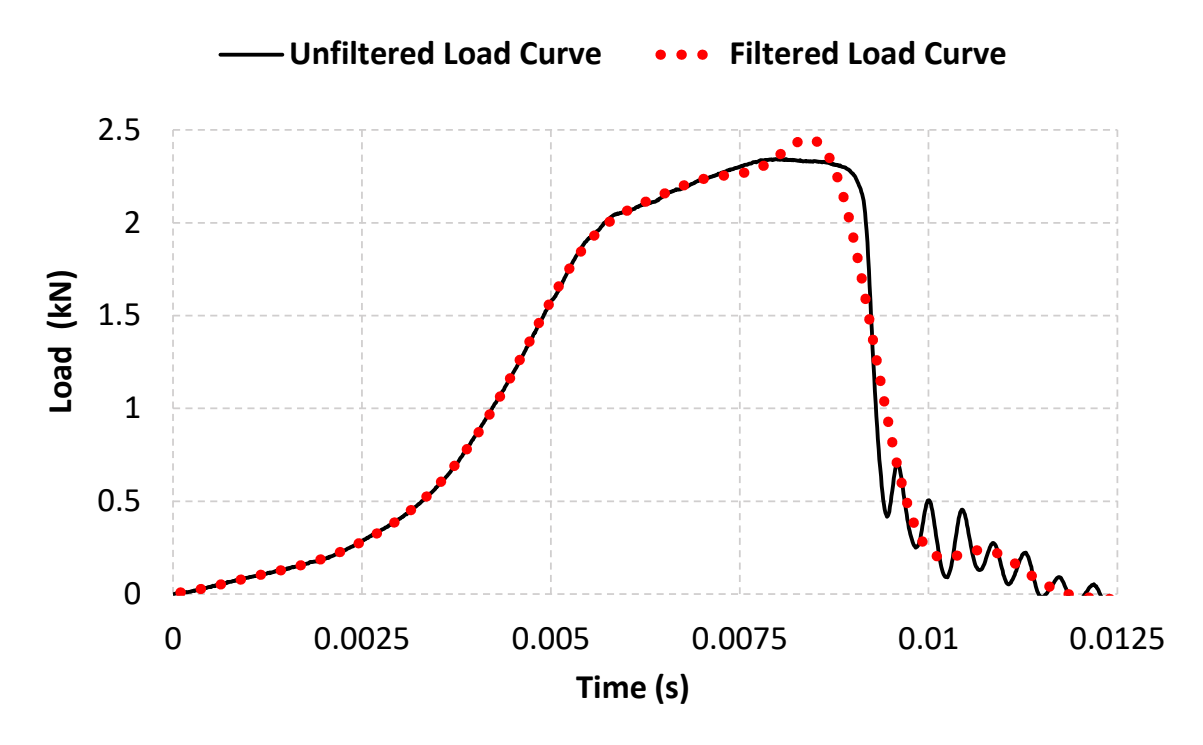


Figure 4.8: Comparison of unfiltered vs. unfiltered load response at a strain rate of 45 s<sup>-1</sup>

Unlike the cited literature, where the elastic region of the deformation flow was constructed artificially based on the quasi-static modulus of the alloy being tested, the experimental elastic region reported is based on actual data. As observed in Figure 4.9 (a) & (b), there is little to no variation in the modulus. The variation can be attributed to the minor vibrations in the system, and can be easily removed by using a curve smoothing method. An unadulterated output response is reported here to signify the quality of the output response. The strain response of the specimens was measured using the DIC technique. In using this technique, the authors ensured that the displacement output was not affected by the compliance of the system.

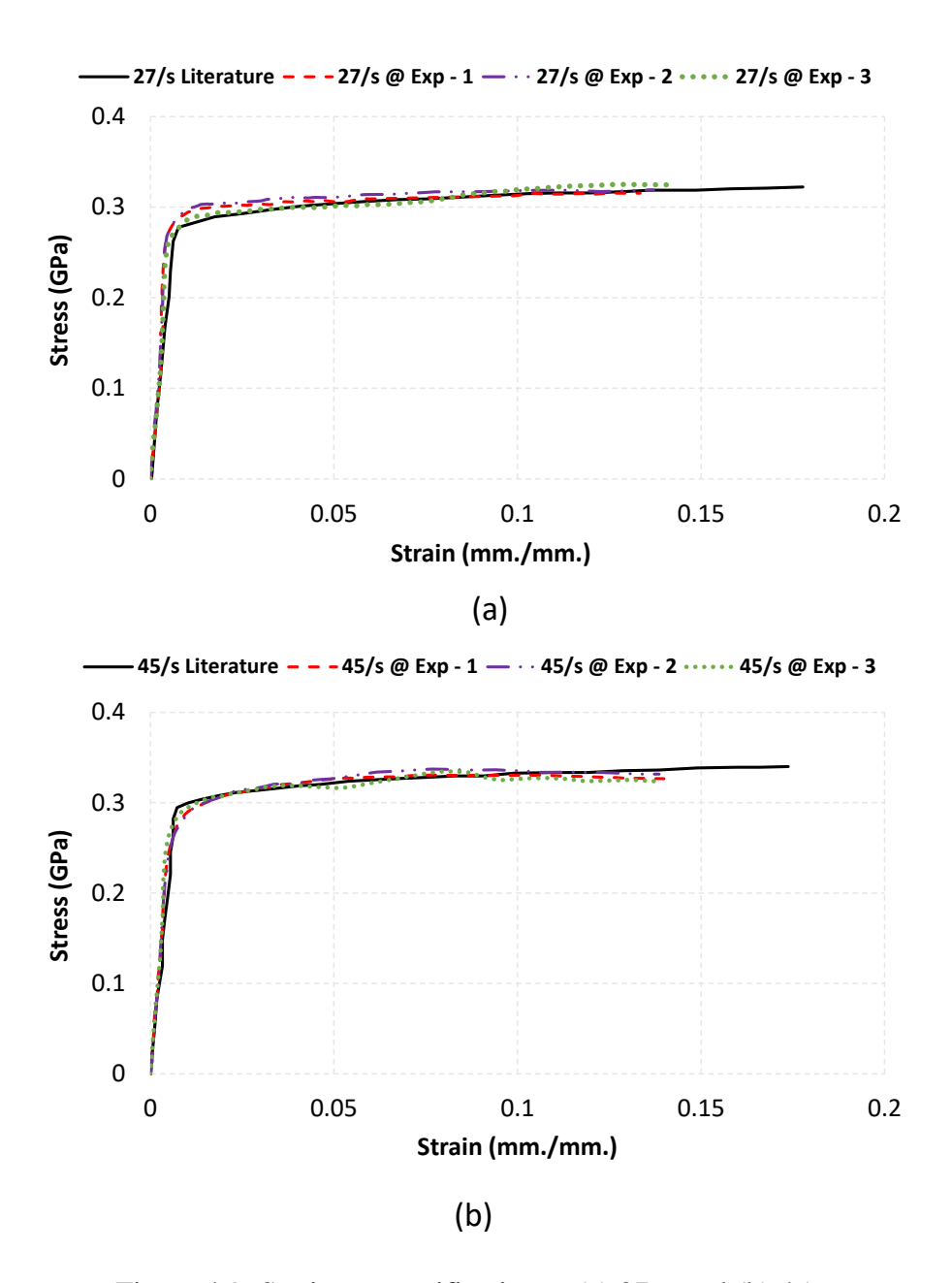


Figure 4.9: Strain rate verification at (a) 27s<sup>-1</sup> and (b) 45s<sup>-1</sup>

Figure 4.9 shows a distinct difference between failure strains cited [14] and current work. There are a number of factors which can cause this behavior, despite the material and temper of the test specimens being uniform. This variation in strain can be due to the difference in the grain structure, small variation in dimensions, method of sample manufacturing and the test temperatures. To illustrate this difference, a graph showing elongation versus strain rate for

AA6061-T6 in literature [14, 44, 45] and present work has been shown in Figure 4.10. The graph clearly indicates the difference in percentage elongation reported in literature. It can be seen that there is a variation in the percentage elongation for the same type of Al 6061, and our work is within the range reported in the literature.

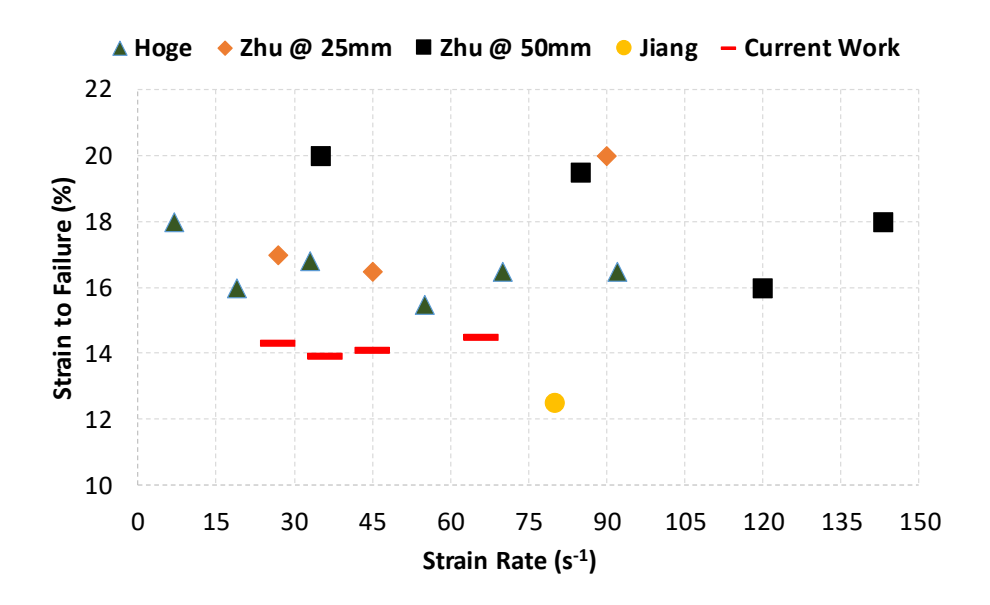


Figure 4.10: Elongation percentage versus strain rate for Aluminum 6061-T6 in literature and present work

## 4.5 Strain Measurement

The strain measurements were carried out using digital image correlation (DIC), a reliable non-contact, non-destructive, full-field deformation measurement technique. In tensile tests carried out at quasi-static speeds, generally an extensometer or a laser extensometer is used to measure the relative displacement of two points on the gage length of the sample. However, for strains experienced during the intermediate strain rate regime, non-contact techniques like linear variable differential transformer (LVDT) and DIC are generally used [5, 14, 26, 46]. Measuring deformations directly from the gage length of the sample is important at intermediate strain rates, because the deformation of other parts of the loading train like grips, load cells, load

frame, connecters, rods etc. may influence the total deformation of the test sample. Depending upon the inertia of the components involved in the loading train, the dominant deformation during a test event might not occur in the gage length of the sample, which could lead to a larger recorded displacements/strains and lower values of elastic modulus. In most high rate servo hydraulic machines which employ LVDT for strain measurement, compliance correction is applied to ensure that only the correct displacement of the sample is measured.

In this work, 2D DIC was used to measure the displacement and strains since the sample failed in pure tension and that there were no out-of-plane displacements involved. Phantom high-speed camera with a frame rate of 14000 fps and a resolution of 640 x 480 was used to capture the images, which were then post processed through a special-use software to extract the displacements and strains. To perform the DIC measurement, an adequate pattern of fiducial markers were sprayed on the surface of the test sample to create a so-called stochastic pattern. An initial coat of aerosol white paint was sprayed on the sample, followed by a fine pattern of black markers. This technique basically creates a reference image at the start of the process and allocates coordinates to the image pixels. The change of pixels in the subsequent images captured during the loading event are compared to the initial reference and the deformation of the object is calculated. For accurate processing of displacement using this technique, a large frame rate is required at a good resolution, in addition to a well-defined stochastic pattern on the test sample.

Figure 4.11 (a) shows the strain-time histories measured using the DIC technique at four different speeds. The slope of the strain curve increases with the increasing strain rate. Derivative of the strain-time history plots yield the strain rate history for these cases as shown in Figure 4.11 (b). After an initial abrupt ramp (initial slope), the strain rate approaches a 'near-constant' value

when the specimen was elongated to a strain of  $\sim 0.02$ . The strain accumulates in the sample during this initial ramp which means that the initial deformation in the test sample does not take place at a constant rate. After this initial jump, the slope stabilizes (secondary slope) and a 'near-constant' strain rate was observed. This secondary slope depends on the strain rate. At lower strain rates, this slope stabilizes quickly, however as the speed of loading increases, near constant strain rates is achieved at higher strain values.

From Figure 4.11(b), the peak strain rate values at the four impactor drop heights, 25, 20, 15 and 10 in, are ~ 73, 46, 37 and 25 s<sup>-1</sup>. These values however are for the representative cases. For each drop height, a total of seven tests were carried out. There were some minor deviations in the recorded strain rates at each drop-height and hence an average was used. The average strain rates recorded against each drop-height along with the standard deviations are shown in Table 4.1.

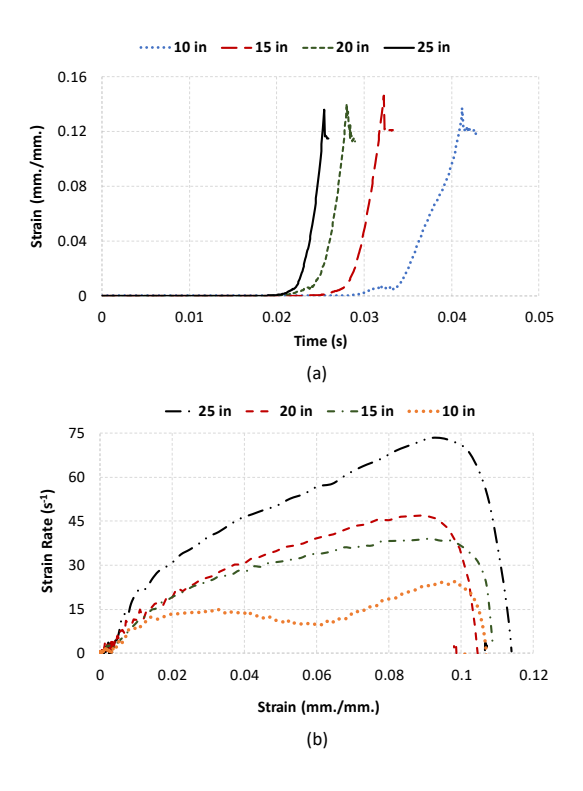


Figure 4.11: (a) Strain-time histories (b) Strain rate histories - at four different drop heights

Table 4.1: Impact drop heights and corresponding strain rates for testing for Al6061-T6 samples

Impactor Drop Height (in.)	Average Corresponding Strain Rate (s <sup>-1</sup> )
25	66 ± 2.64
20	45 ± 1.12
15	$36 \pm 1.66$
10	27 ± 2.21

## 4.6 Strain Rate Characterization of Aluminum 6061-T6

After verification of the tensile test data with established literature, and a qualitative analysis of its output response, the new tensile fixture was used to characterize the strain rate response of Al 6061-T6 samples at four different strain rates mentioned above in Table 4.1.

It is pertinent to mention that this test fixture can successfully conduct testing in the lower spectrum of the intermediate strain rate range. Generally, the high rate servo hydraulic machines and most special use drop weight and hybrid test fixtures experience significant ringing and stress wave propagation issues at lower speed within the intermediate range. These loading rates, ranging from  $10s^{-1}$  to  $50s^{-1}$  are however critical in automotive crashworthiness analysis. In this regard, an intentional effort was made to test the aluminum alloys samples at these lower strain rates.

Figure 4.12 shows the tensile stress-strain curves of Aluminum 6061-T6 at four different strain rates within the intermediate regime. As a baseline, the quasi-static response of this alloy was also incorporated into the figure. This baseline response was recorded at a strain rate of 0.04s<sup>-1</sup> using a conventional MTS hydraulic testing machine. From the representative curves, there does not appear to be any significant increase in flow stress with increasing strain rate,

however there is a distinct increase in tensile strength. Further, there does not appear to be an abrupt change in the amplitude of the flow stress at any strain rate.

The average percentage increase in the tensile strength of the aluminum alloys as it is subjected to higher strain rates within the intermediate regime are reported in Figure 4.13(a). At lower strain rates, 27 s<sup>-1</sup> and 36 s<sup>-1</sup>, the increase in average tensile strength in comparison to the baseline quasi-static strength is approximately 3.6 % and 4.6 % respectively.

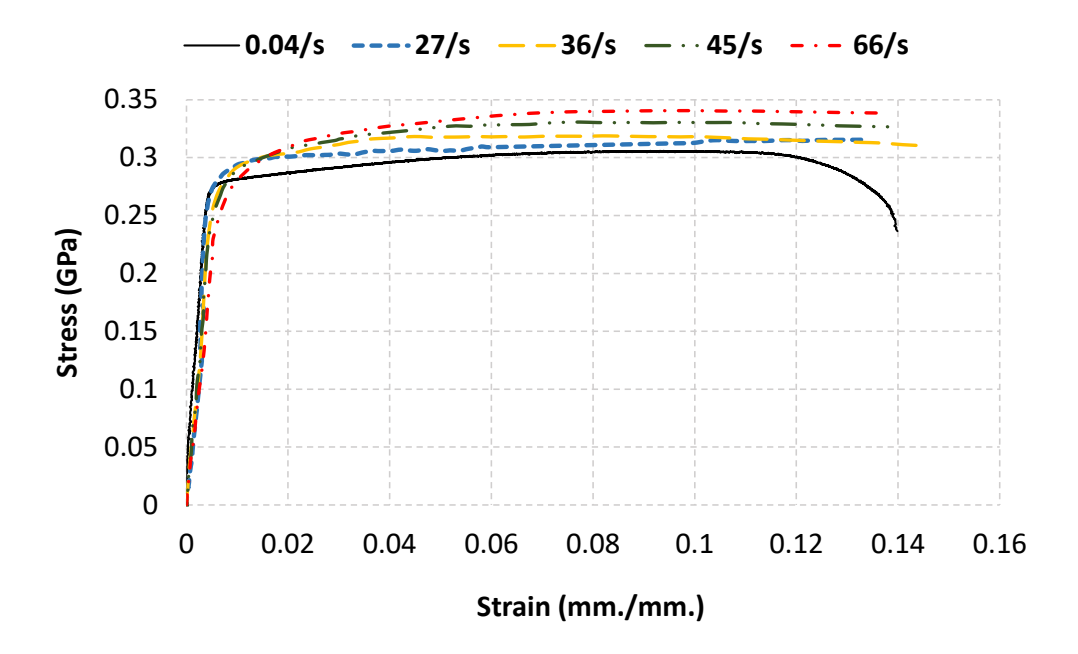


Figure 4.12: Comparison of stress-strain curves of Aluminum 6061-T6 samples at different strain rates

At higher strain rates, the aluminum alloy showed a more pronounced strain rate effect. In going from  $36 \, \text{s}^{-1}$  to  $45 \, \text{s}^{-1}$ , an average increase of  $\sim 4 \, \%$  was observed. The highest tensile strength was reported at  $66 \, \text{s}^{-1}$ . At this loading rate, an average increase by  $\sim 11 \, \%$  was observed relative to its quasi-static strength. From the data, it is clear that there is a sequential increase in tensile strength, which becomes more pronounced at higher rates. This indicates a direct relation between the strength and strain rate, provided the test temperatures are kept constant.

The strain to failure of percentage elongation slightly increased at higher strain rates, however the average percentage increase was not nearly as distinct as was observed in the case of tensile stiffness. Figure 4.13(b) shows the variation of percentage strain to failure with the increasing strain rate compared with values at quasi-static strain rates. In a number of other works involving dynamic loading of Aluminum 6061-T6 at medium and high strain rates, an increase in failure elongation has been reported. However, there is a large data scatter observed at strain rates under 10<sup>3</sup>. The increase in deformation flow becomes more predictable and pronounced after that.

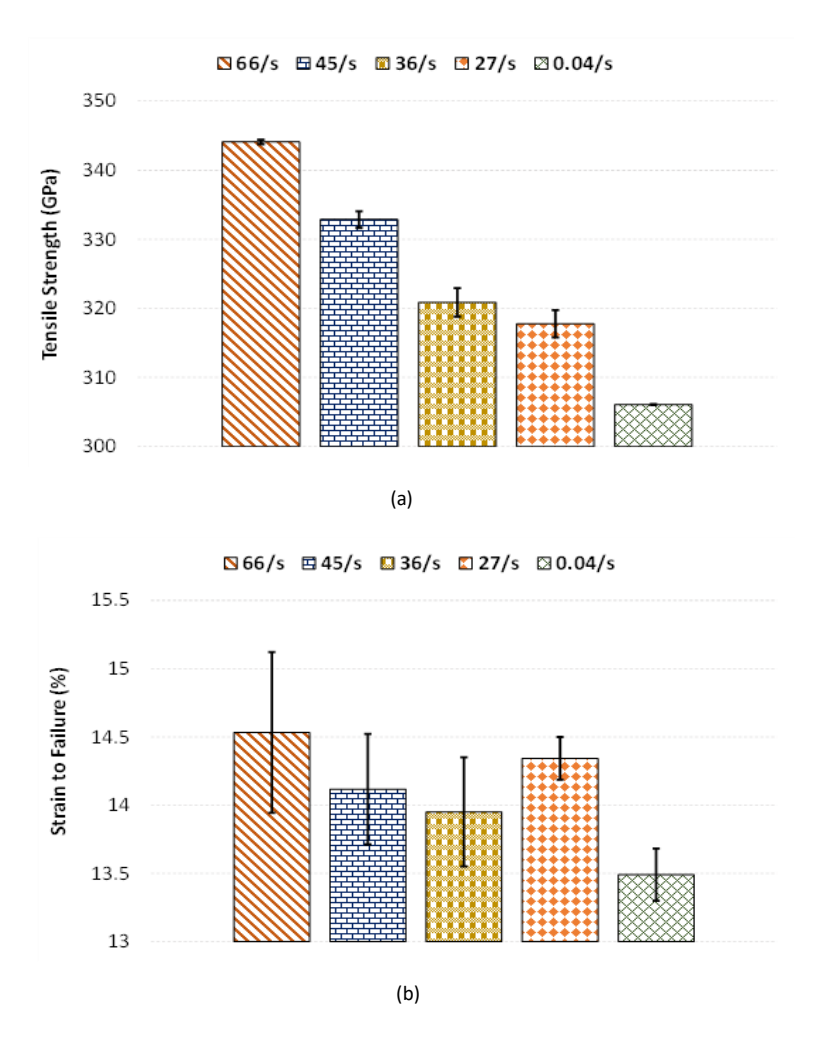


Figure 4.13: Comparison of (a) average tensile strength and (b) strain to failure at different strain rates

## 4.7 Conclusion

A symmetric double acting tensile test fixture for intermediate strain rate characterization of polymers was fabricated in-house. The fixture was designed to overcome the effect of low elastic wave speed, ringing, inertia and sample preload. Experimental verification/validation of the designed test fixture was carried out using Aluminum alloy samples at two intermediate strain rates. Excellent agreement of the experimental data relative to established literature, with a maximum error of ~2.3 % in tensile strength was found. There was however a variation in the strain to failure response of the aluminum alloys samples. This variation was within the data scatter found in established literature. The load cell response was completely in-sync at both ends, verifying the system symmetry and uniform loading. Further, no ringing was observed in the output response, thus eliminating the need of filtration and post-processing of the load signal. Non-contact full field strain calculations were carried out through DIC; all test events recorded at a rate of 14000 frames per second. A maximum 10 % increase in tensile strength was observed from quasi-static to 66s<sup>-1</sup>. The maximum elongation (~ 7 %) was observed at 66 s<sup>-1</sup>, which was in accordance with prior work in literature.

#### REFERENCES

- [1] X. Xiao, "Dynamic tensile testing of plastic materials," Polymer Testing, vol. 27, pp. 164-178, 2008/04/01/2008.
- [2] D. A. Şerban, G. Weber, L. Marşavina, V. V. Silberschmidt, and W. Hufenbach, "Tensile properties of semi-crystalline thermoplastic polymers: Effects of temperature and strain rates," Polymer Testing, vol. 32, pp. 413-425, 2013.
- [3] A. D. Mulliken and M. C. Boyce, "Mechanics of the rate-dependent elastic—plastic deformation of glassy polymers from low to high strain rates," International Journal of Solids and Structures, vol. 43, pp. 1331-1356, 2006/03/01/2006.
- [4] S. M. W. R.W. Armstrong, "High Strain Rate Properties of Metals and Alloys," International Materials Reviews, vol. 53, pp. 105-128, 2008.
- [5] C. R. Siviour and J. L. Jordan, "High strain rate mechanics of polymers: a review," Journal of Dynamic Behavior of Materials, vol. 2, pp. 15-32, 2016.
- [6] S. Walley and J. Field, "Strain rate sensitivity of polymers in compression from low to high rates," DYMAT j, vol. 1, pp. 211-227, 1994.
- [7] A. M. S. Hamouda and M. S. J. Hashmi, "Testing of composite materials at high rates of strain: advances and challenges," Journal of Materials Processing Technology, vol. 77, pp. 327-336, 1998/05/01/1998.
- [8] R. L. Sierakowski, "Strain Rate Effects in Composites," Applied Mechanics Reviews, vol. 50, pp. 741-761, 1997.
- [9] J. E. Field, S. M. Walley, W. G. Proud, H. T. Goldrein, and C. R. Siviour, "Review of experimental techniques for high rate deformation and shock studies," International Journal of Impact Engineering, vol. 30, pp. 725-775, 2004/08/01/2004.
- [10] R. J. Clifton, "High Strain Rate Behavior of Metals," Applied Mechanics Reviews, vol. 43, pp. S9-S22, 1990.
- [11] Y. Xia, J. Zhu, and Q. Zhou, "Verification of a multiple-machine program for material testing from quasi-static to high strain-rate," International Journal of Impact Engineering, vol. 86, pp. 284-294, 2015/12/01/2015.
- [12] T. Bhujangrao, C. Froustey, E. Iriondo, F. Veiga, P. Darnis, and F. G. Mata, "Review of intermediate strain rate testing devices," Metals, vol. 10, p. 894, 2020.
- [13] R. Bardenheier and G. Rogers, "Dynamic impact testing with servohydraulic testing machines," in Journal de Physique IV (Proceedings), 2006, pp. 693-699.

- [14] D. Zhu, B. Mobasher, S. D. Rajan, and P. Peralta, "Characterization of dynamic tensile testing using aluminum alloy 6061-T6 at intermediate strain rates," Journal of Engineering Mechanics, vol. 137, pp. 669-679, 2011.
- [15] A. Rusinek, R. Zaera, P. Forquin, and J. R. Klepaczko, "Effect of plastic deformation and boundary conditions combined with elastic wave propagation on the collapse site of a crash box," Thin-Walled Structures, vol. 46, pp. 1143-1163, 2008/10/01/2008.
- [16] X. Yang, L. Hector Jr, and J. Wang, "A combined theoretical/experimental approach for reducing ringing artifacts in low dynamic testing with servo-hydraulic load frames," Experimental Mechanics, vol. 54, pp. 775-789, 2014.
- [17] M. Rahmat, "Dynamic mechanical characterization of aluminum: analysis of strain-rate-dependent behavior," Mechanics of Time-Dependent Materials, vol. 23, pp. 385-405, 2019/11/01 2019.
- [18] D. Zhu, S. D. Rajan, B. Mobasher, A. Peled, and M. Mignolet, "Modal Analysis of a Servo-Hydraulic High Speed Machine and its Application to Dynamic Tensile Testing at an Intermediate Strain Rate," Experimental Mechanics, vol. 51, pp. 1347-1363, 2011/10/01 2011.
- [19] D. Zhu, B. Mobasher, J. Erni, S. Bansal, and S. D. Rajan, "Strain rate and gage length effects on tensile behavior of Kevlar 49 single yarn," Composites Part A: Applied Science and Manufacturing, vol. 43, pp. 2021-2029, 2012/11/01/2012.
- [20] S. Yoo, D. Schueler, M. Brodbeck, N. Toso, G. Catalanotti, and H. Voggenreiter, "An improved load introduction technique for dynamic material characterisation at intermediate strain rate," in Proceedings, 2018, p. 381.
- [21] I. Uriarte, I. Garitaonandia, T. Guraya, and A. Arriaga, "Suppression of ringing oscillations from high speed rubber compression curves through a detailed modal characterization of servo-hydraulic machines," Polymer Testing, vol. 60, pp. 365-373, 2017/07/01/2017.
- [22] J. ACOSTA, G. OLIVARES, S. KESHAVANARAYANA, M. SIDDIQUI, and I. ECHAVARRI, "Dynamic Material Characterization of Laminated Composite Materials—a Path for Test Method Development."
- [23] H. Jin, B. Sanborn, W. Y. Lu, and B. Song, "Mechanical characterization of 304L-VAR stainless steel in tension with a full coverage of low, intermediate, and high strain rates," Mechanics of Materials, vol. 152, p. 103654, 2021/01/01/2021.
- [24] Z. Qin, W. Li, J. Zhu, and Y. Xia, "Experimental and numerical analysis of the system ringing in intermediate strain rate tests," in ASME 2016 International Mechanical Engineering Congress and Exposition, 2016.

- [25] Z. Qin, J. Zhu, W. Li, Y. Xia, and Q. Zhou, "System ringing in impact test triggered by upper-and-lower yield points of materials," International Journal of Impact Engineering, vol. 108, pp. 295-302, 2017/10/01/2017.
- [26] N. Perogamvros, T. Mitropoulos, and G. Lampeas, "Drop Tower Adaptation for Medium Strain Rate Tensile Testing," Experimental Mechanics, vol. 56, pp. 419-436, 2016/03/01 2016.
- [27] N. Perogamvros and G. Lampeas, "Experimental investigation of composite lockbolt fastened joints under in-plane low velocity impact," Composites Part A: Applied Science and Manufacturing, vol. 90, pp. 510-521, 2016/11/01/2016.
- [28] N. Perogamvros, G. Lampeas, and A. Murphy, "Experimental Investigation of Fastener Pull-out Response in Composite Joints under Static and Dynamic Loading Rates," Applied Composite Materials, vol. 26, pp. 1349-1365, 2019/12/01 2019.
- [29] S. Gurusideswar, R. Velmurugan, and R. Sarathi, "High Strain Rate Studies of Polymer and Hybrid Nanocomposites for Aerospace Application," in Advanced Composites in Aerospace Engineering Applications, ed: Springer, 2022, pp. 55-92.
- [30] S. Gurusideswar, R. Velmurugan, and N. K. Gupta, "Study of rate dependent behavior of glass/epoxy composites with nanofillers using non-contact strain measurement," International Journal of Impact Engineering, vol. 110, pp. 324-337, 2017/12/01/2017.
- [31] S. Gurusideswar, N. Srinivasan, R. Velmurugan, and N. K. Gupta, "Tensile Response of Epoxy and Glass/Epoxy Composites at Low and Medium Strain Rate Regimes," Procedia Engineering, vol. 173, pp. 686-693, 2017/01/01/ 2017.
- [32] D. d. P. C. Antunes, "Development of a drop weight machine for adhesive joints testing," Universidade do Porto (Portugal), 2019.
- [33] R. Othman, P. Guégan, G. Challita, F. Pasco, and D. LeBreton, "A modified servohydraulic machine for testing at intermediate strain rates," International Journal of Impact Engineering, vol. 36, pp. 460-467, 2009/03/01/2009.
- [34] M. LeBlanc and D. Lassila, "A hybrid technique for compression testing at intermediate strain rates," Experimental Techniques, vol. 20, pp. 21-24, 1996.
- [35] B. Song, B. Sanborn, J. D. Heister, R. L. Everett, T. L. Martinez, G. E. Groves, et al., "An Apparatus for Tensile Characterization of Materials within the Upper Intermediate Strain Rate Regime," Experimental Mechanics, vol. 59, pp. 941-951, 2019/09/01 2019.
- [36] W. R. Whittington, A. L. Oppedal, D. K. Francis, and M. F. Horstemeyer, "Robust Intermediate Strain Rate Experimentation Using the Serpentine Transmitted Bar," in Residual Stress, Thermomechanics & Infrared Imaging, Hybrid Techniques and Inverse Problems, Volume 9, Cham, 2016, pp. 167-173.

- [37] W. R. Whittington, A. L. Oppedal, D. K. Francis, and M. F. Horstemeyer, "A novel intermediate strain rate testing device: The serpentine transmitted bar," International Journal of Impact Engineering, vol. 81, pp. 1-7, 2015/07/01/2015.
- [38] A. Gilat, J. D. Seidt, T. A. Matrka, and K. A. Gardner, "A New Device for Tensile and Compressive Testing at Intermediate Strain Rates," Experimental Mechanics, vol. 59, pp. 725-731, 2019/06/01 2019.
- [39] M. Quinlan and M. Hillery, "High-strain-rate testing of beryllium copper at elevated temperatures," Journal of materials processing technology, vol. 153, pp. 1051-1057, 2004.
- [40] T. Bhujangrao, C. Froustey, P. Darnis, F. Veiga, S. Guérard, and F. G. Mata, "Design and Validation of New Torsion Test Bench for Intermediate Strain Rate Testing," Experimental Mechanics, vol. 63, pp. 3-13, 2023/01/01 2023.
- [41] C. M. Roland, J. N. Twigg, Y. Vu, and P. H. Mott, "High strain rate mechanical behavior of polyurea," Polymer, vol. 48, pp. 574-578, 2007/01/12/2007.
- [42] T. Chu, W. Ranson, and M. A. Sutton, "Applications of digital-image-correlation techniques to experimental mechanics," Experimental mechanics, vol. 25, pp. 232-244, 1985.
- [43] M. A. Sutton, J. J. Orteu, and H. Schreier, Image correlation for shape, motion and deformation measurements: basic concepts, theory and applications: Springer Science & Business Media, 2009.
- [44] C. Jiang and M. Chen, "Dynamic Properties of Materials. Part 2. Aluminum Alloys," BOSTON UNIV MA DEPT OF AEROSPACE ENGINEERING1974.
- [45] K. G. Hoge, "Influence of strain rate on mechanical properties of 6061-T6 aluminum under uniaxial and biaxial states of stress: Author presents special technique for determining mechanical properties of materials under dynamic tensile loads," Experimental Mechanics, vol. 6, pp. 204-211, 1966.
- [46] S. Gurusideswar, R. Velmurugan, and N. Gupta, "Study of rate dependent behavior of glass/epoxy composites with nanofillers using non-contact strain measurement," International Journal of Impact Engineering, vol. 110, pp. 324-337, 2017.
- [47] R. Sreidel Jr and C. Makerov, "The tensile properties of some engineering materials at moderate rates of strain," Univ. of California, Livermore1960.

# CHAPTER 5 - INTERMEDIATE STRAIN RATE CHARACTERIZATION OF THERMOPLASTICS

Thermoplastic polymers have experienced an exponential increase in demand in a number of industrial applications ranging from aerospace, automotive, marine and defense to packaging, agriculture, electric component and medical instrument manufacturing. Traditionally, thermosets have been the industrial standard for polymer based structural and semi-structural applications, primarily due to their better strength and stiffness properties. However, development of engineered thermoplastics has afforded design/manufacturing engineers greater flexibility and sophistication in part and process design. A major reason behind the renewed push to incorporate thermoplastic polymers in industrial applications is their reversible nature, which provides limitless potential for healing and health monitoring initiatives. Further, these polymers are suitable for the light-weighting of components which is a critical requirement for automotive manufacturing. These benefits, coupled with the rapid advancements in thermoplastic molding techniques and their compatibility to multiple rapid manufacturing techniques has made thermoplastics a material of choice for parts involving moderate-to-high geometric complexity and greater production volumes. The development of engineered thermoplastics using nanofillers, additives and blends has also helped in incorporating attributes like corrosion resistance, environmental sustainability and most importantly a tailorable combination of mechanical properties.

The increased usage of thermoplastics in mass-produced automotive vehicles necessitates the need for understanding fundamental material behavior at relevant loading rates experienced during automotive crashes and other low velocity impacts. Simulating the exact physical mechanisms encountered by thermoplastic during a dynamic loading event can be achieved by

formulating robust constitutive equations. Developing these equations however requires extensive experimental data over a range of strain rates. Only through these experiments, the dynamic response of the thermoplastic polymers can be identified, characterized and parameterized, and the so called 'digital twins' can be developed.

The development of reliable numerical models to predict the thermoplastic material behavior at intermediate strain rates, generally defined between 1-100s<sup>-1</sup>, [1] is critical. There is however a huge research gap in this domain. As reviewed in Chapter 2, there is an extensive experimental database available for polymers, including thermoplastics, at quasi-static and high strain rates, especially in compressive loading scenarios [2-5]. Tensile mechanical response of polymers, particularly the softer thermoplastics and their composites, at intermediate strain rates remains an anomaly primarily due to the lack of reliable testing machines [4]. Most conventionally designed tensile intermediate strain rate testing machines have complications related to system ringing, high sample preloads, stress wave propagation and load rising time, system inertia, symmetry, torsion/bending of the test sample, size/dimension of the test sample etc.

To overcome this challenge, this work aimed at designing and developing a symmetric double acting drop impact machine, with an aim to test some of the most commonly used thermoplastic polymers at intermediate rates of loading. Details of the fixture and how it operates has been extensively described in Chapter 4. In summary, the newly designed fixture offers the following benefits as compared to pre-existing designs available in literature.

i. Test sample is equally loaded from both sides, leading to a smoother transition to quasidynamic equilibrium along its gauge length.

- ii. The gripping and cable assembly is designed to be extremely lightweight to minimize the inertial effects on the output response. System design also allows for inertial correction.
- iii. The gripping assembly is designed to ensure negligible preload on the test sample.
- iv. Little to no ringing in the output response of the load cells, even at higher rates of loading. Signal filtration is not required.
- v. Samples of multiple sizes and shapes can be tested.
- vi. Test Sample is isolated from any twist/torsion.
- vii. Test Sample experiences a purely tensile deformation.
- viii. Grips are directly connected to inline load cells for acquiring an accurate and unadulterated load response.
- ix. The whole setup is designed to be symmetric.
- x. Relatively low cost as compared to high rate servo hydraulic fixtures

The newly designed test fixture was initially employed to test Aluminum 6061-T6 samples at multiple intermediate strain rates. The experimental data was verified against established literature [6] and the results have been detailed in Chapter 4. Post verification, the fixture was used to evaluate the tensile dynamics response of select thermoplastics – High Density Polyethylene (HDPE), Polypropylene (PP), Acrylonitrile Butadiene Styrene (ABS), Polycarbonate (PC) and Nylon (PA6/6) - at three (03) strain rates within the intermediate regime. These thermoplastics are extensively used in the automotive industry and were selected as part of a scheme in which the polymers were divided into three groups on the basis of their quasi-static mechanical properties. Details of this selection and the baseline quasi-static response of the selected polymers was reported in Chapter 3.

An added objective of this work is to understand the effect of nanofillers on the strain rate behavior of base thermoplastic resin. To this end, an extensively used thermoplastic with good impact properties and toughness - ABS - was selected. Three (03) fillers namely: a) M-5 Graphene granules b) C-750 Graphene platelets and c) Carbon Nanotubes (CNTs) were used. The baseline quasi-static testing for ABS, with and without the nanoparticles, was carried out to evaluate their strain rate sensitivity; results were reported in Chapter 3.

External factors like sample size manufacturing conditions, processing parameters and boundary conditions etc. were kept as uniform as possible. It is important to note that the intrinsic morphology (amorphous/semi-crystalline) of the thermoplastic was intentionally kept inconsistent across the three groups, since the inspiration of material selection was their usage in the automotive industry, and their suitability for various structural, semi-structural and non-structural parts.

## **5.1** Results and Discussion

In this section, the intermediate strain rate response of the selected neat thermoplastic and ABS nanocomposites will be discussed. All the samples were tested at three consistent drop heights of 10, 20 and 25 inches. These drop heights yielded average strain rates of ~ 27, 45 and  $66s^{-1}$  in the aluminum alloys samples. The more ductile thermoplastic test samples were however expected to undergo a different strain response.

It is pertinent to mention that the stack weight, the drop height of the impactor and the corresponding strain rates were chosen to mirror the approximate strain rates experienced in a typical medium to high speed automotive crash. Although there is no unified consensus as to what constitutes a high speed crash, however both the National Highway Traffic Safety Administration (NHTSA), a branch of the Department of Transportation, and the Insurance Institute for Highway Safety (IIHS), an independent safety-research group sponsored by auto insurers, evaluate their

frontal car crash tests at impact speeds of 35 and 40 miles per hour (mph) respectively [7]. Given that the typical size of a standard automotive vehicle is 14.7 feet [8], this constitutes a nominal strain rate of  $\sim 3.5 \, \mathrm{s}^{-1} - 4 \, \mathrm{s}^{-1}$ . The actual strain rates experienced by various car components would obviously be different, depending on the orientation of the parts with respect to the direction of the crash, component material and architecture, whether the crash took place between similar sized cars (heavier vehicle projects more of its crash energy into the smaller one), if the impact took place above or below the bumper line (impact below the bumper line can be more fatal) and a range of other factors [7]. Importantly, the crash will introduce of combination of compressive and tensile forces on the car components.

It is important to note that during crash event or a foreign body impact etc., the component which comes into direct contact will not experience a constant strain rate (something which is an extremely desirable attribute while designing the intermediate strain rate test fixture). Upon impact, stress waves are generated in the component and it experiences varying strain rates as the force of impact is transferred through it, potentially causing damage to it and the surrounding parts. Therefore, while the initial estimated nominal strain rates might be low for an automotive crash, the strain rates experienced by the bumper, hood, engine components can be different and potentially much higher.

Further, while an automotive vehicle might experience crash strain rates at higher velocities, the test samples in the designed test fixture will experience similar strain rates at significantly scaled down velocities. Therefore, the dynamic behavior of multiple thermoplastics was investigated using the most controllable parameter, i.e. by fixing the drop height or the impact force.

Taking these factors into account, it was decided to test the samples at significantly higher strain rates with the intermediate strain rate regime (1-100s<sup>-1</sup>). For Aluminum alloys samples, as mentioned above, these strain rates were 27 s<sup>-1</sup>, 45 s<sup>-1</sup> and 66s<sup>-1</sup>. Consistency in these rates was ensured using same corresponding drop heights (height between the hammer and dampers on top of the impact bar) for testing the thermoplastic samples.

# **5.2** Neat Thermoplastics

Each thermoplastic used to investigate the strain rate effect in this work have different morphologies. This leads to a unique strain response i.e. they would not exhibit the same strain rate sensitivity even if the impact force is kept constant. Therefore, before analyzing the dynamic response of these thermoplastics at consistent drop heights, it was important to investigate the strain rate sensitivity of each thermoplastic. This was carried out by taking the derivate of the strain – time plots at various drop heights for each thermoplastic material. The resultant strain rate histories were analyzed to examine the actual strain rates experienced by each thermoplastic at three uniform drop heights. For ease of understanding and demonstration, strain rate histories of two thermoplastics, HDPE and PA (6/6) are shown in Figure 5.1.

HDPE and PA (6/6) are both semi-crystalline thermoplastics and were selected because the initial quasi-static investigation into their strain rate behavior showed their highly ductile nature. One of the primary challenges in characterizing thermoplastics at intermediate strain rates is their tendency to undergo large deformations before yield and failure. These large deformations prevent the test sample from loading up quickly and achieving a near constant strain rate before failure takes place. This inability of achieving a stable strain rate puts a limitation on the reliability and repeatability of various conventional high rate servo, drop weight and hybrid test fixtures.

Considering these challenges, it was only prudent to investigate their behavior in terms of strain rate history and stability.

From Figure 5.1(a), it was observed that after the initial oscillations and ramp, the strain rates for HDPE test samples at all three drop heights becomes nearly constant at  $\sim 60\text{-}65$  % of the failure strain. For example, at a drop height of 20 in, the strain rate reaches a nearly constant value of  $50 \pm 1 \text{ s}^{-1}$  at a strain of 0.052, which is approximately 65 % of the failure strain (0.084). The initial ramp in the strain rate is expected. This ramp takes place due to the accumulation of strain as the sample tries to load up. It is important to note that for all cases, a stable strain rate is achieved before material failure, which indicates a stable load rising time. The maximum variation in strain rate ( $\pm 5 \text{ s}^{-1}$ ) was observed at 25 in drop height. These variations are expected to get higher at higher strain rates.

The strain history for PA (6/6) samples, commonly known as Nylon (6/6), is shown in Figure 5.1(b). It is evident that at same drop heights the nylon samples experience different strain rates when compared to HDPE. This essentially validates the fact that strain rate of each material is unique and is dependent upon their intrinsic behavior and its microstructure. The nylon samples experienced higher strain rates at same drop heights. A significant observation from their strain rate histories is the larger length of the initial slope. All the strain rate curves stabilize at  $\sim 80\%$  of the failure strain, however there is a larger variation in strain rate when compared to HDPE. For instance, at a drop height of 20 in, the strain rate of the representative curve reaches a 'near-constant' value of  $64 \, \text{s}^{-1}$  at a strain of 0.099 (with a variation of  $\pm 5 \, \text{s}^{-1}$ ) which is 84% of the failure strain. Overall, at least seven iterations were carried out for every thermoplastic at each drop height. Thus, a total of minimum 21 tests were carried out for each thermoplastic at three

different drop heights. The average strain rates (along with the standard deviation) experienced by these polymers at three different drop heights are shown in Table 5.1.

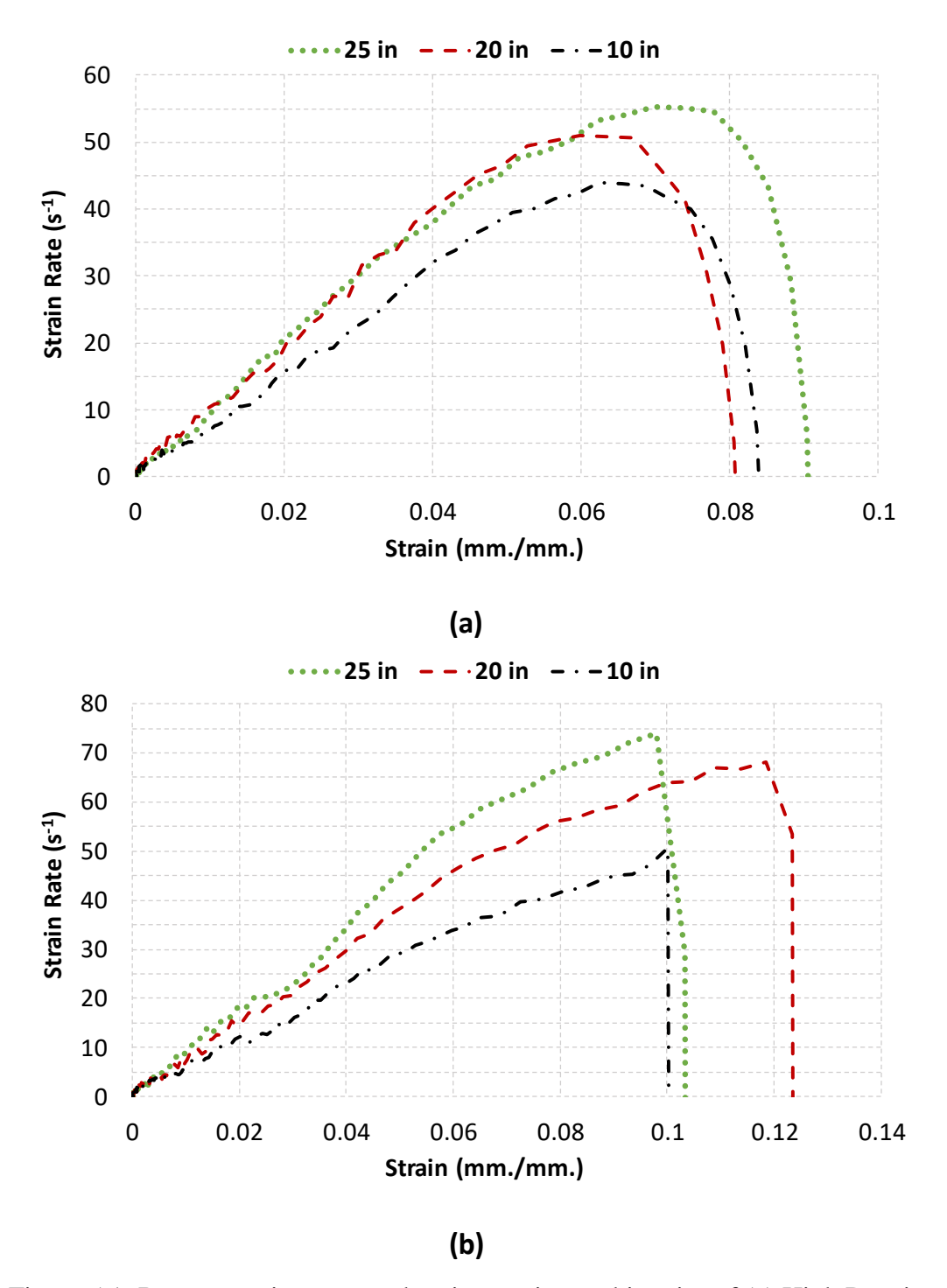


Figure 5.1: Representative curves showing strain rate histories of (a) High Density Polyethylene and (b) Polyamide (6/6)

Table 5.1: Average strain rate values for thermoplastic at three drop heights (All strain rate values have been rounded off to the closest decimal)

Thermoplastics	10 in.	20 in.	25 in.
	Corresponding Strain Rates (s-1)		
HDPE	$46 \pm 2.6$	50 ± 1.6	55 ± 2.6
PP	$49 \pm 2.0$	53 ± 4.2	$60 \pm 5.7$
ABS	$15 \pm 1.9$	$21 \pm 0.8$	27 ± 3.2
PC	$52 \pm 3.5$	$76 \pm 1.2$	82 ± 1.8
PA6/6	$46 \pm 3.4$	$68 \pm 5.5$	$78 \pm 6.2$

Table 5.1 clearly demonstrates that all the polymers exhibit a different strain response when subject to similar loads. The highest strain rate variation was observed in polycarbonate and nylon samples where the strain rate increased by  $\sim 36$ % and 41% respectively as the drop height increased from 10 to 25 inches. ABS samples showed the least strain rate variation among all the polymers tested. Except ABS, the average strain rate in the polymer samples at a drop height of 10 in. was  $49 \pm 3$  s<sup>-1</sup>. However, the average strain in the ABS samples at this height was  $15 \pm 2$  s<sup>-1</sup>. This unique strain rate response of ABS can be attributed to its rubbery nature due to the presence of butadiene monomer, which also contributes to its excellent impact properties. Considering these strain rate responses, the overall stress-strain behavior of the polymers samples was further investigated.

The representative tensile stress-strain curves of all the five thermoplastics at three different impact heights are shown in Figure 5.2. The average tensile strength (in MPa) and the standard deviation are indicated with the representative curves.

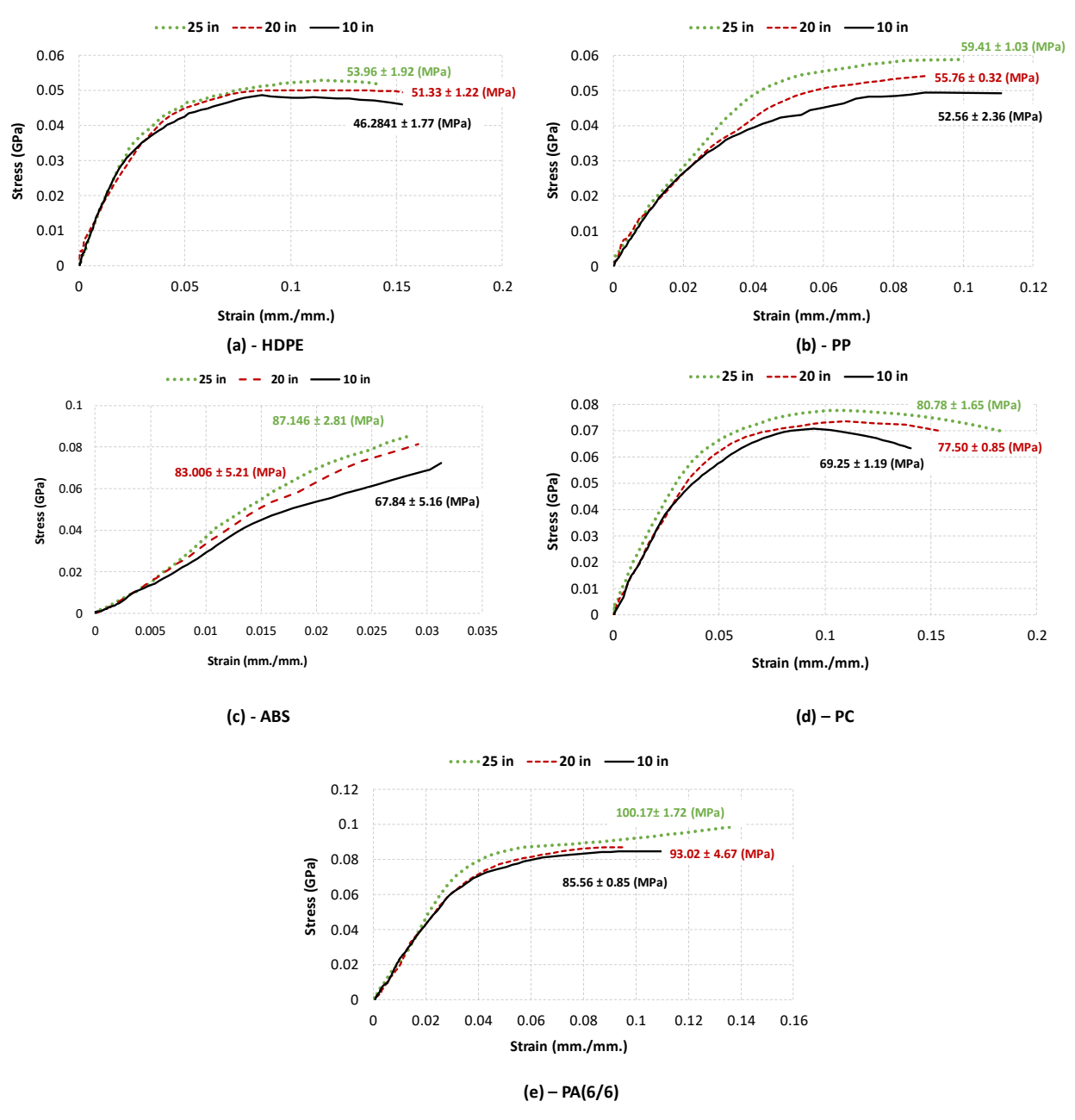


Figure 5.2: Representative curves at three different drop height for the five selected thermoplastics (a) High Density Polyethylene (b) Polypropylene (c) ABS (d) Polycarbonate (e) Polyamide (6/6)

From the figure above, it can be clearly seen that there is a distinct increase in the tensile strength of all the thermoplastic samples as the drop height and the corresponding strain rates increase. In line with the quasi-static response, PA (6/6) show the highest tensile strength. The representative curves show a typical deformation flow in HDPE and PC, starting with a

viscoelastic response, yielding, strain softening and then strain hardening before failure. Strain hardening was not observed for PP, PA (6/6) and ABS, the latter showing the least elongation. While there is a direct relation between tensile strength and the increasing strain rate, the relationship between the failure strain (strain at which the thermoplastic samples break) and the strain rates show considerable variation.

A comprehensive analysis of variations in tensile strength is shown in Figure 5.3. The average percentage variation in the tensile strengths of all the tested polymer samples at intermediate strain rates (defined in Table 5.1) corresponding to three different drop heights are shown in Figure 5.3. It is important to reiterate that the strain rates experienced by polymers samples are not same.

In terms of tensile strength, the highest percentage increase from lowest to the highest drop height was observed in ABS, an ~ 22 % increase in strength. Polypropylene showed the lowest percentage increase in strength at 12 % while the remaining three polymers showed ~14% improvement in tensile strength. Considering that there was an increase of just 12 s<sup>-1</sup> in the strain rates experienced by ABS across the three drop heights, the corresponding average increase in the tensile strength is significant and vividly illustrates the potential of this polymer at higher rates of loading.

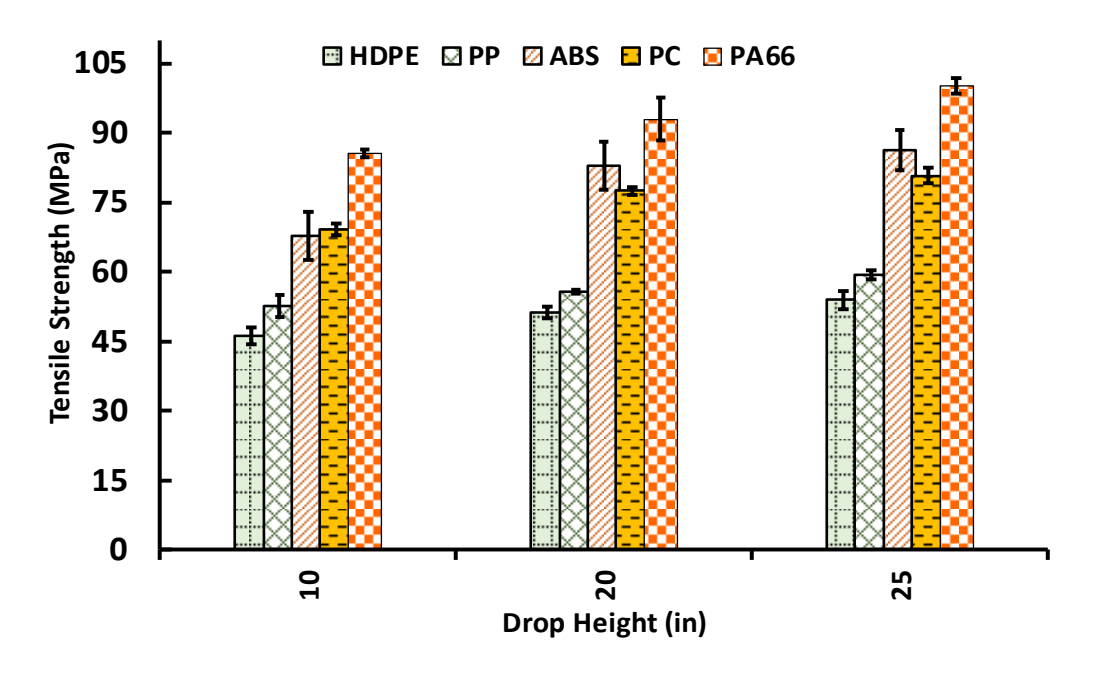


Figure 5.3: Variations in tensile strength experienced by the thermoplastics at three different drop heights

The drastic increase in the tensile strength of ABS is also significant in view of its quasistatic response. To illustrate that, a log graph indicating the average tensile strength values of all the tested polymers both in quasi-static and intermediate strain rate regimes is shown in Figure 5.4. As observed, the tensile strength of PC was distinctly higher than ABS at quasi-static rates of loading, an average difference of ~40 % at the four strain rates within the quasi-static regime. However, at intermediate strain rates, the tensile strength of ABS actually exceeded the tensile strength of PC. At a drop height of 10 in, PC showed slightly better (~2 %) strength than ABS, however at drop height of 20 and 25 inches, the average tensile strength of ABS was approximately 6.5 % higher than PC. Table 5.2 shows the percentage increase in stiffness which the thermoplastic polymers experienced from a quasi-static strain rate of 0.01s<sup>-1</sup> to strain rates corresponding to a drop height of 25 inches.

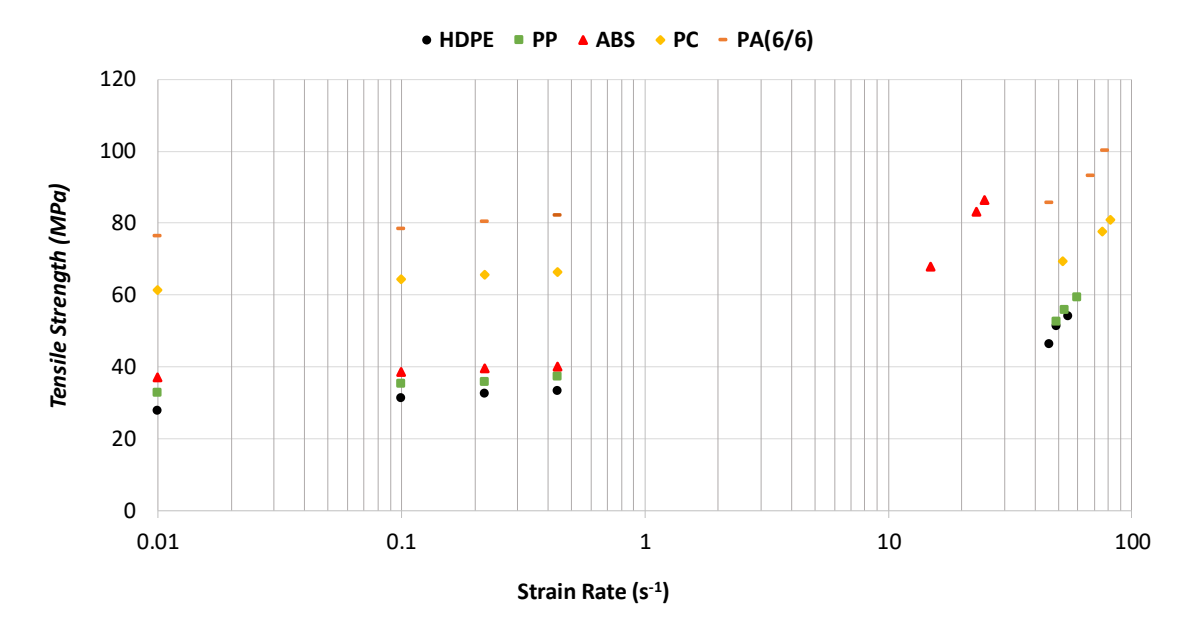


Figure 5.4: Log graph indicating the variation of average percentage tensile stiffness from quasistatic to intermediate testing regime. Error bars were not added intentionally to ensure clarity of representation

Table 5.2: Percentage increase in average stiffness from 0.01s<sup>-1</sup> to strain rates corresponding to a drop height of 25 inches

	Tensile Strength (MPa)			
Thermoplastics	At Quasi-static Strain Rate (0.01s <sup>-1</sup> )	At Intermediate Strain  Rates corresponding to 25  in. drop height (s <sup>-1</sup> )	%age Difference	
HDPE	27.84	53.97	48.41	
PP	32.78	59.42	44.84	
ABS	37.04	86.34	57.09	
PC	61.43	80.80	23.97	
PA (6/6)	76.29	100.17	23.84	

Tensile strengths of HDPE, PP and ABS experience a considerable increase at higher rates of loading as shown in Table 5.2. The highest increase in strength (57 %) was observed in the ABS samples. However, PC and PA (6/6) samples only showed an approximately 24 % increase in average tensile strength.

The average percentage strain to failure experienced by all thermoplastics at the three drop heights are shown in Figure 5.5.

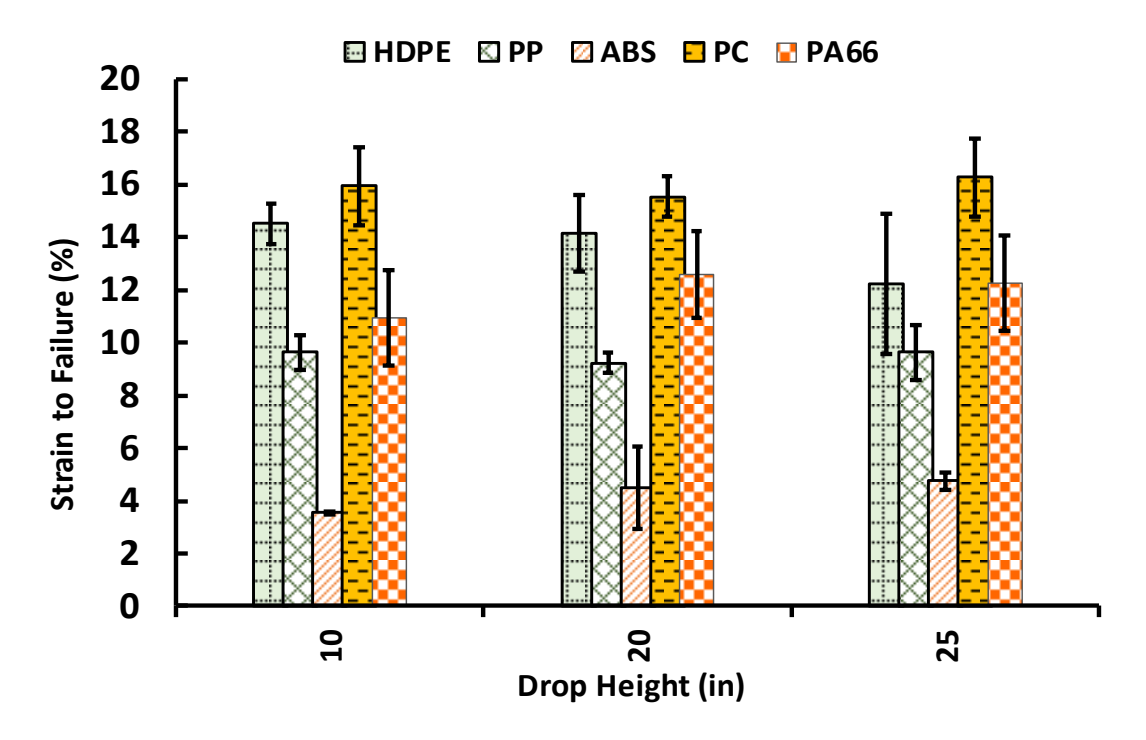


Figure 5.5: Variations in strain to failure experienced by the thermoplastics at three different drop heights

From the Figure 5.5, it is clear that PC test samples experienced the highest failure strains at all the drop heights. Unlike the tensile strength, the average percentage strain to failure or percentage of elongation did not increase with the increasing strain rates. In case of HDPE, the ductility dropped by ~ 16 % as the drop height increased from 10 to 25 inches. For PP and PC, the percentage strain to failure was observed to be nearly same for all drop heights. The highest variation in strain to failure was observed in ABS test samples. The average percentage strain to

failure in ABS samples increased with the increase in strain rates. There was an increase of  $\sim$ 21 % during transition from a drop height of 10 to 20 inches and a further increase of  $\sim$  6 % from 20 to 25 inches. For PA (6/6) samples, the average strain to failure first increased by  $\sim$  13 % from 10 to 20 inches and then decreased by 2.5 % as the drop height increased from 20 to 25 inches.

From the observations above, it is evident that each thermoplastic displayed a unique elongation behavior with varying strain rates. ABS samples failed the quickest which was inagreement with their quasi-static response as shown in Figure 5.6. The variation of average strain to failure from quasi-static to intermediate testing regime of all polymers in this study are shown in Figure 5.6.

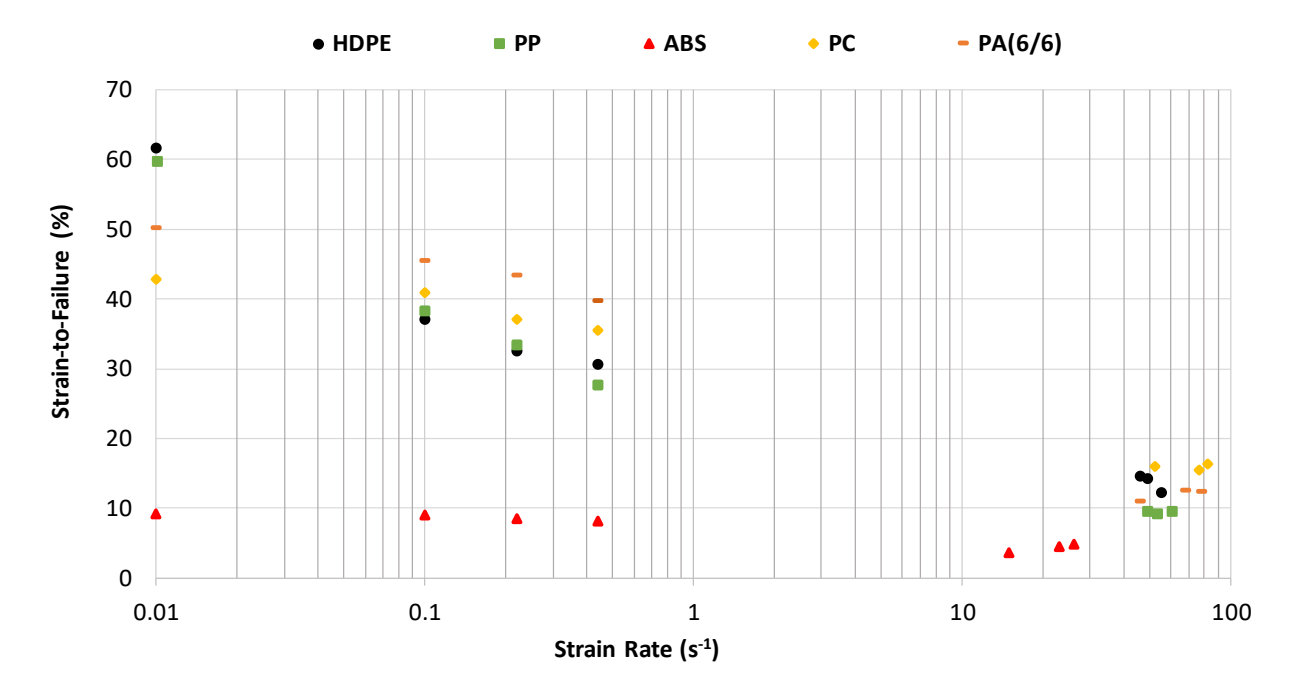


Figure 5.6: Log graph indicating the variation of average strain to failure from quasi-static to intermediate testing regime. Error bars were not added intentionally to ensure clarity of representation

From the figure above, it is evident that from quasi-static to intermediate strain rates, there is a sharp decline in the percentage strain to failure. Table 5.3 shows the average

percentage decrease in strain to failure which the thermoplastic polymers experienced from a quasi-static strain rate of  $0.01s^{-1}$  to material specific strain rates corresponding to the drop height of 25 inches. HDPE underwent the highest decreases in strain to failure at ~ 84 %. ABS samples showed the lowest percentage reduction however they did fail significantly quickly than other thermoplastics.

Table 5.3: Percentage decrease in strain to failure from 0.01s<sup>-1</sup> to strain rates corresponding to a drop height of 25 inches

	Percentage (%) Strain to Failure			
Thermoplastics	At Quasi-static Strain  Rate (0.01s <sup>-1</sup> )	At Intermediate Strain  Rates Corresponding to  25 in. drop height (s <sup>-1</sup> )	%age Difference	
HDPE	61.62	9.64	84.36	
PP	59.75	12.24	79.52	
ABS	9.16	4.76	48.05	
PC	42.84	16.27	62.02	
PA (6/6)	50.22	12.28	75.55	

From the data above the intermediate strain rate behavior of the five automotive thermoplastics used in this study can be summarized as follows.

### **5.2.1** High Density Polyethylene (HDPE)

HDPE displayed the lowest tensile strength and highest ductility during quasi-static testing. These polymers showed high strain rate sensitivity which translated into an  $\sim 48$  % increase in tensile strength and  $\sim 84$  % decrease in the percentage elongation at the highest strain

rate. The spread of intermediate strain rate across the three different drop heights was however limited to 9 s<sup>-1</sup>.

### **5.2.2** Polypropylene (PP)

PP, much like HDPE, showed high strain sensitivity leading to a radical increase in strength and reduction in strain to failure at intermediate strain rates. Their intermediate strain rate spread was limited at 11s<sup>-1</sup> between the three drop heights.

## **5.2.3** Acrylonitrile Styrene Butadiene (ABS)

ABS polymer samples failed quickly upon application of load. At quasi-static strain rates, their average strain to failure was ~ 8.7 % (for the four quasi-static strain rate cases), significantly lower than the elongation observed in other thermoplastics. Similarly, in terms of tensile strength at quasi-static strain rates, ABS showed only a slightly better response as compared to HDPE and PP, which were earmarked as thermoplastic polymers having the lowest strength and highest ductility in the initial categorization explained in Section 3.1. However, upon being tested in the intermediate strain rates, the ABS samples showed remarkable improvement in strength. At high intermediate strain rates, the tensile strength of ABS samples was  $\sim 0.86$  times the strength of the nylon (6/6) samples, which were initially categorized as the highest strength plastics to be tested. Importantly, the reduction in percentage strain to failure at higher strain rates was also around 48 %, which was comparatively much lower than other thermoplastic samples. Another important feature of the ABS samples was their strain response at different heights i.e. increasing strain rates. At a drop height of 10 inches, the average strain rate in the ABS samples was 15 s<sup>-1</sup>, which was significantly lower than the strain rates in other thermoplastics as shown in Table 5.1. The maximum strain rate experienced by the ABS samples at a drop height of 25 inches was 27 s<sup>-1</sup>, which was significantly lower than the lowest

intermediate strain rates experienced by other thermoplastic samples tested in this work (at the smallest drop height of 10 inches). The intermediate strain rate spread of ABS was 12 s<sup>-1</sup>.

### **5.2.4** Polycarbonate (PC)

PC test samples exhibited a strain rate spread of 30 s<sup>-1</sup> across the three drop heights. Despite that, the average strain to failure values at all three intermediate strain rates were consistently around 16 %. This was the highest intermediate strain response observed among all thermoplastic samples tested in this work. Overall, between the quasi-static and intermediate loading regime, there was an average decrease of 62 % in average percentage strain to failure. The tensile strength properties of PC also improved at higher strain rates, but this improvement was not nearly of the same magnitude as observed in ABS samples. A 24 % increase in tensile strength was observed between the lowest and highest strain rates at which the PC samples were tested.

### **5.2.5** Polyamide (6/6) or PA (6/6)

The Nylon samples exhibited the best load characteristics at higher strain rates, however much like PC, the average increase in strength was not significant (~ 24 %). A drastic dip in the average strain to failure was also observed as shown in Table 5.3. These plastics however exhibited high strain rates at the three drop heights, with a 32 s<sup>-1</sup> variation between the drop heights of 10 and 25 inches.

#### **5.3** ABS Nanocomposites

The second part of this study was to investigate the effect of nanoparticles on the strain rate response of ABS thermoplastic. In this regard, three ABS nanocomposites were tested at drop heights of 10, 20 and 25 inches. Details of the ABS nanocomposites were provided in section 3.5.2. Before investigating the effect of inclusions on the strain rate response of ABS, the

strain rates experienced by the nanocomposites were evaluated using the strain history plots. The resultant strain rates are reported in Table 5.4.

Table 5.4: Average strain rate values for ABS and its nanocomposites at three drop heights

	10 in.	20 in.	25 in.
ABS/ ABS Nanocomposites			
	Corresponding Strain Rates (s-1)		
		T	
ABS	$15 \pm 1.9$	$21 \pm 0.8$	$27 \pm 3.2$
ABS - M5	$14 \pm 1.8$	$20 \pm 3.0$	$25 \pm 5.4$
ABS - C750	$18 \pm 1.8$	$24 \pm 3.2$	$29 \pm 6.6$
ABS - CNT	$19 \pm 1.3$	$23 \pm 3.7$	$27 \pm 1.2$

From the table above, it is evident that the strain rates experienced by the ABS nanocomposite are approximately similar to the neat ABS samples. The tensile strain rate response of these nanocomposites was however observed to be markedly different. The variation in the tensile strength and strain to failure of neat ABS and its nanocomposites at the three drop heights are shown in Figure 5.7. It is clear from Figure 5.7 that neat ABS test samples exhibited a distinct improvement in tensile strength at intermediate strain rates. This trend was also seen in the nanocomposites, indicating that an increase in strain rates increases the tensile strength of both neat and reinforced ABS samples. There was however a variation in the magnitude of the strength improvement. This indicates that the presence of nanoparticles (fillers) in the base matrix influences the strain rate response of ABS.

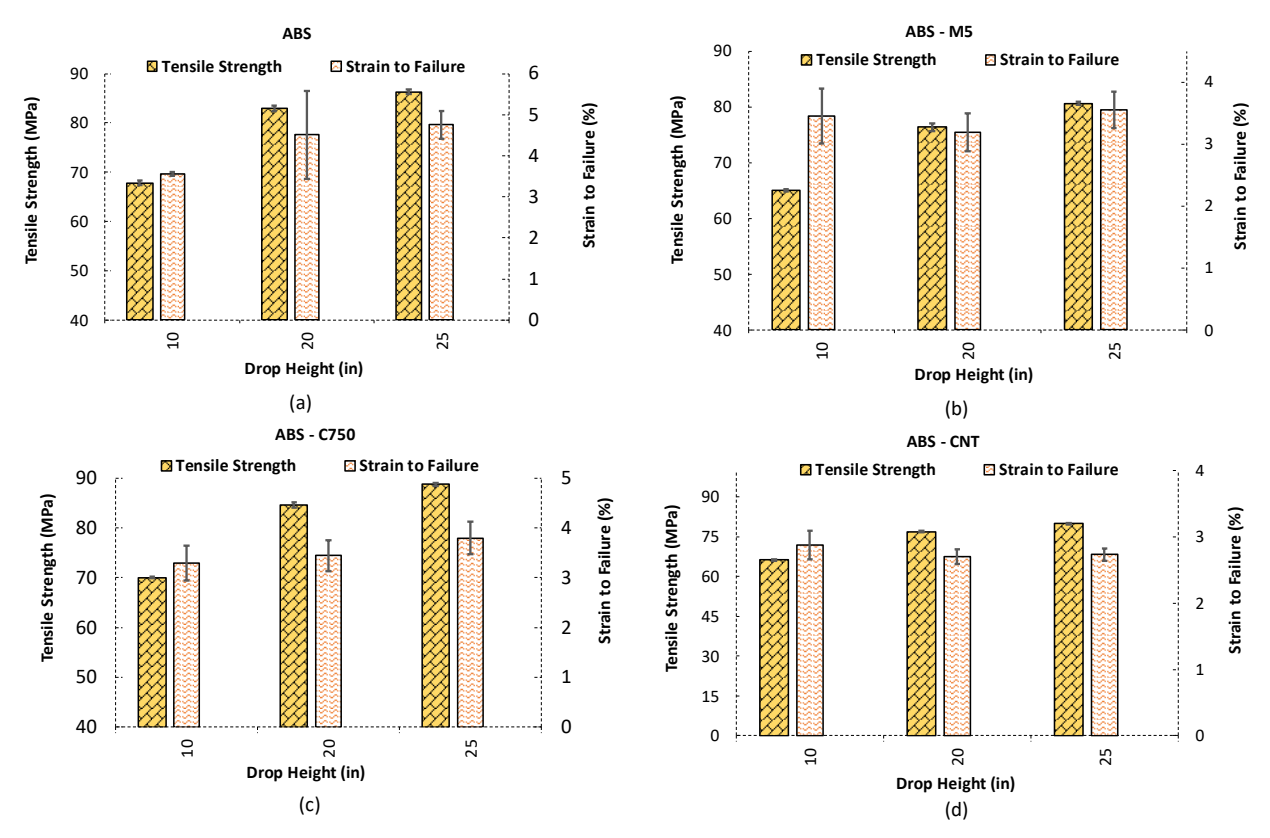


Figure 5.7: Average tensile strength and strain to failure values at three drop heights for (a) ABS (b) ABS – M5 nanocomposite (c) ABS – C750 nanocomposite and (d) ABS – CNT nanocomposite

The highest percentage increase in the tensile stiffness (~ 21 %) was observed in ABS – C750 samples, which actually mirrors the average increase in strength for neat ABS samples. For ABS – M5 and ABS – CNT samples, the percentage increase in strength across the three drop heights was slightly less (approximately 19 % and 17 % respectively). Further, the strain to failure behavior of ABS nanocomposites was poor as compared to neat ABS.

Figure 5.8 shows the comparative analysis of variation in average tensile strength of ABS and its nanocomposites when subjected to intermediate strain rates corresponding to drop heights of 10, 20 and 25 inches. This graph details interesting results, especially in the context of the quasi-static strain rate testing already carried out in Chapter 3. The highest magnitude increase in tensile strength was observed in ABS – C750 samples, whereas the tensile strength of ABS – M5

and ABS – CNT actually decreased as compared to the neat ABS samples. This is in stark contrast to the quasi-static observations, where out of the three nanoparticles, CNT based nanocomposites showed the highest increase in strength at increasing strain rates. For ease of understanding, the rate dependent behavior of these samples is re-plotted in Figure 5.9.

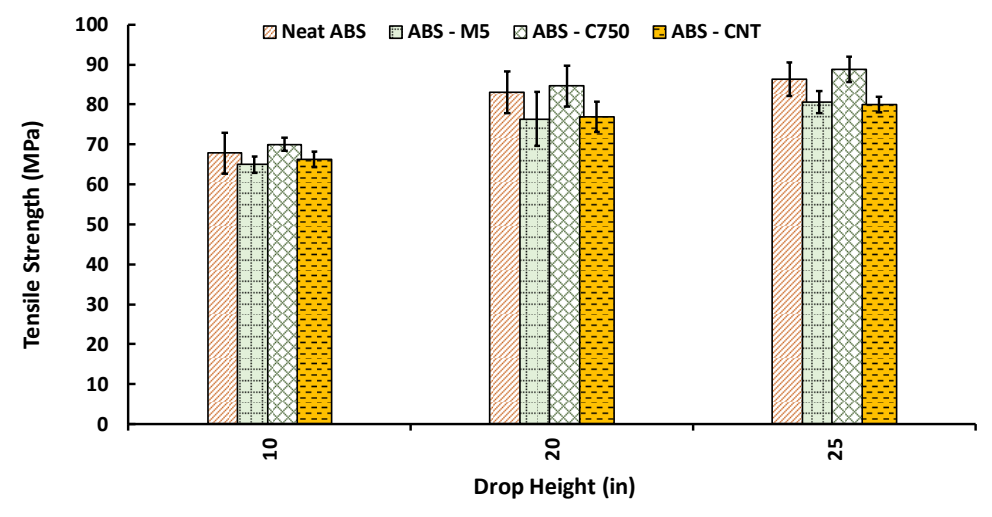


Figure 5.8: Average tensile strength of ABS/ABS Nanocomposites at three different drop heights

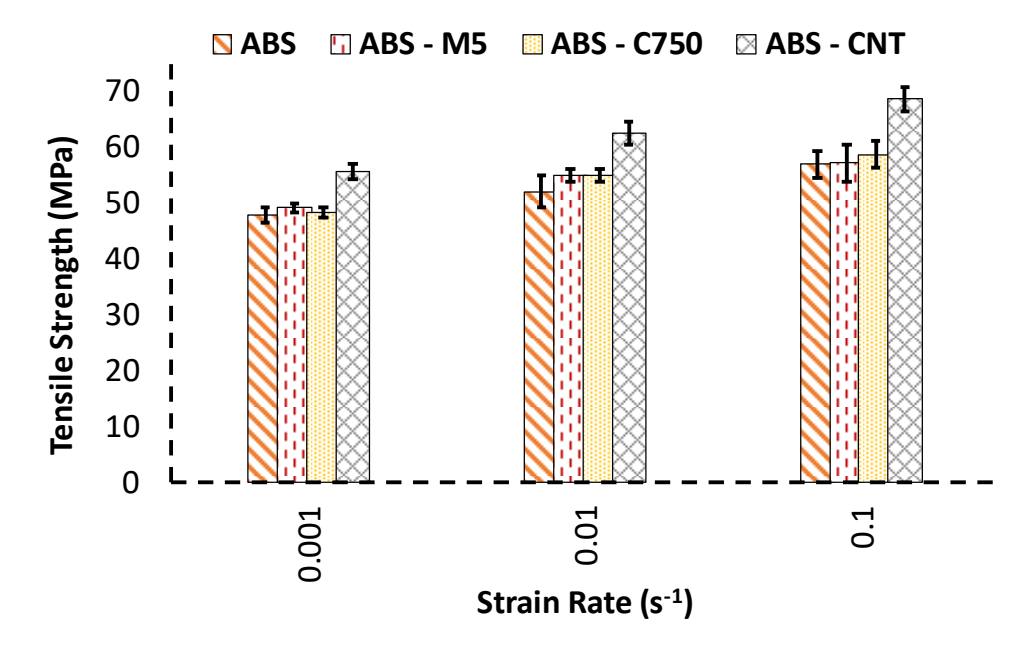


Figure 5.9: Average tensile strength of ABS/ABS Nanocomposites at quasi-static strain rates

This unique behavior, especially in the case of ABS – CNT composites can be attributed to the high aspect ratios of CNT and the lack of particle functionalization for this specific study. In general, nanoparticles having higher aspect ratios are preferred since they facilitate better load transfer between the matrix and the particles. This is especially true at quasi-static strain rates where the CNT's have enough time to align with the direction of load during the deformation flow process. This argument stands true even for the highest strain rate (0.1 s<sup>-1</sup>), at which the samples were tested during the quasi-static strain rate sensitivity study. At intermediate strain rates however, the failure occurs so quickly that CNT tube structures are unable to align in the direction of the load. Therefore, rather than acting as short fibers oriented in the load direction, these CNT's disrupt the loading process by acting as stress discontinuities leading to a brittle behavior and low strain to failures.

The behavior of large aspect ratio nanoparticles at intermediate strain rates also emphasizes the need for proper dispersion of nanoparticles. Particle dispersion through ultrasonic treatment, usage of high shear mixing instrument, or ball mill treatment etc. can allow a design engineer to control key physiochemical properties, such as particle size/size distribution, shape, aggregation/agglomeration etc. within the ABS matrix and subsequently tailor the strain rate response. In this study, as mentioned earlier, mechanical mixing was used and no specialized technique was used to disperse the nanoparticles into the ABS matrix and the potential of agglomeration was high. This was by design to establish the baseline/control behavior of asreceived materials. Any further improvements will only add value to the material behavior and hence this work is aimed as a launch-pad for further detailed studies.

Another important factor which can lead to reduction in stiffness at higher strain rates is the presence, or lack thereof the oxygen functional groups. The presence of functionalized

oxygen groups is critical in ensuring a strong bond between the matrix and the nanoparticle which is essential in properly utilizing the stiffness of the nanoparticles. If the bond between the matrix and the nanoparticle is weak, interfacial debonding will take place before the load can be completely transferred to the nanoparticle leading to an abrupt failure. Chemical functionalization of nanoparticles is therefore critical in ensuring compatibility between the nanoparticle and the host polymer, which can lead to higher tensile strengths.

For this work, CNTs and the graphene nanoparticles were not functionalized. Lack of these functional groups can reduce or eliminate the effect of higher aspect ratios, especially at higher strain rates. At quasi-static strain rates, since the translational/rotational motion of ABS chains is slow, adequate interfacial adhesion takes place even with nonfunctionalized carbon nanotubes owing to their large aspect ratios. At higher speeds however, deformation takes place quickly and with no oxygen functional groups attached to the nanotubes, the tensile strength of ABS nanocomposites is reduced in comparison to the graphene platelets which inherently comprise of oxygen functional groups as part of their microstructure.

The atomic concentration of oxygen for GnP - C750 was more than two times higher than the oxygen concentration of GnP - M5 [9]. The presence of these functional groups can be attributed to the higher tensile strength of ABS – C750 nanocomposites as compared to CNT and M5. It is important to mention that an increase in tensile strength of ABS – C750 particles was observed despite their tendency to agglomerate. These particles possess a high surface area (750 m<sup>2</sup>/g) and oxygen groups tend to aggregate through  $\pi$ - $\pi$  stacking [9].

The high specific surface area of contact in C-750 graphene particles also helps in improving the elongation properties of the nanocomposite, because it increases the contact area

with the host matrix. These particles have the highest specific surface area among the three nanoparticles C-750 (750  $m^2/g$ ) > CNT (200  $m^2/g$ ) > M-5 (150  $m^2/g$ ) [10].

A comparative analysis of the average strain to failure experienced by neat and reinforced ABS tensile test samples is shown in Figure 5.10. It is clear from the figure that the addition of non-dispersed and non-functionalized nanoparticles in the ABS matrix compromised their elongation properties. Theoretically, the addition of nanoparticles should increase the brittle behavior of the thermoplastics however from Figure 5.8 it was observed that only ABS – C750 nanocomposites showed an improvement in strength. These nanocomposites also display the best strain response, most probably due to its oxygen functional groups and higher specific surface area. This deformation behavior is in-agreement with the quasi-static failure strain response evaluated in Chapter 3. There is however no overall advantage of nanoparticles on the strain response of the system.

Considering the above observations and the inputs from the quasi-static strain rate analysis, it can be concluded that while non-dispersed and non-functionalized nanoparticles may provide a tangible increase in strength at increasing rates within the quasi-static regime, at intermediate strain rates, these nanoparticles are do more harm than good. It is therefore recommended that for testing at dynamic loading rates, the nanoparticles or inclusion must be properly dispersed and functionalized to extract maximum advantage from their strength and toughness properties.

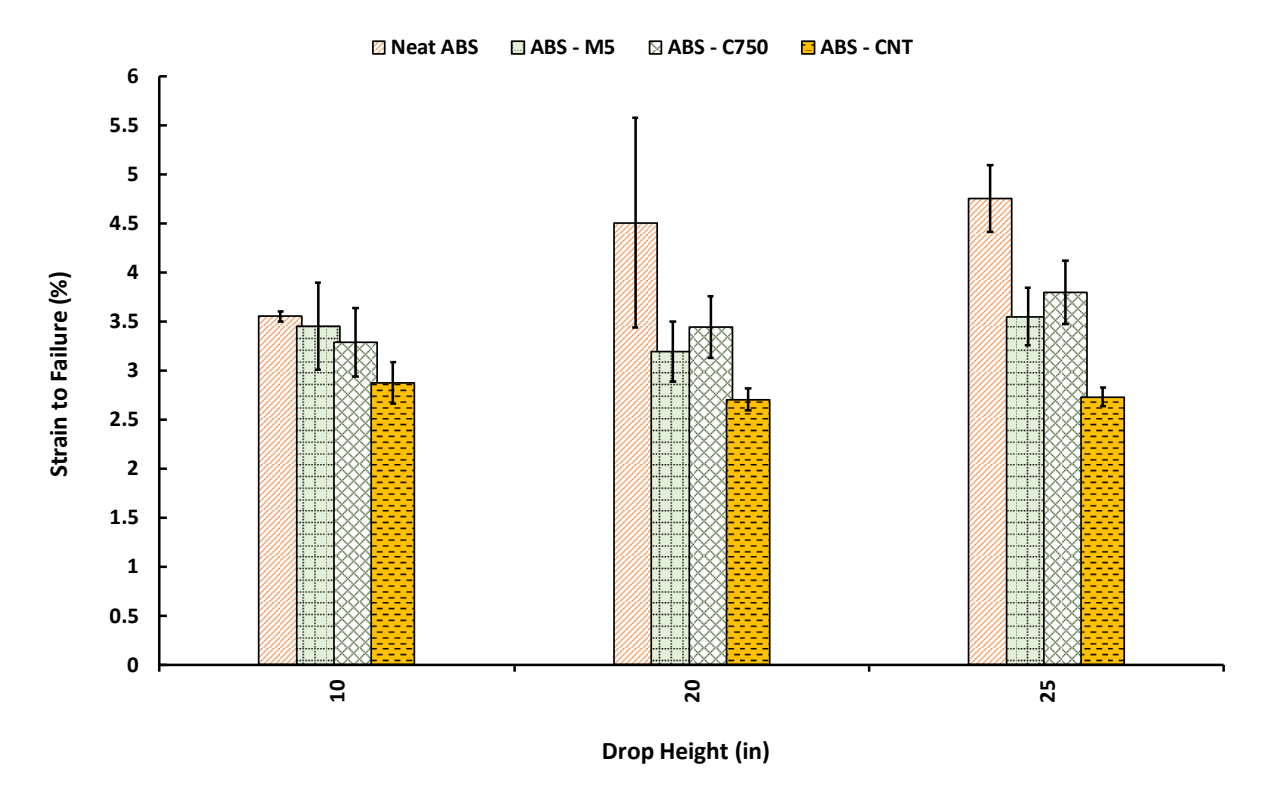


Figure 5.10: Average percentage strain to failure of ABS/ABS Nanocomposites at intermediate strain rates

### 5.4 Conclusion

In this chapter, intermediate strain rate testing of 'select' thermoplastics was carried out using the newly developed tensile fixture. All the selected thermoplastic polymer samples were tested at three constant drop heights. It was observed that polymers exhibit unique strain responses when subjected to similar loads. The highest strain rate variation was observed in PC and PA (6/6) samples where the strain rate increased by ~ 36 % and 41 % respectively as the drop height increased from 10 to 25 inches. ABS samples showed the least strain rate variation among all the polymers tested.

The highest percentage increase (22 %) in strength was observed in ABS whereas PP showed the lowest percentage increase in strength at 12 %. The tensile behavior of polymers was found to be distinctively different at intermediate strain rates when compared to their quasi-static

response. For example, at quasi-static loading, the tensile strength of PC was ~40 % higher than ABS. However, at a drop height of 25 in, the tensile strength of ABS (86.30 MPa) was observed to be higher than that of PC (80.80 MPa), clearly indicating that the intermediate strain rate behavior of each polymer is unique and cannot be estimated based on its quasi-static response. Similarly, unlike the quasi-static response, the average percentage strain to failure did not decrease with the increasing strain rates. The percentage elongation in each polymer was unique, with the PC test samples experiencing the highest overall failure strains at all drop heights.

Investigation into the effect of three carbon-based nanoparticle fillers on the intermediate strain rate properties of ABS was also carried out. At all drop heights, the strain rates experienced by the ABS nanocomposites were approximately similar to the neat ABS samples. The highest magnitude increase in tensile strength was observed in ABS – C750 samples, whereas the tensile strength of ABS – M5 and ABS – CNT decreased as compared to the neat ABS samples. This observation was in stark contrast to the quasi-static test results wherein, out of the three nanoparticles, ABS – CNT showed the highest increase in strength at increasing strain rates. This unique behavior, especially in the case of ABS – CNT composites, can be attributed to the comparatively high aspect ratios of CNT, random dispersion and the lack of particle functionalization. ABS – C750 shows comparatively better response which can be attributed to its higher surface area and inherently more oxygen functional groups. It was concluded that there was no overall benefit of adding unfunctionalized and poorly dispersed nanoparticles in the thermoplastic matrix. Nevertheless, chemically functionalized nanoparticles that are compatible with the host polymer are expected to show better enhancements than what was observed in this study. This was done 'by design' to create the benchmark performance of these polymers with 'as-received,' non-functionalized nano-fillers. Future work will showcase

the enhancement of each of these polymers based on chemical functionalization, varying particle concentrations, varying process parameters, etc. In short, this work creates the launchpad for a wide range of exploration on high-strain rate testing of polymers.

#### REFERENCES

- [1] X. Xiao, "Dynamic tensile testing of plastic materials," Polymer Testing, vol. 27, pp. 164-178, 2008/04/01/2008.
- [2] J. E. Field, S. M. Walley, W. G. Proud, H. T. Goldrein, and C. R. Siviour, "Review of experimental techniques for high rate deformation and shock studies," International Journal of Impact Engineering, vol. 30, pp. 725-775, 2004/08/01/2004.
- [3] S. Walley and J. Field, "Strain rate sensitivity of polymers in compression from low to high rates," DYMAT j, vol. 1, pp. 211-227, 1994.
- [4] C. R. Siviour and J. L. Jordan, "High strain rate mechanics of polymers: a review," Journal of Dynamic Behavior of Materials, vol. 2, pp. 15-32, 2016.
- [5] J. L. Jordan, C. Siviour, and B. Woodworth, "High strain rate tensile and compressive effects in glassy polymers," in EPJ web of conferences, 2012, p. 01001.
- [6] D. Zhu, B. Mobasher, S. D. Rajan, and P. Peralta, "Characterization of dynamic tensile testing using aluminum alloy 6061-T6 at intermediate strain rates," Journal of Engineering Mechanics, vol. 137, pp. 669-679, 2011.
- [7] Consumer Reports. (April 2014). NHTSA Crash Test 101. Available: consumerreports.org/cro/2011/08/crash-test-101/index.htm
- [8] Engineerine.com. (2023). Car's Average Length By Model [Why is it Important?]. Available: engineerine.com/cars-average-length/
- [9] F. Wang, L. T. Drzal, Y. Qin, and Z. Huang, "Mechanical properties and thermal conductivity of graphene nanoplatelet/epoxy composites," Journal of materials science, vol. 50, pp. 1082-1093, 2015.
- [10] XG Sciences Our Proprietary xGnP Graphene Formulas. Available: xgsciences.com/graphene/